University of Alberta

Aviat Diamonds: A Window into the deep Lithospheric Mantle beneath the Northern Churchill Province

by

Jennifer Elizabeth Peats

A thesis submitted to the Faculty of Graduate Studies and Research
in partial fulfillment of the requirements for the degree of

Master of Science

Earth and Atmospheric Sciences

Fall 2011
Edmonton, Alberta

Abstract

The northern Churchill Province is an intensely explored, yet poorly researched target area for diamonds. I examined the mantle sources and residence history of diamonds from Aviat, located on the Melville Peninsula. Aviat diamonds display a $\delta^{13}C$ range extending far below the average mantle value of -5‰ indicating eclogitic sources must be present. Crustal protoliths, carrying the organic matter implied by strongly ^{13}C depleted diamond compositions, likely were supplied via subduction. The main population of diamonds around -5‰ may be either eclogitic or peridotitic. The CL patterns and variation of $\delta^{13}C$ values within diamonds indicate that at least two diamond growth events, interrupted by periods of resorption, occurred at Aviat. Nitrogen and $\delta^{13}C$ are decoupled indicating that multiple fluid sources contributed to diamond formation at Aviat. Mantle residence temperatures for most Aviat diamonds range from ~1050-1150°C, indicating a range of source depths.

Acknowledgements

First I would like to thank all of the members of my examining committee: Thomas Stachel, Karlis Muehlenbachs, and Claire Currie, for taking the time to read this thesis and for providing valuable feedback which subsequently improved it. Thank you to John Armstrong of Stornoway Diamond Corporation for providing the samples for this project. Many thanks go out to the staff of the CCIM, Richard Stern and Gayle Hatchard, for their assistance with the SIMS and CL work presented in this thesis. The support and knowledge of my fellow members of the Diamond Research Group: Greg Melton, Lucy Hunt, Catherine Johnson, and Karen Smit, were invaluable in the completion of this thesis. Lastly, I want to thank my supervisor Thomas Stachel for giving me the opportunity to undertake this thesis in the first place and for all of the guidance along the way.

Table of Contents

List of Tables

List of Figures

List of Abbreviations and Symbols

‰	per mille
at.ppm	atomic parts per million
CL	Cathodoluminescence
FTIR	Fourier Transform Infrared Spectroscopy
SIMS	Secondary Ion Mass Spectrometry
STZ	Snowbird Tectonic Zone
IUGS	International Union of Geological Sciences
Ma	Megaannum (one million years)
Ga	Gigaannum (one billion years)
et.al.	et alia (and others)
mW/m^2	milliWatts per square meter
NW	northwest
SE	southeast
cpht	carats per hundred tonnes
DTC	Diamond Trading Company
IR	Infrared
VPDB	Vienna Pee Dee Belemnite
CCIM	Canadian Centre for Isotopic Microanalysis
IPG	Institut de Physique du Globe de Paris
cts/sec	counts per second
WDS	Wavelength Dispersive Spectrometry
NV	Nitrogen Vacancies
ES	Eastern Sheet Complex

In Tables:

agg	aggregate
b	brown
c	colourless
d	dodecahedral
f	fragment
gn	green
g	grey
i	irregular
l	light
o	octahedral
PD	plastic deformation
N/A	not available

Chapter 1: Introduction

1.1. Introduction

Diamond mining has become a lucrative industry in northern Canada accounting for 97% of the 2.1 billion dollar mineral production in the Northwest Territories and Nunavut (2008 data; Northern Mining News, 2009). Exploration is the key to finding new deposits and continuing to expand the industry; to accomplish this, advancements in geochemical data and indicator mineral assessment, and target area selection must come from research on diamonds and their associated mineral inclusions obtained from existing deposits.

The basic principle in diamond exploration is “Clifford’s Rule” that diamondiferous kimberlites intrude cratons; pieces of old continental crust which have remained stable for long periods of time (Clifford, 1966), preferably since the Archean (Janse, 1994). Underneath these cratons are thick layers of lithospheric mantle which during formation in the Archean experienced high degrees of melt extraction stripping out most of the heat producing radioactive element budget, leaving the subcratonic lithosphere colder than at other locations at equivalent depth (e.g. Pollack and Chapman, 1977). These cratons also experienced dehydration and iron loss (e.g. Lee et al., 2008). Therefore, beneath cratons the temperature sensitive graphite/diamond transition occurs at a shallower depth, making them the only locations globally where lithospheric keels and diamond stable conditions overlap (e.g. Boyd and Gurney, 1986). This corresponds to temperatures and pressures of formation for most diamonds of 900-1500°C and 50-60 kbar respectively (Figure 1-1) (Haggerty, 1986; Meyer, 1987, Harris, 1992). Kimberlites and lamproites, two very deep seated magma types, then sample these keels and entrain diamonds during their swift ascent towards the Earth's surface.

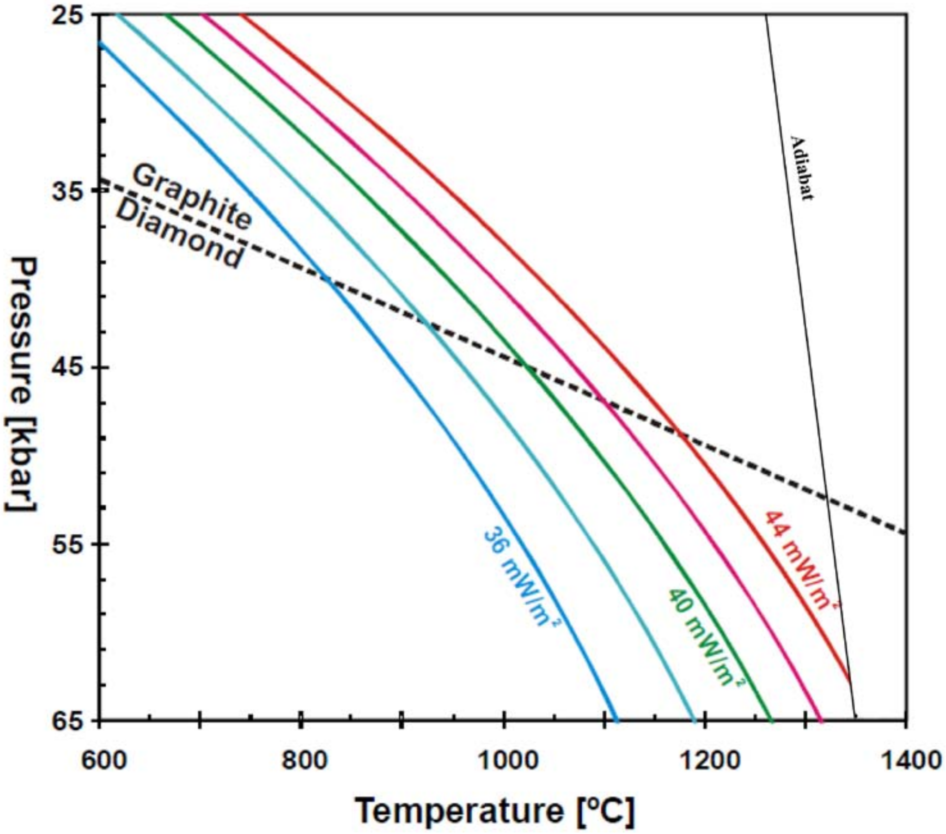

Figure 1-1 Reference conductive mantle geotherms.
After Pollack and Chapman (1977), reference conductive mantle geotherms superimposed with the graphite-diamond transition line. Where a geotherm crosses this graphite-diamond line delimits the beginning of the window of diamond formation within the mantle. Where the same geotherm is cross-cut by the mantle adiabat delimits the end of the diamond window.

1.2. Geochemistry

1.2.1. Source Rock Geochemistry

The host rocks for diamond formation in the lithospheric mantle are peridotite, eclogite, and websterite (pyroxenite). Studies of inclusion bearing diamonds indicate that peridotitic associations are most common (65%) followed by eclogitic (33%) and websteritic (2%) source lithologies (Stachel and Harris, 2009). Peridotite is an olivine rich (>40 vol.%) ultramafic rock which has several subdivisions based on its complete mineralogy. Peridotite composed of olivine, clinopyroxene, and orthopyroxene (plus usually some garnet as the aluminum bearing phase at diamond stable conditions) is a lherzolite; if the clinopyroxene is no longer present due to very strong melt depletion then it is termed a harzburgite. Further depletion where both pyroxenes are removed results in a rock with >90% olivine, termed dunite. Another variant, which can occur due to metasomatic overprinting (introduction of secondary clinopyroxene), is wehrlite which has clinopyroxene but almost no orthopyroxene. Eclogites are made up of >90% clinopyroxene and garnet (in roughly similar proportions) and are the metamorphic high pressure equivalent of basalt. Websterite was first introduced by Gurney (1984) as a third principal diamond paragenesis and has since then been loosely defined to describe diamond source rocks with compositions intermediate to eclogites and peridotites. Note that this loose definition overlaps with, but is not restricted to, the IUGS approved classification of websterite as an olivine poor (<5%) two pyroxene pyroxenite (Le Maitre, 2002).

Geochemical characterization of diamonds and their host kimberlites is an important routine procedure as diamonds from each host kimberlite have a unique carbon and nitrogen signature (e.g. Galimov, 1991). These chemical signatures provide information on the mantle residence (length of time or temperature) of diamonds, their source paragenesis, and conditions in the region where the diamonds were formed.

1.2.2. Inclusions in Diamond

Many different mineral inclusions have been documented in diamond. These inclusions are important in determining the source paragenesis and the physical conditions during formation of their host diamonds. Once included within diamond, the inclusions are well protected by their hosts from alteration e.g. during transport in a kimberlite magma, thus providing accurate chemical data for the mantle from which they came (Meyer and Boyd, 1972). Diamonds can contain one or more inclusions, and the inclusions may be separate or touching in the host (Meyer and Boyd, 1972). Inclusion size varies, but commonly is on the order of 100 μm in diameter (Meyer and Boyd, 1972). Inclusions may be either protogenetic, crystallizing before their diamond host, syngenetic, crystallizing simultaneously with their host, or epigenetic, crystallizing after the diamond host (Bulanova, 1995). For rare “super-deep” diamonds (~200-230 km depth) of sublithospheric origin, Harte (2010) postulates that the distribution of their mineral inclusions suggests that their formation within the mantle is a function of dehydration (associated for example with the wadsleyite to olivine transition) and fluid/melt production in their growth regions.

The majority of diamonds form in the lithospheric mantle between 150 to 200 km depth and up to a maximum of about 240 km depth (Stachel and Harris, 1997). Inclusions in lithospheric diamonds reflect the mineralogy of the peridotites, eclogites or websterites in which they formed (e.g. Meyer and Boyd, 1972).

Diamonds which include majoritic garnet indicate formation in the deep lithosphere, asthenosphere, or transition zone ranging from approximately 230-

660 km in depth (Stachel et al., 2005). Almost exclusively, these majoritic inclusions are of eclogitic paragenesis which led to the interpretation that asthenosphere and transition zone diamonds have a subduction related origin (Stachel, 2001).

Another source region for diamonds is the lower mantle (depths >660 km) (Ringwood, 1982; Harris, 1992). To be classified as deriving from the lower mantle, diamonds must feature coexisting inclusions of ferroperriclase and either CaSi-perovskite, MgSi-perovskite or stishovite (Stachel et al., 2005). Ferroperriclase alone is not enough to definitively classify a diamond as lower mantle in origin because while it is not present in the majority of upper mantle rocks, as there are localized areas of low silica in this region (Stachel et al., 2005). Thus, a coexisting inclusion of perovskite or stishovite is necessary to unequivocally prove a lower mantle origin (Stachel et al., 2005).

1.2.3. Diamond Geochemistry

The carbon isotopic composition of diamond is reported in the standard delta notation (δ^{13}Csample = ((^{13}C/^{12}Csample – ^{13}C/^{12}Cstandard)/^{13}C/^{12}Cstandard) x 1000).

Ranges in δ^{13}C values for diamonds from individual occurrences can sometimes aid in the determination of source paragenesis, as each paragenesis has a unique range of values (Sobolev et al., 1979). The bulk of peridotitic diamonds display a restricted range of δ^{13}C values from -10 to -1‰ (Galimov, 1991; Kirkley et al., 1991). A much broader range of values are exhibited by eclogitic diamonds (Sobolev et al., 1979), from -41 (De Stefano et al., 2009) to +2.9‰ (Davies et al., 2003). A mode at -5 ± 1‰ is the generally accepted value for mantle derived carbon, and is common to both parageneses (Deines, 1980; Cartigny, 2005). Diamonds of eclogitic paragenesis, however, show a bimodal distribution with an indistinct second “mode” between approximately -19 and -8‰ which likely reflects several overlapping modes from different diamond mines/districts (e.g. Stachel and Harris, 2009). An explanation for the highly negative $\delta^{13}C$ values observed in eclogitic diamonds has been the subject of much debate. The proposed explanations include: (1.) contribution of carbon derived from graphitized organic matter contained in subducted oceanic crust (Sobolev and Sobolev, 1980; Milledge et al., 1983; Kirkley et al., 1991), (2.) mantle inhomogeneity (Deines, 1980), (3.) isotopic fractionation of carbon dissolved in mantle minerals (Deines, 2002), or (4.) isotopic fractionation in an open system environment (Javoy et al., 1986; Cartigny, 2005).

Nitrogen is the primary impurity present in diamond due to its similarity to carbon in size and valence. With increasing mantle residence time nitrogen aggregation progresses from single N atoms (C centre), to pairs of N atoms (A centre), and finally to rings of four N atoms surrounding a vacancy (B centre) (e.g. Evans et al., 1995). Almost exclusively, the transition from C to A centre is completed in monocrystalline, mantle derived diamonds (e.g. Gurney, 1989). Consequently, nitrogen aggregation is usually expressed as the relative abundance of A and B centres (%B = 100B/[A+B] in atomic ppm).

Diamonds are classified as either Type I (nitrogen bearing), or Type II (nitrogen free). Type Ia diamonds contain only aggregated nitrogen (no C centres) and are subdivided according to their exact nitrogen aggregation state: Type IaA

= 0-10%B, Type IaAB = 10-90%B, Type IaB = 90-100%B. The aggregation from A to B centres in diamond is accompanied by the formation of platelets (defects in the diamond lattice not associated with nitrogen) which produce a sharp absorption peak in the range of 1358-1378 cm^{-1} (Sobolev et al., 1968).

1.3. Thesis Intent

Together, carbon isotopic composition, and nitrogen characteristics (content and aggregation state) provide a geochemical fingerprint for diamonds present at any given location, yielding important information on their mantle residence history and source paragenesis, thereby providing information on the composition and evolution of the associated lithospheric mantle. This project endeavors to use such analyses to glean the aforementioned information for diamonds from the Aviat diamond property, located in a poorly studied area of Canada’s arctic, the Rae Craton of the northern Churchill Province.

References

Boyd, F.R. and Gurney, J.J. (1986) Diamonds and the African lithosphere. *Science* **232**, 472-477.

Bulanova, G.P. (1995) The formation of diamond. *J. Geochem. Explor.* **53**, 1-23.

Cartigny P. (2005) Stable isotopes and the origin of diamond. *Elements* **1,** 79-84.

Clifford T.N. (1966) Tectono-metallogenic units and metallogenic provinces of Africa. *Earth Planet. Sci. Lett.* **1,** 421-434.

Davies R.M., Griffin W.L., O'Reilly S.Y. and Andrew A.S. (2003) Unusual mineral inclusions and carbon isotopes of alluvial diamonds from Bingara, eastern Australia. *Lithos* **69,** 51-66.

De Stefano A., Kopylova M.G., Cartigny P. and Afansiev V. (2009) Diamonds and eclogites of the Jericho kimberlite (Northern Canada). *Contrib. Mineral. Petrol.* **158,** 295-315.

Deines P. (1980) The carbon isotopic composition of diamonds: relationship to diamond shape, color, occurrence and vapor composition. *Geochim. Cosmochim. Acta* **44,** 943-961.

Evans, T., Kiflawi, I., Luyten, W., van Tendeloo, G., and Woods, G.S. (1995) Conversion of platelets into dislocation loops and voidite formation in type IaB diamonds. *Proc. R. Soc. Lond. Ser. A,* **449**, 295-313.

Galimov E.M. (1991) Isotope fractionation related to kimberlite magmatism and diamond formation. *Geochim. Cosmochim. Acta* **55,** 1697-1708.

Gurney J.J. (1989) Diamonds. *In* Kimberlites and Related Rocks: Proceedings of the IVth International Kimberlite Conference (eds. J. Ross, A.L. Jaques, J. Ferguson, D.H. Green, S.Y. O'Reilly, R.V. Danchin, A.J.A. Janse). Geological Society of Australia Special Publication, vol. **14**. Blackwell, Carlton, pp. 935-965.

Gurney, J.J., Harris, J.W., and Richard R.S. (1984) Silicate and oxide inclusions in diamonds from the Orapa Mine, Botswana. *In* Kimberlites II: the mantle and crust-mantle relationships (ed. J. Kornprobst). Elsevier, Amsterdam, pp.3-9.

Haggerty, S.E. (1986) Diamond genesis in a multiply-constrained model. *Nature*, **320**(6057), 34-38.

Harris J.W. (1992) Diamond Geology. *In* The properties of natural and synthetic diamond (ed. A. C. Field). Academic Press, London. pp. 345-393.

Harte B. (2010) Diamond formation in the deep mantle: the record of mineral inclusions and their distribution in relation to mantle dehydration zones. *Mineral. Mag.* **74,** 189-215.

Janse, A.J.A. (1994) Is Clifford's rule still valid? Affirmative examples from around the world. *In* Diamonds: characterization, genesis and exploration. (eds. H.O.A. Meyer and O.H. Leonardos), CPRM Spec. Publ. Jan/94, Brasilia, pp.215-235.

Javoy M., Pineau F. and Delorme H. (1986) Carbon and nitrogen isotopes in the mantle. Chem. Geol. **57**, 41-62.

Kirkley M.B., Gurney J.J., Otter M.L., Hill S.J. and Daniels L.R. (1991) The application of C isotopes measurements to the identification of the sources of C in diamonds: a review. *Appl. Geochem.* **6,** 477-494.

Lee, C.A., Luffi, P., Höink, T., Li, Z.A., Lenardic, A. (2008) The role of serpentine in preferential carbon formation in the late Archean by lithosphere underthrusting. *Earth Planet. Sci. Lett*. **269**, 96-104.

Le Maitre, R.W. (2002) Igneous rocks - A classification and glossary of terms. Cambridge University Press, 236 pp.

Meyer H.O.A. and Boyd F.R. (1972) Composition and origin of crystalline inclusions in natural diamonds. *Geochim. Cosmochim. Acta* **36,** 1255-1273.

Meyer, H.O.A. (1987) Inclusions in diamond. Mantle Xenoliths (ed. P.X. Nixon), John Wiley & Sons Ltd., New York. pp.501-533

Milledge H.J., Mendelssohn M.J., Seal M., Rouse J.E., Swart P.K. and Pillinger C.T. (1983) Carbon isotopic variation in spectral type II diamonds. *Nature* **303,** 791-792.

Northern Mining News (July 2009) **2**:3.

Pollack H.N. and Chapman D.S. (1977) On the regional variation of heat flow, geotherms, and lithospheric thickness. *Tectonophysics* **38,** 279-296.

Ringwood A.E. (1982) Phase-transformations and differentiation in subducted lithosphere-implications for mantle dynamics, basalt petrogenesis, and crustal evolution. *J. Geol.* **90,** 611-643.

Sobolev V.S. and Sobolev N.V. (1980) New Proof on very deep subsidence of eclogitized crustal rocks. *Doklady Akad. Nauk SSSR* **250,** 683-685.

Sobolev E.V., Lenskaya S.V. and Lisoivan V.I. (1968) Lamellar formations in the structure of natural diamonds. *Jour. Struc. Chem. (Engl. Transl.)* **9,** 917-920.

Sobolev N. V., Galimov E. M., Ivanovskaia I. N. and Yefimova E. S. (1979) Isotopic composition of carbon from diamonds containing crystalline inclusions (in Russian). *Doklady Akad. Nauk SSSR* **5,** 1217-1220.

Stachel T. (2001) Diamonds from the asthenosphere and the transition zone. *Eur. J. Mineral.* **13,** 883-892.

Stachel T. and Harris J.W. (1997) Syngenetic inclusions in diamond from the Birim field (Ghana) - a deep peridotitic profile with a history of depletion and re-enrichment. *Contrib. Mineral. Petrol.* **127,** 336-352.

Stachel T. and Harris J.W. (2009) Formation of diamond in the Earth's mantle. *J. Phys: Condens. Matter* **21,** June 23, 2010.

Stachel, T., Brey, G.P., and Harris, J.W. (2005) Inclusions in sublithospheric diamonds: Glimpses of deep Earth. *Elements*. **1**, 73-78.

Chapter 2: Geological History

2.1. The Churchill Province

The Churchill Province is divided into the Rae and Hearne cratons by the Snowbird tectonic zone (STZ) (Figure 2-1) (Gibb and Walcott, 1971; Hoffman, 1988,1990; Berman et al., 2005). Recently, several authors have delineated the "Chesterfield Block", centered around the community of Chesterfield Inlet, Nunavut, as a separate component in the northeast Churchill Province, unique from both the Rae and Hearne cratons (Berman et al., 2007). The Churchill Province is broadly described as consisting of 2.7-2.6 Ga greenschist to amphibolite facies supracrustal rocks with felsic intrusions (Berman et al., 2005).

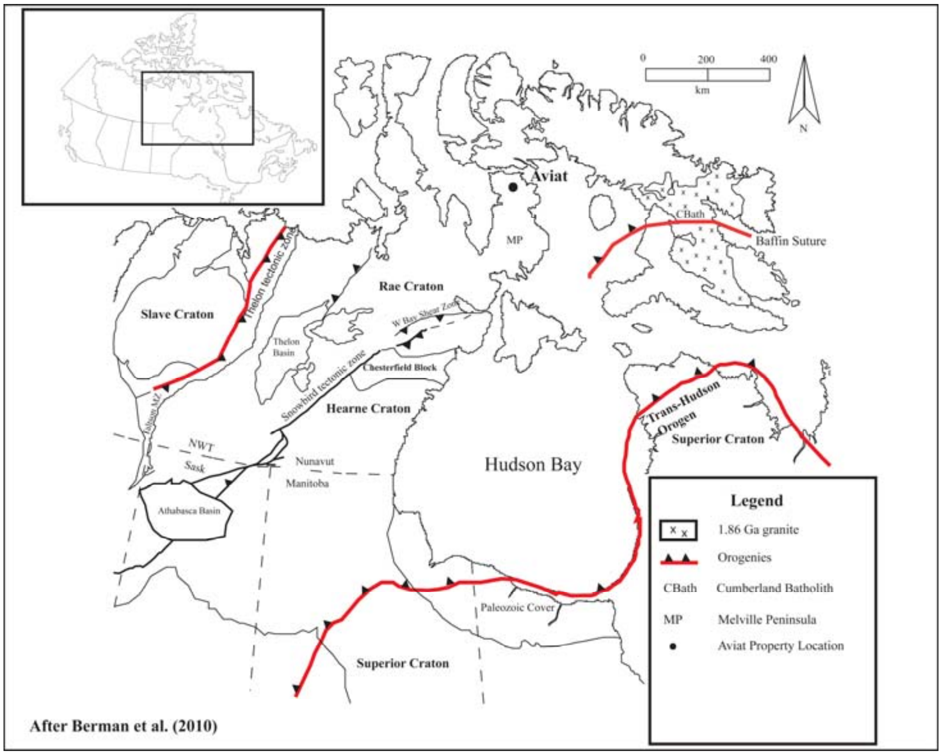

Figure 2-1 Location of the Aviat property
Property location is projected onto a map of the Canadian Shield adapted from Berman et al. (2010).

2.2. The Rae Craton

The Rae craton, which hosts the Aviat kimberlites studied here, can be divided into two portions, a northern portion <3.0 Ga in age, and a southern portion >3.0 Ga in age (Hartlaub et al., 2005). The Rae is dominantly made up of Archean granitoid rocks and supracrustal belts as well as Paleoproterozoic metasedimentary rocks chiefly of amphibolite facies (Skulski et al., 2003a,b; Berman et al., 2010). The majority of the granitoid rocks were emplaced during two separate pulses of magmatism from 2.9-2.85 and 2.72-2.58 Ga (e.g. Skulski et al., 2003a,b). Further granitoid emplacement, related to the Trans-Hudson orogen, took place from 1.85-1.81 Ga (Peterson et al., 2002).What distinguishes the Rae from the Hearne craton is the presence of greenstone belts and komatiitic flows (e.g. Berman et al., 2005).

2.2.1. The Northern Melville Peninsula

The northern (above 68^{o} latitude) Melville Peninsula features Precambrian bedrock which displays southeast to northeast trending structures, with Paleozoic sediments surrounding these crystalline basement rocks (Dredge, 2009). Archean tonalite, pyroxene gneiss, and granite exist at the heart of the Melville (Schau, 1984,1993; Dredge, 2009). The area features rocks of the Prince Albert (banded iron formations, komatiites, and mafic to ultramafic volcanics) and Penrhyn (supracrustal marble and pelitic gneiss) Groups (Scott and deKemp, 1998; Dredge, 2009). The Prince Albert Group has been metamorphosed from upper greenschist to amphibolite grade and was subjected to periods of folding, faulting, and granitoid plutonism during the formation of the Foxe Fold Belt (Schau, 1984; Scott and deKemp, 1998). The Penrhyn Group is present mostly in the southern portions of the northern Melville and is metamorphosed to amphibolite grade (Schau, 1993). Unconformably overlying the Archean basement on the Melville are Proterozoic quartzite, metamorphosed conglomerate, and sandstones which are topped by Paleozoic sandstones, limestones, and dolostones (Schau, 1984).

2.3. Orogenic Events

2.3.1. The Snowbird Tectonic Zone and Amalgamation of the Churchill Province

A first amalgamation event in the Churchill Province took place before 2.62-2.58 Ga, as plutonism of this age is present in both the Rae and Chesterfield Block but absent in the Hearne indicating that the Rae and Chesterfield Block came together before this phase of plutonism occurred (Davis et al., 2006; Berman et al., 2007). The process of amalgamation of the Rae and Hearne cratons is less certain, stemming from the controversial nature of the Snowbird Tectonic Zone (STZ), the division between the two. The STZ is a geophysical (both gravity and magnetic) anomaly which runs from Alberta in the SW to the Hudson Bay in the NE spanning approximately 2800 km in length (Berman et al., 2007). Several models exist regarding the STZ. The first is that it is a suture, a remnant from the <1.9 Ga collision of the Rae and Hearne cratons (Gibb and Walcott, 1971; Hoffman, 1988,1990; Berman et al., 2005; Berman et al., 2007). Another viewpoint is that the STZ represents an intracontinental shear zone (Hanmer, et al., 1995). A third interpretation is that within the context of a 2.55 Ga orogeny, the STZ represents the beginnings of an intracontinental rift environment (Flowers et al., 2006). Thus, depending on the interpretation of the STZ, the exact timing of the merger of the Rae and Hearne cratons varies.

2.3.2. The Arrowsmith Orogeny

Continental arc magmatism followed by a collisional orogenesis (the Arrowsmith orogeny) resulted in compression, thickening and reworking of the Churchill Province at 2.35 Ga (Berman et al., 2005). An orogenic event was indicated by several lines of evidence. Firstly, analysis of zircons from igneous rocks along the western margin of the Churchill revealed a distribution of 2.4-2.3 Ga magmatic rocks (Hartlaub et al., 2007). Next, deformation and metamorphism in the area from 2.4-2.3 Ga was taken as further evidence of a collisional event, an event which possibly featured eastward directed subduction along the western boundary of the Churchill (Berman et al., 2005; Hartlaub et al., 2007). Hartlaub et al. (2007) note that due to a lack of data, pinpointing which terranes were involved in the collisional event of the Arrowsmith orogeny is difficult; they suggest the Queen Maud Block and the Churchill Province as likely candidates.

2.3.3. The Taltson-Thelon Orogeny

The Rae craton collided with the Slave craton during the 2.0-1.9 Ga Taltson-Thelon orogeny (Hoffman, 1988). Following the collision event, the hinterland of the Rae was indented by the foreland of the Slave through crustal shortening in the Queen Maud Block and slip along the intracontinental Great Slave Lake shear zone (e.g. Hoffman, 1988). The Taltson and Thelon magmatic zones are made up of a series of 2.0-1.9 Ga granitoids extending along the Slave/Rae boundary, with the Taltson referring to the southern portion and the Thelon referring to the northern portion of this 2500 km zone (Hoffman, 1988; Bostock and van Breeman, 1994; Chacko et al., 2000). The Taltson and Thelon magmatic zones are interpreted to have formed during subduction and collision of the Slave and Rae (Ross et al., 1991; Bostock and van Breeman, 1994). The 2.4-2.0 Ga granites which intruded the Archean rocks of the Taltson magmatic zone have been interpreted as being produced during eastward directed subduction along the western boundary of the Rae craton before its collision with the Slave (Hoffman, 1990; Bostock and van Breeman, 1994). Chacko et al. (2000) suggest the Taltson magmatic zone formed in an intracrustal setting, contending that the continental arc is older, and was simply reactivated from 2.0-1.9 Ga while in the plate interior to form the granitoid bodies of the magmatic zone.

2.3.4. The Trans-Hudson Orogeny

The Trans-Hudson orogeny was a collisional event which took place from 1.85-1.83 Ga between the Churchill Province and the Superior craton in which the active continental margin resided on the Churchill (Hoffman, 1988,1990). Northward subduction of oceanic lithosphere accommodated the convergence and collision which took place during this orogeny (Hoffman, 1988). Continental volcanic arc magmatism during the Trans-Hudson orogeny resulted in the development of the Cumberland batholith, located on Baffin Island (Whalen et al., 2010). The Trans-Hudson orogenic zone is made up of plutonic, metavolcanic, and metasedimentary rocks which are subdivided into distinct belts (Hoffman, 1988).

2.4. Kimberlites of the Northern Churchill Province

There are many individual kimberlite discoveries and exploration properties in the northern Churchill. The kimberlite fields and clusters in the northern Churchill as grouped by Kjarsgaard (2007), following the terminology of Mitchell (1986), are: Aviat, Somerset Island, Brodeur Peninsula, Baffin Island, Boothia Peninsula, Wales Island, Repulse Bay, and Rankin Inlet.

Limited information is available about the Aviat kimberlite cluster. Several kimberlite pipes and dykes, which were emplaced ~558 Ma ago (Scott Smith, 2008), exist on the Aviat property. The dykes form what has been termed the Eastern Sheet Complex, which is a series of stacked, shallowly dipping kimberlite dykes each separated vertically by 10-30 m (Stornoway Diamond Corporation, 2011). The model geotherm beneath Aviat is relatively cool, corresponding to 38 mW/m^2 surface heat flow, which is conducive to diamond formation and preservation (Snyder and Grütter, 2010). Geotherms were derived by Pollack and Chapman (1977) based on the principle that there is equilibrium between surface heat flow, and heat generated by radioactive decay plus heat flowing into the base of the lithosphere. The model of Pollack and Chapman (1977) takes into account regional variations in the aforementioned paramenters. Both peridotitic and eclogitic garnets have been found in till samples on the property, indicating that diamonds of both parageneses may be present at Aviat (Besserer, 2008).

The best studied kimberlites on the Churchill Province are in the Somerset Island field which was emplaced into Archean basement during the Cretaceous (~100 Ma ago) forming a belt of kimberlitic bodies trending northeast-southwest (Schmidberger et al., 2002; Irvine et al., 2003). The emplacement age paleo-geotherm beneath Somerset Island was relatively hot (equivalent to 44 mW/m^2

surface heat flow) and not “diamond friendly” (Irvine et al., 2003). The Rankin Inlet kimberlite field exhibits Mesozoic kimberlites manifested as pipes and dykes (Zurevinski et al., 2008). Kimberlite pipes exhibit emplacement ages spanning from 225-170 Ma (Zurevinski et al., 2008) and kimberlite dykes (from a different exploration property in the Rankin Inlet region) display a more restricted emplacement age range from 214 Ma (Davis and Miller, 2001) to 196 Ma (Heaman and Kjarsgaard, 2000). A paleogeotherm based on Cretaceous kimberlite activity on the Brodeur Peninsula is also relatively hot (equivalent to 42 mW/m^2 surface heat flow) with a narrow diamond window between 1050-1100°C (Cross, 2009).

2.4.1. Exploration History at Aviat

The Aviat exploration property is a joint venture between Stornoway Diamond Corporation (90%) and Hunter Exploration Group (10%). The property is located on the northern portion of the Melville Peninsula in eastern Nunavut. The first publicly announced kimberlite discovery on the Melville Peninsula was made at Aviat in 2002 (Besserer, 2008). Since that time, 12 kimberlite bodies, including both pipes and dykes, have been discovered on the property. The Aviat kimberlites are mostly macrocrystal and of hypabyssal facies, but areas with kimberlite breccias have also been observed (Stornoway Diamond Corporation, 2011). A resource study by SRK Consulting delineated the diamond potential for Aviat as 24.1 to 40.3 million carats in 12.4 to 16.0 million tonnes of kimberlite. Till sampling, diamond drilling, mini-bulk sampling, prospecting and ground and airborne geophysical surveys have been completed on the Aviat property

(Besserer, 2008). The largest diamond found in the exploration process at Aviat thus far is 3.99 carats (Stornoway Diamond Corporation, 2011). Further bulk sampling is planned for the future (Stornoway Diamond Corporation, 2011).

References

Berman R.G., Davis W.J. and Pehrsson S. (2007) Collisional Snowbird tectonic zone resurrected: Growth of Laurentia during the 1.9 Ga accretionary phase of the Hudsonian orogeny. *Geology* **35,** 911-914.

Berman R.G., Sanborn-Barrie M., Rayner N., Carson C., Sandeman H.A. and Skulski T. (2010) Petrological and *in situ* SHRIMP geochronological constraints on the tectonometamorphic evolution of the Committee Bay belt, Rae Province, Nunavut. *Precamb. Res.* **181,** 1-20.

Berman R.G., Sanborn-Barrie M., Stern R.A. and Carson C.J. (2005) Tectonometamorphism at *ca*. 2.35 and 1.85 Ga in the Rae Domain, Western Churchill Prince, Nunavut, Canada: Insights from structural, metamorphic and *in situ* geochronological analysis of the southwestern Committee Bay Belt. *Can. Mineral.* **43,** 409-442.

Besserer D.J. (2008) Technical report for the Aviat Property Melville Peninsula, Nunavut, Canada. 1-61.

Bostock H.H. and van Breeman O. (1994) Ages of detrital and metamorphic zircons and monazites from a pre-Taltson magmatic zone basin at the western margin of the Rae Province. *Can. J. Earth Sci.* **31,** 1353-1364.

Chacko T., De S.K., Creaser R.A. and Muehlenbachs K. (2000) Tectonic setting of the Taltson magmatic zone at 1.9-2.0 Ga: a granitoid-based perspective. *Can. J. Earth Sci.* **37,** 1597-1609.

Cross J. (2009) The diamond potential of the Tuwawi kimberlite (Baffin Island, Nunavut). Undergraduate thesis, University of British Columbia, Vancouver, BC.

Davis W. J. and Miller A. R. (2001) A late Triassic Rb-Sr phlogopite isochron age for a kimberlite dyke from the Rankin Inlet area, Nunavut. Geol. Surv. Can. Curr. Res. **2001-F3**, 1-12.

Davis, W.J., Hanmer, S., Tella, S., Sandeman, H., Ryan, J.J. (2006) U-Pb Geochonology of the MacQuoid supracrustal belt and Cross Bay plutonic complex: Key components of the northwestern Hearne subdomain, Western Churchill Province, Nunavut, Canada. *Precamb. Res*. **145**, 53-80.

Dredge L.A. (2009) Till geochemistry, and results of lithological, carbonate and textural analyses, northern Melville Peninsula, Nunavut (NTS 47A,B,C,D). Open File **6285,** 1-11.

Flowers, R.M., Bowring, S.A., Williams, M.L. (2006) Timescales and significance of high-pressure, high-temperature metamorphism and mafic dike anatexis, Snowbird tectonic zone, Canada. *Contrib. Mineral. Petrol*. **151**, 558-581.

Gibb R.A. and Walcott R.I. (1971) A Precambrian suture in the Canadian shield. *Earth Planet. Sci. Lett.* **10,** 417-422.

Hanmer, S., Williams, M., Kopf, C. (1995) Striding-Athabasca mylonite zone: implications for the Archean and Early Proterozoic tectonics of the western Canadian Shield. *Can. J. Earth Sci*. **32**, 178-196.

Hartlaub R.P., Chacko T., Heaman L.M., Creaser R.A., Ashton K.E. and Simonetti A. (2005) Ancient (Meso- to Paleoarchean) crust in the Rae Province, Canada: Evidence from Sm-Nd and U-Pb constraints. *Precamb Res.* **141,** 137-153.

Hartlaub R.P., Heaman L.M., Chacko T. and Ashton K.E. (2007) Circa 2.3-Ga magmatism of the Arrowsmith Orogeny, Uranium City Region, Western Churchill Craton, Canada. *J. Geol.* **115,** 181-195.

Heaman L.M. and Kjarsgaard B.A. (2000) Timing of eastern North American kimberlite magmatism: continental extension of the Great Meteor Hotspot Track? *Earth Planet. Sci. Lett.* **178,** 253-268.

Hoffman P.F. (1990) Subdivision of the Churchill Province and extent of the Trans-Hudson Orogen. *In* The Early Proterozoic Trans-Hudson Orogen of North America (eds. J. F. Lewry and M. R. Stauffer). Geological Association of Canada Special Paper, 15-38.

Hoffman P.F. (1988) United plates of America, the birth of a craton: Early Proterozoic assembly and growth of Laurentia. *Ann. Rev. Planet. Sci.* **16,** 543-603.

Irvine G.J., Pearson G., Kjarsgaard B.A., Carlson R.W., Kopylova M.G. and Dreibus G. (2003) A Re-Os isotope and PGE study of kimberlite-derived peridotite xenoliths from Somerset Island and a comparison to the Slave and Kaapvaal cratons. *Lithos* **71,** 461-488.

Kjarsgaard B.A. (2007) Kimberlite diamond deposits. *In* Mineral Deposits of Canada: A Synthesis of Major Deposit Types, District Metallogeny, the Evolution of Geological Provinces, and Exploration Methods (ed. W. D. Goodfellow). Geological Association of Canada, Mineral Deposits Division, 245-272.

Mitchell R.H. (1986) *Kimberlites: mineralogy, geochemistry, and petrology.* Plenum Press, New York.

Peterson, T.D., Van Breeman, O., Sandeman, H., and Cousens, B. (2002) Proterozoic (1.85-1.75 Ga) igneous suites of the Western Churchill Province: granitoid and ultrapotassic magmatism in a reworked Archean hinterland. *Precamb. Res*. **119**, 73-100.

Pollack, H.N. and Chapman, D.S. (1977) On the regional variation of heat flow, geotherms, and lithospheric thickness. *Tectonophysics*, **38**, 279-296.

Ross G.M., Parrish R.R., Villeneuve M.E. and Bowring S.A. (1991) Geophysics and geochronology of the crystalline basement of the Alberta Basin, western Canada. *Can. J. Earth Sci.* **28,** 512-522.

Schau M. (1993) Northern Melville Peninsula. Geol. Surv. Can. Open File **2594** (scale: 1:500000**).**

Schau M. (1984) Northern Melville Peninsula. Geol. Surv. Can. Open File **1046** (scale: 1:500000**).**

Schmidberger S.S., Simonetti A., Francis D. and Gariepy C. (2002) Probing Archean lithosphere using the Lu-Hf isotope systematics of peridotite xenoliths from Somerset Island kimberlites, Canada. *Earth Planet. Sci. Lett.* **197,** 245-259.

Scott Smith B.H. (2008) Canadian kimberlites: Geological characteristics relevant to emplacement. *J. Volcanol. Geotherm. Res.* **174,** 9-19.

Scott D.J. and deKemp E.A. (1998) Bedrock geology compilation, northern Baffin Island and northern Melville Peninsula, Northwest Territories. Geol. Surv. Can. Open File **3633,** 3 sheets.

Skulski T., Sanborn-Barrie M. and Sandeman H. (2003b) Geology, Walker Lake and Arrowsmith River area, Nunavut. Geol. Surv. Can. Open File, **3777.**

Skulski T., Sandeman H., Sanborn-Barrie M., MacHattie T., Young M., Carson C., Berman R., Brown J., Rayner N., Panagapko D., Byrne D. and Deyell C. (2003a) Bedrock geology of the Ellice Hills map area and new constraints on the regional geology of the Committee Bay area, Nunavut. Geol. Surv. Can. Curr. Res. **C22,** 1-11.

Snyder D.B. and Grütter H.S. (2010) Lithoprobe's impact on the Canadian diamond-exploration industry. *Can. J. Earth Sci.* **47,** 783-800.

Stornoway Diamond Corporation (2011), http://www.stornowaydiamonds.com/advanced/aviat (accessed February 1, 2011).

Whalen J.B., Wodicka N., Taylor B.E. and Jackson G.D. (2010) Cumberland batholith, Trans-Hudson Orogen, Canada: Petrogenesis and implications for Paleoproterozoic crustal and orogenic processes. *Lithos* **117,** 99-118.

Zurevinski S.E., Heaman L.M., Creaser R.A. and Strand P. (2008) The Churchill kimberlite field, Nunavut, Canada: petrography, mineral chemistry, and geochronology. *Can. J. Earth Sci.* **45,** 1039-1059.

Chapter 3: Aviat Diamonds: A Window Into The Deep Lithospheric Mantle Beneath The Northern Churchill Province

3.1. Introduction

Geochemical characterization of diamonds and their host kimberlites can yield valuable information about the underlying subcontinental lithospheric mantle. It has been demonstrated that for each region and each kimberlite there are unique carbon and nitrogen signatures due to distinct compositions of source fluids and rocks (Galimov, 1991). For the northern Churchill Province, very little diamond data, and consequently very limited information on the sublithospheric mantle is available despite this area having proven highly prospective for diamonds in recent years. To address this lack of data for the northern Churchill Province, diamonds from the Aviat kimberlites have been analyzed for their carbon isotopic composition, nitrogen concentration, and nitrogen aggregation state. The carbon isotopic composition of diamond can help to delineate source parageneses in the lithospheric mantle of the northern Churchill. In combination, nitrogen concentration and aggregation data allow us to constrain the mantle residence history of diamonds, and by extension, to interpret the thermal history of the lithospheric mantle in the region. Together, these data provide the first insights into the origin of diamonds and the evolution of their mantle source regions in this poorly studied region of the Canadian Shield.

For this study, Stornoway Diamond Corporation provided a suite of diamonds from the Aviat kimberlite cluster, located on the northern portion of the Melville Peninsula in northeastern Nunavut. The area is part of the Rae craton within the Churchill Province. The Aviat kimberlites were emplaced ~558 Ma ago (Scott Smith, 2008) with a diamond friendly "cool" conductive mantle geotherm equivalent to 38 mW/m^2 surface heat flow (Pollack and Chapman, 1977; Stornoway Diamond Corporation, 2006; Snyder and Grütter, 2010). This was determined by analyzing down-ice tills on the Aviat property for their compositions, and performing xenolith or clinopyroxene thermobarometry which was then referenced to the model geotherms of Pollack and Chapman (1977) (Snyder and Grütter, 2010).

3.2. Regional Geologic Context

The Churchill Province is divided into the Rae (NW) and Hearne (SE) cratons by the Snowbird tectonic zone (Gibb and Walcott, 1971; Hoffman, 1988,1990; Berman et al., 2005). The Rae craton, which is host to the Aviat kimberlites, is largely made up of Archean granitoid rocks and supracrustal belts as well as Paleoproterozoic metasedimentary rocks predominantly of amphibolite facies (Skulski et al., 2003a,b; Berman et al., 2010).

The amalgamated Churchill Province collided with the Slave and Superior Provinces during the 2.0-1.9 Ga Taltson-Thelon and 1.85-1.83 Ga Trans-Hudson orogenies, respectively (Hoffman, 1990; Hartlaub et al., 2007). The bulk of the Churchill Province underwent greenschist to amphibolite facies metamorphism connected to the Trans-Hudson orogeny (Hoffman, 1990). During the Trans-Hudson orogeny northward directed subduction took place (Hoffman, 1988).

The region around the Melville Peninsula was subject to compression resulting in crustal thickening during two orogenic events at 2.35 Ga and 1.85 Ga

(Berman et al., 2005). The former is thought to be related to a collisional event which followed or was concurrent with continental arc magmatism occurring on the western boundary of the Rae craton (Berman et al., 2005; Hartlaub et al., 2007). This 2.35 Ga event has been referred to as the Arrowsmith orogeny (Berman et al., 2005; Hartlaub et al., 2007). The tectonometamorphic event at 1.85 Ga has been associated with a 1.88-1.86 Ga accretionary stage of the Trans-Hudson orogeny (Hoffman, 1990; Berman et al., 2005).

3.3. Samples

3.3.1. Diamonds

In 2008, bulk sampling of the AV2 and AV6 kimberlites (which represent opposite ends of the Eastern Sheet Complex) was conducted by Stornoway Diamond Corporation (Figure 3-1). The AV2 sample had a dry weight of 148.3 tonnes and an estimated diamond content of 144 carats per hundred tonnes (cpht) based on stones of +1 DTC sieve size, i.e. retained on a sieve with circular apertures of 1.092mm (Stornoway Diamond Corporation, 2009). The AV6 sample had a dry weight of 42.7 tonnes and an estimated diamond content of 210 cpht based on stones retained on +1 DTC sieve size (Stornoway Diamond Corporation, 2009).

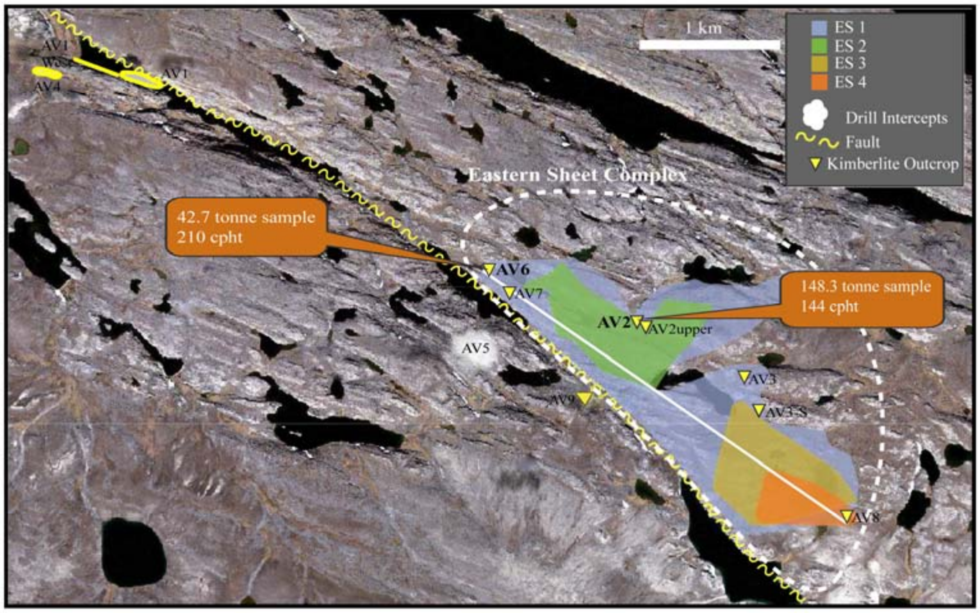

Figure 3-1. Aviat kimberlite location map.
Modified from Stornoway (2011), map delineating kimberlite outcrops and drill intersections on the Aviat exploration property.

These kimberlite samples were processed using dense media separation making use of both an X-Ray sorter and a grease table to extract the entrained diamonds (Stornoway Diamond Corporation, 2009). Two hundred diamonds below 1.1mm in diameter from both the AV2 and AV6 samples were obtained for this study. Of these, 70, ranging in length of the longest axis from 0.8-1.9 mm, were randomly selected for analyses. Weights of the diamonds analyzed range from 0.1-2.4 mg (Table 3-1).

In addition to the AV2 and AV6 diamond suites, a small eclogite sample from the AV6 kimberlite was provided by Stornoway, along with one diamond (AV6E) which had been extracted from the eclogite. This is the only diamond in this study of known source paragenesis.

3.4. Methods

3.4.1. Fourier Transform Infrared (FTIR) Nitrogen Analyses

Samples were analyzed for their nitrogen content and aggregation state using a Thermo-Nicolet Nexus 470 Fourier Transform Infrared (FTIR) spectrometer joined with a Continuum IR microscope outfitted with a KBr beam splitter. A constant environment was maintained in the instrument by purging it with a dry nitrogen-oxygen mixture. Sample spectra (4000-650 cm^{-1}) were collected for 200 cycles. After base line correction and conversion to absorption coefficient (normalization to 1cm sample thickness), spectra were deconvoluted to determine nitrogen content and aggregation state. Lower detection limits range from 5-15 atomic ppm (at.ppm), with errors typically in the range of 5-10% of the total nitrogen concentration. The exact values of the detection limits and errors are strongly dependent upon the quality of the samples, (i.e. sample shape and state of resorption).

Where present in the spectra, the intensities of the platelet peak and the hydrogen related peak at 3107 cm^{-1} were measured by integrating the peak area using the OMNIC software.

3.4.2. Conventional Carbon Isotopic Analyses

Ten samples with masses >0.5 mg were analyzed for their carbon isotopic compositions using sealed tube combustion and subsequent gas flow mass spectrometry. Samples (1.1 mg-2.4 mg) were loaded into silica glass tubes together with 1-2 grams of copper oxide as an oxygen donor. Tubes were then evacuated, sealed with a blowtorch, and loaded into a furnace at 980°C for approximately 12 hours to combust the diamonds. Following combustion, the sample gas was analyzed using a Finnigan Mat 252 dual inlet mass spectrometer. Analyses are reported as $\delta^{13}C$ relative to the Vienna Pee Dee Belemnite (VPDB) standard. Total analytical precision was determined to be better than ±0.1‰ based on repeat analyses of multiple fragments of a single diamond (Donnelly, 2006).

3.4.3. SIMS Carbon Isotope and Nitrogen Analyses

Sixty-one samples were analyzed for their carbon isotopic composition using secondary ion mass spectrometry (SIMS) on a Cameca IMS1280 ion microprobe at the Canadian Centre for Isotopic Microanalysis (CCIM) at the University of Alberta. The diamonds were embedded in epoxy and polished in two steps using metal plates embedded with 15 micron and 6 micron diamond grit. The samples were then analyzed for their cathodoluminescence (CL) patterns using a Zeiss EVO 15 scanning electron microscope equipped with both Gatan Chroma and Robinson wide spectrum CL detectors at CCIM. Following CL characterization, the epoxy pucks were cored out to yield disks of embedded diamonds less than 0.5 cm in diameter and approximately 3 mm in thickness. These epoxy disks were pressed into indium around a centrally positioned diamond standard with the maximum distance between the samples and the standard being <1.0 cm. The finished indium mounts were coated with a 3 nm layer of gold before analysis. The standard used for analysis - 1808/16L-2(i), (CCIM standards S0011B and S0011C) - is an isotopically homogeneous section through a {100} growth sector of a synthetic diamond provided through David Fisher, The Diamond Trading Company, Maidenhead, UK. Conventional carbon isotopic analysis of the standard was performed by Pierre Cartigny (IPG, Paris) and yielded a $\delta^{13}C$ value of -22.576 ± 0.017‰. The standard was analyzed after every five analyses of unknowns, and the values for the unknowns were corrected to account for instrumental drift. The standard error (2σ) for individual point analyses ranged from 0.1‰ to 0.2‰. A single sample, left unpolished due to its small size, has a larger 2σ error of 0.3‰.

In a second step, the sixty-one samples were analyzed for their nitrogen content at the exact same points analyzed for $\delta^{13}C$. A different slab - 1808/16L-2(ii) (CCIM standard S0011G) – of the same diamond standard with a nitrogen content of 470 at.ppm (determined in house using FTIR) across the compositionally homogeneous {100} sector was used. A 4 nA Cs beam was employed for the analyses. Two Faraday cups simultaneously collected ^{12}C-^{14}N ions and ^{12}C-^{12}C ions, from which total N content was calculated in ppm. For samples with low count rates (a cut off of 5×10^4 cts/sec was used) an electron multiplier was utilized. The relative uncertainty associated with these analyses is ± 10-11% and is mainly due to the large uncertainty of FTIR analyses, which established the standard composition.

3.4.4. Electron Microprobe Analysis of Garnet

Ten garnet crystals were extracted from a diamondiferous eclogite sample, embedded in Araldite® epoxy resin within 5 mm brass rings and polished for analysis. The garnets were analyzed for their major element compositions using wavelength dispersive spectrometry (WDS) on a Cameca SX100 electron microprobe at the University of Alberta. Each of the 10 garnets was analyzed at two separate points: at the centre and towards the rim.

3.5. Results

3.5.1. Color and Morphology

The Aviat diamonds display a range of colors (Table 3-1) including colorless, brown, grey, and green with grey being dominant (39%) followed by colorless (28%). Diamonds were categorized into various morphological groups (octahedral or dodecahedral) based on their shape and surface features. Diamonds which did not exhibit a shape or surface features associated with either morphology were classified as irregular. For diamonds which displayed attributes of both octahedral (o) and dodecahedral (d) morphology an o-d or d-o classification was used, the second letter denoting the dominant morphology. The majority of the diamonds are irregular in shape (51%) followed by dodecahedral (24%), octahedral (20%), and mixed octahedral-dodecahedral morphologies (5%). A large proportion of the diamonds are fragments (38% of the 71 diamond set). In addition, one twin, (a macle characterized by a herringbone pattern outlining the compositional plane) and two aggregates (two or more intergrown diamonds) were observed in the sample set. There are no cubic diamonds present.

The octahedral diamonds in this sample set display any combination of the following characteristics: stacked growth layering, negative trigons, and shallow resorption pits. Some of the dodecahedral stones display hillocks and shallow pits. Plastic deformation lines are apparent on some of the dodecahedral faces.

Table 3-1 Physical and Chemical Characteristics of Aviat Diamonds

Sample	Weight	Color	Morphology	P.D.	δ^{13}C	N	Average N	%B	Type	3107 cm^{-1} Peak	Integrated Platelet
	(mg)				(‰)	(at.ppm)	(at.ppm)			(cm^{-2})	(cm^{-2})
AV2-010	0.9	c	o-frag	n	-5.8*	338	N/A	36	IaAB	22.82	
AV2-012	1.3	y	d-o	n	-5.3*	928	N/A	36	IaAB	20.24	
AV2-014	2.4	g-b	d	y	-3.5*	487	N/A	33	IaAB		91.74
AV2-016	1.1	b	d	y	-6.0*	1467	N/A	34	IaAB	108.63	22.00
AV2-017	1.1	c	o	y	-5.58	325	N/A	37	IaAB	13.54	65.56
AV2-021	0.9	g	d-o frag	y	-4.89	326	406	54	IaAB	7.44	106.45
AV2-022	1.5	g	d-o frag	y	-5.06	450	689	18	IaAB	4.73	6.60
AV2-023	1.7	c to lb	o frag	y	-4.13	13	6	60	IaAB	1.40	
AV2-024	2.0	lgn	d	y	-4.73	687	N/A	32	IaAB	3.81	75.13
AV2-026	2.5	c	d	y	-3.54	676	597	50	IaAB	5.17	235.86
AV2-027	2.7	c to gn	d	y	-5.31	557	N/A	0	IaA	3.37	
AV2-028	2.5	lg	d	y	-5.55	899	630	56	IaAB	3.94	
AV2-029	1.4	b	o	y	-3.65	899	1072	56	IaAB	27.98	251.89
AV2-031	1.1	gn	o agg frag	y	-4.15	643	768	12	IaAB	4.94	
AV2-033	0.6	lb	d frag	y	-6.00	918	878	31	IaAB	13.36	
AV2-044	0.7	lb	o	y	-6.97	1098	1015	19	IaAB	20.63	7.88
AV2-050	0.4	g-b	o frag	y	-6.00	511	665	4	IaA	25.85	
AV2-072	0.3	g	i frag	y	-5.91	880	872	37	IaAB	8.54	
AV2-084	0.7	c	i	n	-7.00	753	837	11	IaAB	6.91	
AV2-093	0.7	g	i	y	-4.50	841	796	19	IaAB	25.30	24.61
AV2-107	0.8	lb	i	y	-5.03	740	795	7	IaA	8.71	
AV2-111	0.7	b-g	i	y	-4.77	210	754	10	IaA	8.46	4.06
AV2-117	0.8	gn	o-d	y	-4.70	664	432	43	IaAB	22.13	185.70
AV2-131	0.5	c	o	n	-4.80	699	717	0	IaA	6.35	
AV2-144	0.7	g	i	y	-7.00	288	253	23	IaAB	10.08	45.58
AV2-155	0.4	c	i frag	n	-16.43	18	31	0	IaA	1.21	
AV2-168	0.8	g	i frag	y	-7.15	909	1352	4	IaA	33.53	
AV2-179	0.8	g	d	y	-5.75	509	570	8	IaA	6.52	10.61
AV2-180	0.8	g	i	n	-6.45	1039	442	6	IaA	12.32	
AV2-189	0.5	b	i agg	y	-5.31	630	515	22	IaAB	5.54	
AV2-193	0.5	g to gn	i	n	-6.44	636	1091	13	IaAB	12.92	33.90
AV2-194	0.5	b	i	y	-5.16	431	475	10	IaAB	13.77	29.48
AV2-196	0.2	g	i	n	-5.55	554	721	5	IaA	12.26	12.12
AV6-004	1.9	lgn	d	y	-3.33	242	529	48	IaAB	17.70	92.50
AV6-005	1.6	lg	d	y	-4.1*	163	N/A	45	IaAB		
AV6-006	1.2mg	b	d	y	-29.7*	147	N/A	98	IaB	16.06	
AV6-012	1.3	c	d	y	-5.3*	747	N/A	29	IaAB	1.33	100.48
AV6-015	1.5	c	d	y	-5.4*	595	N/A	0	IaA	2.83	
AV6-016	1.2	c	o -twin	y	-5.8*	796	N/A	6	IaA	10.56	
AV6-017	1.2	lg	d	y	-5.7*	905	N/A	10	IaA	9.78	
AV6-024	1.3	lg	d	y	-4.37	667	301	28	IaAB	6.61	39.70
AV6-032	1.2	c	d frag	y	-4.19	1042	391	15	IaAB	2.81	140.72
AV6-036	0.8	g	i	y	-1.68	322	358	55	IaAB	4.53	117.11
AV6-040	0.8	c	i frag	y	-4.37	681	550	6	IaA	7.48	
AV6-054	0.3	g	o frag	n	-3.25	957	1004	11	IaAB	10.15	
AV6-068	0.5	lb	i frag	y	-4.37	45	564	7	IaA	17.54	
AV6-107	0.7	lb	i	y	-3.80	198	320	0	IaA		
AV6-111	0.6	g	o frag	n	-11.47	524	558	52	IaAB	25.64	72.34
AV6-115	0.4	g	i frag	n	-16.36	1064	459	32	IaAB	70.73	10.53
AV6-124	0.1	g	i	n	-3.84	543	287	15	IaAB	16.54	18.77
AV6-131	0.7	b	i frag	y	-5.15	709	716	15	IaAB	15.11	
AV6-133	0.5	b	i frag	y	-4.17	352	596	37	IaAB	6.52	90.92
AV6-134	0.6	b	i	y	-2.90	336	339	26	IaAB	26.14	71.65
AV6-136	0.7	g	i	n	-4.35	693	745	12	IaAB		
AV6-138	0.5	lb	i	y	-6.14	671	735	0	IaA	5.61	
AV6-142	0.8	c	i frag	n	-6.06	775	877	3	IaA	8.86	
AV6-148	0.7	c	i frag	n	-5.44	953	828	19	IaAB	4.80	53.71
AV6-155	0.6	g	i frag	n	-6.17	687	557	29	IaAB	11.02	
AV6-168	0.7	g-b	oct frag	y	-5.50	679	253	2	IaA	19.36	16.65
AV6-169	0.6	b	oct frag	y	-4.88	420	697	0	IaA	5.05	7.47
AV6-170	0.8	c	i frag	n	-5.22	504	530	1	IaA		
AV6-171	0.8	c	i frag	n	-5.35	689	596	13	IaAB	6.98	7.64
AV6-172	0.4	g	i	n	-5.88	680	732	9	IaA	6.05	
AV6-173	0.6	b	i	y	-5.55	735	414	4	IaA	11.34	
AV6-175	0.5	g	i frag	y	-5.24	1096	1035	5	IaA	22.08	
AV6-176	0.7	b to c	i	y	-5.01	416	587	49	IaAB	41.82	109.85
AV6-177	0.6	c	o frag	n	-5.72	451	1034	6	IaA	2.84	
AV6-181	0.6	c	i	y	-6.09	182	673	19	IaAB	11.93	15.84
AV6-183	0.6	g	d	y	-5.24	502	424	17	IaAB		
AV6-190	0.8	g	i	y	-4.81	439	673	18	IaAB	11.01	36.35
AV6-E	0.1	c	o	n	-4.95	749	582	7	IaA	60.39	14.67

Table 3-1. Physical and chemical characteristics of Aviat diamonds
PD = plastic deformation, g=grey, gn=green, l=light, c=colorless, b=brown, o=octahedral, d=dodecahedral, frag=fragment, i=irregular, agg=aggregate. 3107 cm^{-1} Peak refers to the H-related peak area. Integrated platelet refers to the area beneath the peak at approximately 1350-1380 cm^{-1}. Blank spaces in the hydrogen and platelet peak columns indicate that no peak was detected. Nitrogen concentrations were obtained by FTIR and δ^{13}C values are average SIMS values or values obtained by conventional methods denoted with a *. Average N refers to SIMS point analyses averaged to one value for the whole diamond, N/A = not available (e.g. nitrogen aggregation state for diamonds only analyzed by SIMS.

3.5.2. Inclusions in Diamond

Many of the 71 diamonds analyzed for their carbon isotopic composition and nitrogen content and aggregation state displayed small, generally near-surface graphite inclusions, but no other mineral inclusions were observed.

3.5.3. FTIR Spectroscopy

The nitrogen content of Aviat diamonds ranges from 13 to 1467 at.ppm. Nitrogen aggregation in diamond progresses from single atoms (C centre), to pairs of nitrogen atoms (A centre), through to rings of four nitrogen atoms surrounding a vacancy (B centre) (Evans et al., 1995). With rare exceptions, the transition from C to A centre is completed in monocrystalline, mantle derived diamonds (e.g. Gurney, 1989) and accordingly, nitrogen is not present in C centres in the current sample set. Nitrogen aggregation is quantified as %B (100B/[A+B]) which expresses how much nitrogen is contained in the A and B centres. Type Ia diamonds (i.e. diamonds containing only aggregated nitrogen) are subdivided into several categories based on the relative abundance of the B component: Type IaA = 0-10 %B, Type IaAB = 10-90 %B, Type IaB = 90-100 %B. For Aviat diamonds, the relative proportion of the B component ranges from 0% to 98%, with the majority classifying as Type IaAB (62%), followed by Type IaA (37%), and a minor Type IaB population (1%).

Increasing aggregation from A to B centres is accompanied by formation of "platelets", nm to μm sized planar defects in the diamond lattice not related to nitrogen, with an associated sharp absorption peak in the range 1358-1378 cm^{-1} (Sobolev et al., 1968). Of the Type IaAB diamonds studied here, 34% have no platelet peak.

The majority of the Aviat FTIR spectra exhibit one or more absorption peaks at 3107 cm^{-1}, 2786 cm^{-1} and 1404 cm^{-1}; a group of related peaks which are the result of the bending and stretching of the vinylidene group ($C=CH_2$) in diamond (Charette, 1959; Runciman and Carter, 1971; Woods and Collins, 1983; Davies et al., 1984). A peak at 3237 cm^{-1} was also present in some Aviat diamonds; this peak is C-H related, but is not related to the bending and stretching of the vinylidene group like the aforementioned peaks (Charette, 1959; Fritsch et al., 2007). Surface contamination was excluded as a cause since the absorption peaks persisted through repeated cleaning with various agents including eucalyptus oil, petrol-ether, HNO_3, and HF. The Aviat diamonds overall are high in hydrogen; one diamond classifies as "hydrogen-rich" as defined by Fritsch et al. (2007) in that the hydrogen absorption peak at 3107 cm^{-1} is higher than the diamond peak at 2450 cm^{-1}. The area underneath the hydrogen related absorption peak at 3107 cm^{-1} is reported in Table 3-1.

Some of the Aviat diamonds display one or more peaks at 2337 cm^{-1} (nine of 71 diamonds), 1100 cm^{-1} (13 diamonds), 1000 cm^{-1} (six diamonds) and 874 cm^{-1} (two diamonds) related to various molecular species. The peak at 2337 cm^{-1} is likely due to CO_2, the exact position of the peak varying slightly with concentration (Rudolph et al., 2006; Kopylova et al., 2010). As the Aviat diamonds are rich in nitrogen, the peaks at 1100 cm^{-1} and 1000 cm^{-1} are likely due to slight shifts of the 1013 cm^{-1} and 1172 cm^{-1} peaks which are produced by the nitrogen B centre (Iakoubovskii and Adriaenssens, 2002; Thongnopkun and Ekgasit, 2005). The peak at 874 cm^{-1} is likely the same as a peak at 880 cm^{-1} described by Chrenko et al. (1967) which is attributed to carbonate.

3.5.4. SIMS Nitrogen Analyses

Point analyses for nitrogen content yielded values ranging from <1 to 1724 at.ppm, a larger range than obtained by FTIR analyses (13 to 1467 at.ppm). Average nitrogen contents for each diamond range from 6 to 1353 at.ppm, which compares very well with the FTIR data.

3.5.5. Bulk Carbon Isotopic Analyses

Ten microdiamonds were analyzed conventionally for their $\delta^{13}C$ values producing nine values ranging from -6.0 to -3.5‰ as well as one value of -29.7‰. A plot combining the conventional bulk analyses and SIMS individual point analyses of $\delta^{13}C$ is provided in Figure 3-2. The range of $\delta^{13}C$ is broadly similar to that of the Slave craton which exhibits a mode at -5‰ and a string of more negative values (e.g. Stachel et al., 2009).

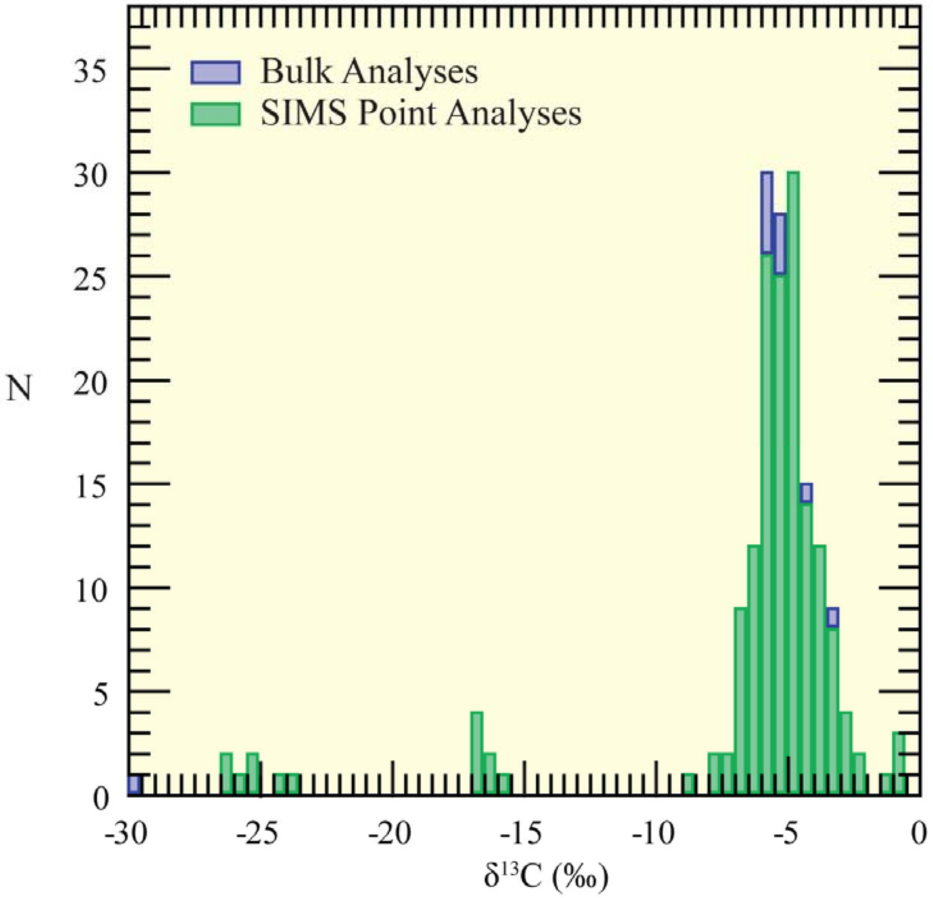

Figure 3-2. Histogram of δ^{13}C values for Aviat diamonds.
This plot reveals a pronounced mode at -5‰ with several negative outliers. SIMS values are individual point analyses (not diamond averages), bulk analyses refer to δ^{13}C values obtained conventionally through sealed tube combustion.

3.5.6. Cathodoluminescence and SIMS

Due to mounting and polishing procedures used (see above), the studied sections through the Aviat diamonds are oriented in random directions and generally, crystal cores were not exposed. Consequently, many of the cathodoluminescence images do not show systematic growth zonations but appear artificially complex. A number of CL images, where simple core rim zonations can be identified, are displayed along with their corresponding δ^{13}C and nitrogen analyses in Figure 3-3.

Two trends in carbon isotopic composition were observed in zoned crystals: (1.) several crystals have cores with highly negative $\delta^{13}C$ values and rim compositions around -5‰, with evidence for resorption occurring between the two growth stages (Figure 3-3f-h). This trend of increasing $\delta^{13}C$ from core to rim can also be much more subdued (Figure 3-3e). (2.) Several crystals display core compositions near -5‰ and rims with slightly more negative $\delta^{13}C$ values (0.7-2.0‰ difference), again with evidence for resorption in between (Figure 3-3a-d). No correlation is observed between $\delta^{13}C$ values and nitrogen content and aggregation state.

As multiple points were analyzed on each diamond (all individual points are shown in Fig. 3-2), these values were averaged to obtain a single $\delta^{13}C$ value for each diamond for Table 3-1. Point analyses range from -26.2‰ to -0.7‰ whilst the averaged $\delta^{13}C$ values fall between -16.4 to -2.9‰.

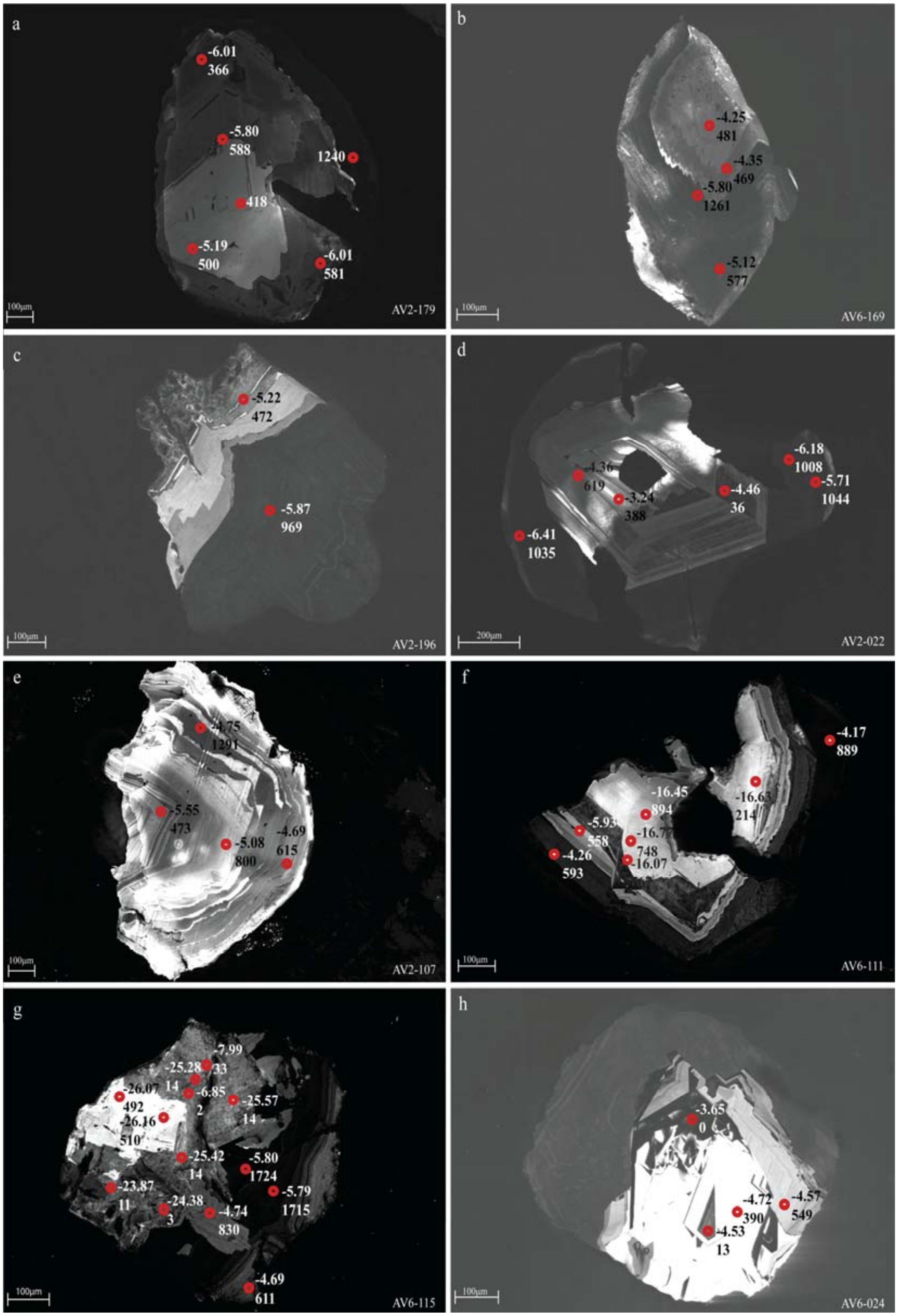

Figure 3-3. δ^{13}C values and nitrogen contents for zoned Aviat diamonds with discernable growth directions.

Nitrogen content (in at.ppm) always appears below the δ^{13}C value (in ‰). Diamonds a-d become isotopically lighter at the rim whereas diamonds e-h become isotopically heavier towards the rim. Evidence for resorption between different growth layers indicates multiple

growth events. Diamonds g and h demonstrate a disconnect between variations in $\delta^{13}C$ and nitrogen content.

3.5.7. Garnet Chemistry

Examining the Cr_2O_3 and CaO contents of the garnet xenolith crystals, all of the analyses fall within the field of low-Ca eclogitic (G4) garnet with Cr_2O_3 values <<1 wt% and CaO values between 2 and 6 wt% (Table 3-2). All of the garnets have Na_2O values >0.07 wt%, the threshold value for enhanced diamond potential (Gurney, 1984; Gurney et al., 1993), consistent with the observed presence of diamond within the sample.

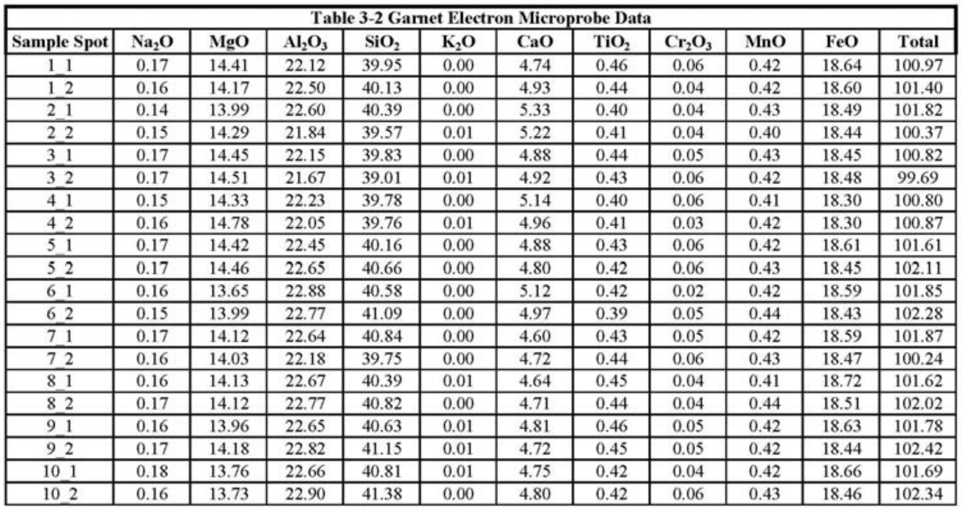

Table 3-2 Garnet Electron Microprobe Data

Sample Spot	Na_2O	MgO	Al_2O_3	SiO_2	K_2O	CaO	TiO_2	Cr_2O_3	MnO	FeO	Total
1_1	0.17	14.41	22.12	39.95	0.00	4.74	0.46	0.06	0.42	18.64	100.97
1_2	0.16	14.17	22.50	40.13	0.00	4.93	0.44	0.04	0.42	18.60	101.40
2_1	0.14	13.99	22.60	40.39	0.00	5.33	0.40	0.04	0.43	18.49	101.82
2_2	0.15	14.29	21.84	39.57	0.01	5.22	0.41	0.04	0.40	18.44	100.37
3_1	0.17	14.45	22.15	39.83	0.00	4.88	0.44	0.05	0.43	18.45	100.82
3_2	0.17	14.51	21.67	39.01	0.01	4.92	0.43	0.06	0.42	18.48	99.69
4_1	0.15	14.33	22.23	39.78	0.00	5.14	0.40	0.06	0.41	18.30	100.80
4_2	0.16	14.78	22.05	39.76	0.01	4.96	0.41	0.03	0.42	18.30	100.87
5_1	0.17	14.42	22.45	40.16	0.00	4.88	0.43	0.06	0.42	18.61	101.61
5_2	0.17	14.46	22.65	40.66	0.00	4.80	0.42	0.06	0.43	18.45	102.11
6_1	0.16	13.65	22.88	40.58	0.00	5.12	0.42	0.02	0.42	18.59	101.85
6_2	0.15	13.99	22.77	41.09	0.00	4.97	0.39	0.05	0.44	18.43	102.28
7_1	0.17	14.12	22.64	40.84	0.00	4.60	0.43	0.05	0.42	18.59	101.87
7_2	0.16	14.03	22.18	39.75	0.00	4.72	0.44	0.06	0.43	18.47	100.24
8_1	0.16	14.13	22.67	40.39	0.01	4.64	0.45	0.04	0.41	18.72	101.62
8_2	0.17	14.12	22.77	40.82	0.00	4.71	0.44	0.04	0.44	18.51	102.02
9_1	0.16	13.96	22.65	40.63	0.01	4.81	0.46	0.05	0.42	18.63	101.78
9_2	0.17	14.18	22.82	41.15	0.01	4.72	0.45	0.05	0.42	18.44	102.42
10_1	0.18	13.76	22.66	40.81	0.01	4.75	0.42	0.04	0.42	18.66	101.69
10_2	0.16	13.73	22.90	41.38	0.00	4.80	0.42	0.06	0.43	18.46	102.34

Table 3-2. Garnet Electron Microprobe Data
Garnets were extracted from an eclogite xenolith from Aviat. Sample spot numbers X_1 indicate analyses from the centre of the crystals and X_2 indicate analyses from the crystal rims.

3.6. Discussion

3.6.1. Source Parageneses of Aviat Diamonds

Compiling both conventional and SIMS carbon isotopic analyses, the Aviat diamonds display a pronounced mode at -5‰, with clusters of outliers from -15.5 to -17‰, -23.5 to -26.5‰, and a single outlier at -29‰ (Figure 3-2). In total, 14 point analyses (representing three diamonds) and one bulk diamond analysis fall below a $\delta^{13}C$ of -10‰ (Figure 3-2). Peridotitic diamonds have $\delta^{13}C$ values around -5‰, with the bulk of the values lying from -10 to -1‰ (Galimov, 1991; Kirkley, et al., 1991). Stachel et al. (2009) noted that only 1.3% of inclusion bearing peridotitic diamonds worldwide have $\delta^{13}C$ values which fall below -10‰. Eclogitic (and some rare websteritic) diamonds, however, may display a much wider range of values (Sobolev and Sobolev, 1980), and therefore, the occurrence of several strongly ^{13}C depleted diamonds is taken as evidence for the presence of an eclogitic diamond population at Aviat, consistent with the observation of a diamondiferous eclogite xenolith.

The pronounced mode in $\delta^{13}C$ values around -5‰ is common for both peridotitic and eclogitic diamonds (e.g. Harris, 1992). An indication that the main mode at -5‰ at Aviat may represent eclogitic diamonds (partially or wholly) comes from the diamondiferous eclogite xenolith sample: diamond AV6E yielded $\delta^{13}C$ values around -5‰. Besserer (2008) documented that mantle derived garnets with both peridotitic (G9, G10, and G12; G classification of Grutter et al., 2004) and eclogitic (G3 and G4) chemistries occur in till samples on the Aviat property. Therefore, in the absence of data on inclusions in Aviat diamonds, it cannot be ruled out that the mode at -5‰ represents both eclogitic and peridotitic source parageneses.

3.6.2. Evidence for Multiple Growth Events and Fluid Sources

SIMS profiling revealed that diamond with isotopically light (eclogitic signature) carbon isotopic composition may be overgrown by a second generation of diamond with $\delta^{13}C$ values around -5‰ (mantle signature). Evidence for a resorption event at the interface between these isotopically distinct growth zones indicates two separate diamond growth stages. Other diamonds display the reverse zoning trend; core values between about -3 to -5‰ and rim values that are 0.7 to 2‰ lower. Again, these diamonds were produced during two or more separate growth events, in either eclogitic or peridotitic sources.

Examining carbon and nitrogen point analyses for Aviat diamonds (Figure 3-4) reveals a trend of decreasing maximum nitrogen content with decreasing $\delta^{13}C$, as previously noted by Stachel and Harris (1997). Cartigny et al. (2001) interpreted this relationship as representing a "limit sector" (or a bounding curve) that results from open system isotopic fractionation, through separation of CO_2 fluid from a residual carbonate bearing melt that becomes increasingly depleted in ^{13}C and nitrogen. However, due to clustering of carbon isotopic data for Aviat the trend is not continuous, and may equally reflect multiple fluids originating from different sources.

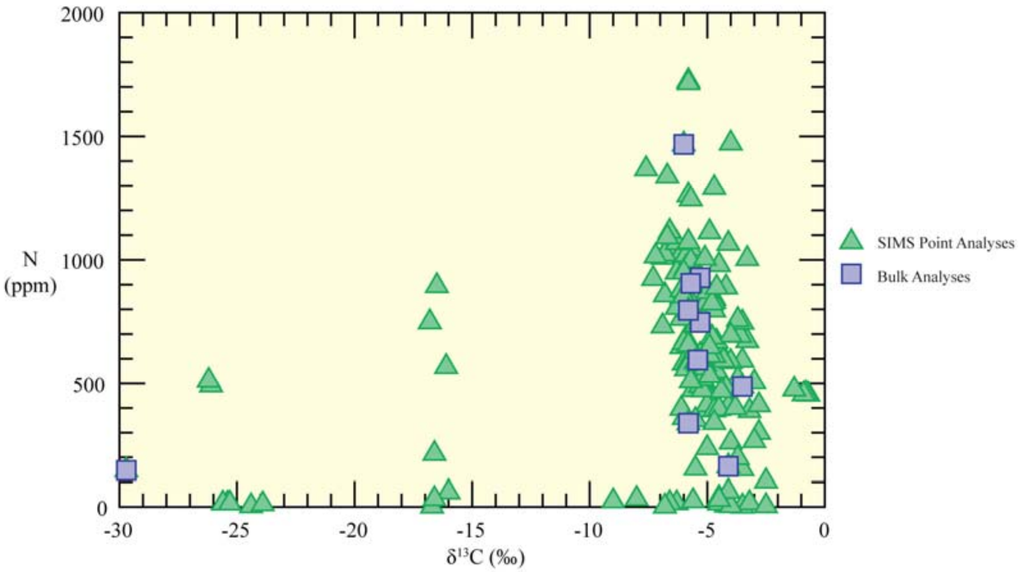

Figure 3-4. Nitrogen content vs. δ^{13}C values for Aviat diamonds.
Each point analysis (δ^{13}C and N) performed by SIMS is recorded as well as the ten diamonds analyzed conventionally for δ^{13}C and by FTIR for nitrogen. The Aviat diamonds with higher δ^{13}C values exhibit higher maximum nitrogen contents as well as a larger range of values. The cluster of data points around -16‰ represents two separate diamonds. A second cluster at -26‰ to -25‰ represents one diamond; such large variations in nitrogen content without associated systematic variations in δ^{13}C provide evidence of a decoupling of nitrogen and δ^{13}C on the scale of individual diamond growth sectors.

Comparing carbon and nitrogen point analyses within the diamonds, the dominant trend is increasing δ^{13}C with decreasing nitrogen content which is indicative of diamond formation via reduction of carbonates (Stachel et al., 2009). On the scale of individual diamond growth sectors, however, carbon and nitrogen are generally decoupled in Aviat diamonds, with large variations in nitrogen content with no associated change in δ^{13}C and vice versa (Figure 3-3). This indicates that closed system Rayleigh fractionation was not dominant during diamond formation at Aviat, and instead suggests that variations in nitrogen content and δ^{13}C reflect multiple pulses of fluid derived from distinct sources instead.

Examining the relationship between CL response and nitrogen content, the dominant association observed in Aviat diamonds are cores with a visible CL response with fairly low nitrogen contents (~3-400 at.ppm) and rims with dark CL colors and high nitrogen contents (~850-1725 at.ppm). However, it should be noted that the reverse CL pattern was also observed, where dark cores corresponded to low nitrogen content and bright rims featured high nitrogen content.

In diamond, it has been demonstrated that nitrogen abundance correlates with CL colour: the higher the nitrogen content, the brighter the CL (e.g. Fitzsimons et al., 1999; Harte et al., 1999; Hauri et al., 2002). However, the vast majority of Aviat diamonds display the reverse trend, with very dark areas in CL corresponding to high nitrogen contents. Studies of fluorescence in synthetic diamonds have revealed that when surface bonds are hydrogen-terminated rather than oxygen-terminated, the charge of nitrogen vacancies (NV) changes from negative (NV^-) to neutral (NV^0) which suppresses fluorescence (Hauf et al., 2011). As Aviat diamonds are hydrogen-rich, this may provide an explanation for the lack of cathodoluminescence in nitrogen-rich areas of the diamonds.

A plot of the intensity of the H-related peak at 3107cm^{-1} (quantified as peak area) versus nitrogen content (at.ppm) reveals a linear relationship for some diamonds similar to observations for Argyle (Western Australia) diamonds by Iakoubovskii and Adriaenssens (2002) (Figure 3-5). These authors suggested that diamonds showing such a positive linear correlation grew from a source rich in NH_3 and NH_4^+, whereas diamonds which exhibit low H and high nitrogen grew

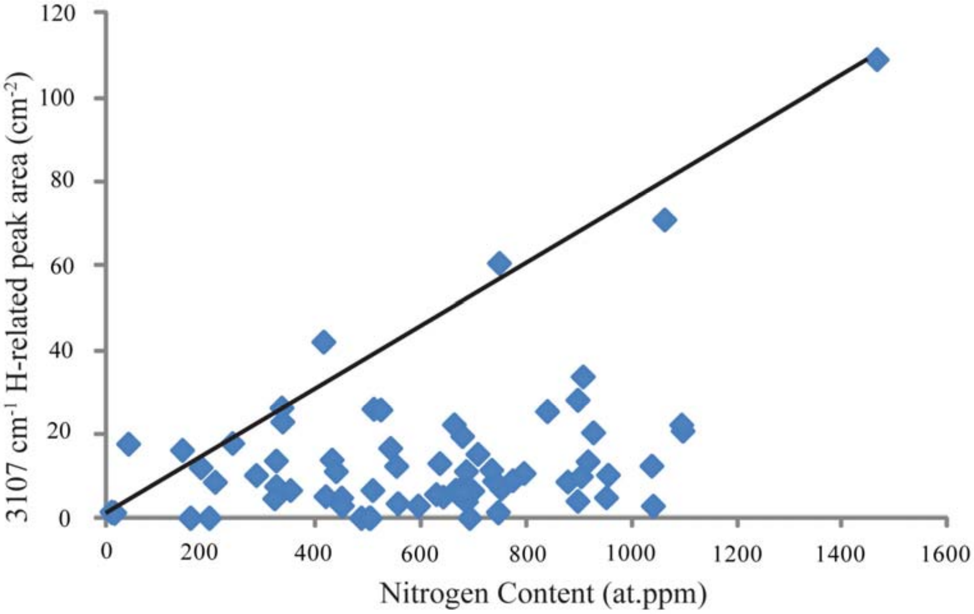

Figure 3-5. 3107cm^{-1} H peak intensity (cm^{-2}) vs. nitrogen content.
Nitrogen content plotted was measured using FTIR. A population of diamonds exhibits a linear relationship as observed for diamonds at Argyle by Iakoubovskii and Adriaenssens

(2002). However, a significant proportion of Aviat diamonds does not follow this linear trend.

from a source rich in N_2. Both “trends” are observed at Aviat, thus providing further evidence for the involvement of multiple fluids derived from distinct sources. The data also indicate that these fluids must have had unique N speciation and nitrogen contents.

3.6.3. Thermal History during Mantle Residence

A plot of bulk nitrogen content vs. %B component (both obtained via FTIR) reveals that Aviat diamonds span a range of time averaged mantle residence temperatures (isotherms were calculated after Taylor et al. (1990) and Leahy and Taylor, (1997)) from ~1050-1300°C, for a mantle residence of 1 Ga, indicating derivation of diamonds from various depths beneath Aviat (Figure 3-6).

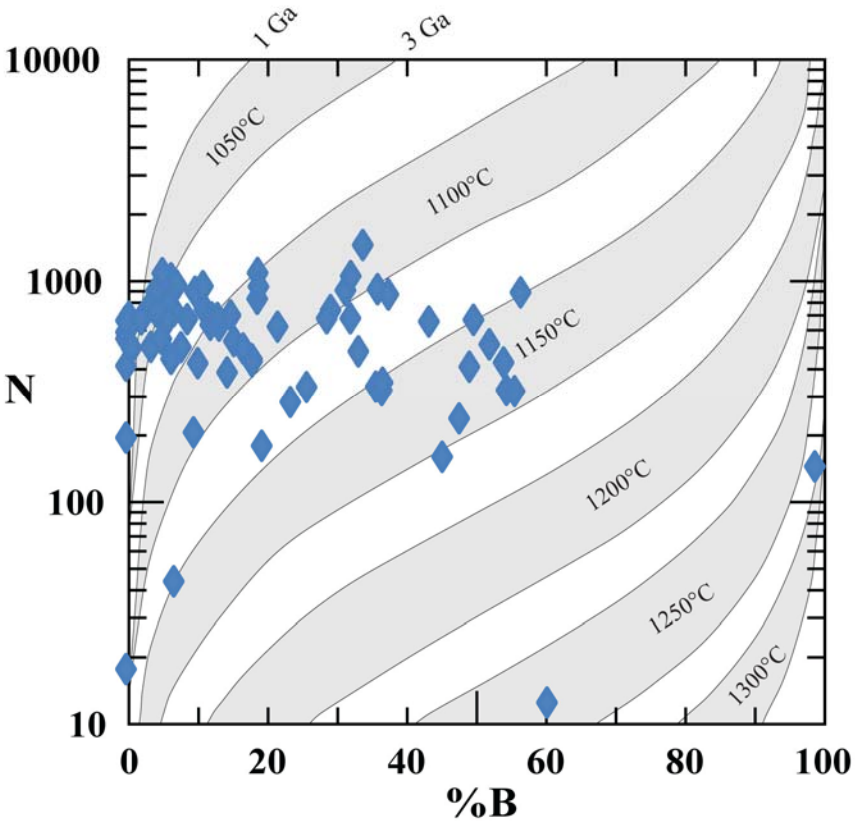

Figure 3-6. Nitrogen content (at.ppm) vs. %B component for Aviat diamonds obtained via FTIR bulk analyses.
Isotherms for 3 and 1 Ga mantle residence were calculated after Taylor et al. (1990) and Leahy and Taylor (1997). Aviat diamonds illustrate a spread of temperatures indicating variation in depth of origin, based on the assumption of mantle residence along a steady state conductive geotherm. The samples cluster at nitrogen contents between 100-1700 at.ppm and aggregation states of 0-60 %B, with a few outliers.

For "regular" diamonds Woods (1986) observed a linear relationship between the integrated strength of the platelet peak (I(B')) and the nitrogen B centre related absorption coefficient (μ_B) at 1282 cm^{-1}. In Figure 3-7, for simplicity, we replaced μ_B with the concentration of nitrogen in B aggregates (at.ppm) and derived the slope for "regular" diamonds from evaluation of several in-house data sets. The majority of Aviat diamonds plot below the linear trend for "regular" diamonds (Figure 3-7) and according to Woods (1986) classify as being "irregular". The breakdown of a linear relationship between I(B') and at.ppm nitrogen in B centres indicates that "catastrophic platelet degradation" occurred, which relates either to transient heating events or deformation (or a combination of both) during mantle residence (Woods, 1986; Evans et al., 1995).

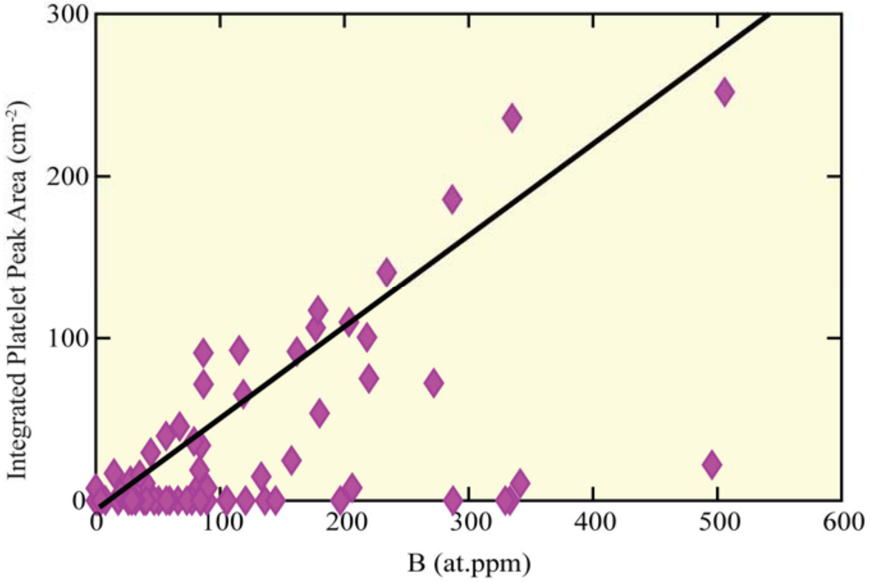

Figure 3-7. Integrated strength of the platelet peak (cm^{-2}) vs. the concentration of nitrogen as B component (at.ppm) for Aviat diamonds.
The solid line represents the strict proportionality between platelet intensity and absorbance associated with nitrogen in B centres for "regular" diamonds, similar to Fig. 5 of Woods (1986). Many of the diamonds in this diagram plot below the line for regular diamonds and hence likely underwent "catastrophic platelet degradation" probably caused by transient heating events and/or shearing during mantle residence (Woods, 1986; Evans et al., 1995).

3.6.4. Origin of Eclogitic Diamond Sources and Diamond Forming Events Beneath Aviat

Several orogenic events may have involved subduction of basaltic lithologies and graphitized organic matter beneath the Melville Peninsula, two examples are: (1.) east-dipping subduction on the western margin of the Rae craton, likely concurrent with the 2.35 Ga Arrowsmith orogeny (Berman et al., 2005; Hartlaub et al., 2007) and (2.) northward directed subduction during the 1.9 Ga Trans-Hudson orogeny (Berman et al., 2005; Berman et al., 2010). Either/both of these orogenies, or others that occurred in the area can equally be employed to explain the presence of eclogitic diamond sources and the occurrence of light carbon isotopic signatures among Aviat diamonds.

These eclogitic carbon reservoirs were tapped during an initial phase of diamond growth producing diamonds with a low $\delta^{13}C$ signature. This growth event was followed by a period of diamond resorption. A subsequent diamond growth event with a mantle like carbon isotopic signature affected eclogitic and possibly additional peridotitic sources. Several diamonds record a third growth event of mantle like signatures. If additional subsequent diamond growth events occurred before kimberlite emplacement and diamond exhumation took place at ~558 Ma (Scott Smith, 2008) cannot be constrained on the basis of the present data set.

3.7. Conclusions

The evaluation of the carbon isotopic composition, nitrogen content, and nitrogen aggregation state of Aviat diamonds allows preliminary conclusions about diamond sources in the lithospheric mantle beneath the northern Churchill Province:

(1.) There are likely multiple diamond sources in the lithospheric mantle beneath Aviat with diamond formation occurring at various times and depths to produce diamonds with differing carbon isotopic signatures.

(2.) The presence of an eclogitic subpopulation is certain, but it cannot be excluded that peridotitic diamonds are present at Aviat as well.

(3.) Fluids from multiple sources must have contributed to the formation of Aviat diamonds, evidenced for example, by the decoupling of nitrogen content and $\delta^{13}C$ on the scale of individual growth sectors.

(4.) The occurrence of multiple diamond growth events is indicated by zoning of crystals in CL, coinciding with distinct carbon isotopic signatures, separated by resorption events.

(5.) Orogenic events with subduction directed towards the Melville Peninsula likely supplied the crustal protolith for eclogitic sources and provided ^{13}C depleted carbon for some Aviat diamonds.

References

Berman R.G., Sanborn-Barrie M., Stern R.A. and Carson C.J. (2005) Tectonometamorphism at *ca*. 2.35 and 1.85 Ga in the Rae Domain, Western Churchill Prince, Nunavut, Canada: Insights from structural, metamorphic and *in situ* geochronological analysis of the southwestern Committee Bay Belt. *Can. Mineral.* **43,** 409-442.

Berman R.G., Sanborn-Barrie M., Rayner N., Carson C., Sandeman H.A. and Skulski T. (2010) Petrological and *in situ* SHRIMP geochronological constraints on the tectonometamorphic evolution of the Committee Bay belt, Rae Province, Nunavut. *Precamb. Res.* **181,** 1-20.

Besserer, D.J. (2008) Technical report for the Aviat property Melville Peninsula, Nunavut, Canada. 1-61.

Cartigny P., Harris J.W. and Javoy M. (2001) Diamond genesis, mantle fractionations and mantle nitrogen content: a study of δ^{13}C-N concentrations in diamonds. *Earth Planet. Sci. Lett.* **185,** 85-98.

Charette J.J. (1959) Le Spectre Infra-rouge a grande dispersion des trois types de diamants et ses variations en fonction de la temperature. *Physica* **25,** 1303-1312.

Chrenko R.M., McDonald R.S. and Darrow K.A. (1967) Infra-red spectra of diamond coat. *Nature* **213,** 474-476.

Davies G., Collins A.T. and Spear P. (1984) Sharp infra-red absorption lines in diamond. *Solid State Commun.* **49,** 433-436.

Donnelly C. (2006) The characterization of diamonds and their mineral inclusions from the Diaviak diamond mine, Lac de Gras, Northwest Territories, Canada. MSc. thesis, University of Alberta, Edmonton, Alberta pp.1-187.

Evans T., Kiflawi, I., Luyten, W., Vantendeloo G. and Woods G.S. (1995) Conversion of platelets into dislocation loops and voidite formation in Type IaB diamonds. *Proc. R. Soc. London, Ser. A* **449 (1936),** 295-313.

Fitzsimons, I.C.W., Harte, B., Chinn, I.L., Gurney, J.J., and Taylor, W.R. (1999) Extreme chemical variation in complex diamonds from George Creek, Colorado: a SIMS study of carbon isotope composition and nitrogen abundance. *Mineral. Mag.* **63**, 857-878.

Fritsch E., Hainschwang T., Massi L. and Rondeau B. (2007) Hydrogen-related optical centers in natural diamond: An update. *New Diamond and Front. Carbon Technol.* **17,** 63-89.

Galimov E.M. (1991) Isotope fractionation related to kimberlite magmatism and diamond formation. *Geochim. Cosmochim. Acta* **55,** 1697-1708.

Gibb R.A. and Walcott R. I. (1971) A Precambrian suture in the Canadian shield. *Earth Planet. Sci. Lett.* **10,** 417-422.

Grütter, H.S., Gurney, J.J., Menzies, A.H., and Winter, F. (2004) An updated classification scheme for mantle-derived garnet, for use by diamond explorers. *Lithos* **77**, 841-857.

Gurney, J.J. (1984) A correlation between garnets and diamonds in kimberlites. Publications of the Geology Department and Department of Extension. University of Western Australia, Perth. pp.143-166.

Gurney J.J. (1989) Diamonds. *In* Kimberlites and Related Rocks: Proceedings of the IVth International Kimberlite Conference (eds. J. Ross, A.L. Jaques, J. Ferguson, D.H. Green, S.Y. O'Reilly, R.V. Dancin, A.J.A. Janse). Geological Society of Australia Special Publication, vol. **14**. Blackwell, Carlton. pp. 935-965.

Gurney, J.J., Helmstaedt, H.H., Moore, R.O. (1993) A review of the use and application of mantle mineral geochemistry in diamond exploration. Pure and Applied Chemistry **65**, 2423-2442.

Harris J.W. (1992) Diamond Geology. *In* The properties of natural and synthetic diamond (ed. A. C. Field). Academic Press, London. pp. 345-393.

Harte, B., Fitzsimons, I.C.W., Harris, J.W., and Otter, M.L. (1999) Carbon isotope ratios and nitrogen abundances in relation to cathodoluminescence characteristics for some diamonds from the Kaapvaal Province, S. Africa. *Mineral. Mag.* **63**, 829-856.

Hartlaub R.P., Heaman L.M., Chacko T. and Ashton K.E. (2007) Circa 2.3-Ga magmatism of the Arrowsmith Orogeny, Uranium City Region, Western Churchill Craton, Canada. *J. Geol.* **115,** 181-195.

Hauf, M.V., Grotz, B., Naydenov, B., Dankerl, M., Pezzagna, S., Meijer, J., Jelezko, F., Wrachtrup, J., Stutzmann, M., Reinhard, F., and Garrido, J.A. (2011) Chemical control of the charge state of nitrogen-vacancy centers in diamond. *Phys. Rev. B* **83**, 081304(R).

Hauri, E.H., Wang, J. Pearson, D.G., and Bulanova, G.P. (2002) Microanalysis of $\delta^{13}C$, $\delta^{15}N$, and N abundances in diamonds by secondary ion mass spectrometry. *Chem. Geol.* **185**, 149-163.

Hoffman P.F. (1988) United plates of America, the birth of a craton: Early Proterozoic assembly and growth of Laurentia. *Ann. Rev. Planet. Sci.* **16,** 543-603.

Hoffman P.F. (1990) Subdivision of the Churchill Province and extent of the Trans-Hudson Orogen. *In* The Early Proterozoic Trans-Hudson Orogen of North America (eds. J.F. Lewry and M.R. Stauffer). Geological Association of Canada Special Paper, pp. 15-38.

Iakoubovskii K. and Adriaenssens G.J. (2002) Optical characterization of natural Argyle diamonds. *Diamond Relat. Mater.* **11***,* 125-131.

Kirkley M.B., Gurney J.J., Otter M.L., Hill S.J. and Daniels L.R. (1991) The application of C isotopes measurements to the identification of the sources of C in diamonds: a review. *Appl. Geochem.* **6,** 477-494.

Kopylova M., Navon O., Dubrovinsky L. and Khachatryan G. (2010) Carbonatitic mineralogy of natural diamond-forming fluids. *Earth Planet. Sci. Lett.* **291,** 126-137.

Leahy K. and Taylor W.R. (1997) The influence of the Glennie domain deep structure on the diamonds in Saskatchewan kimberlites. *Russ. Geol. Geophys.* **38,** 481-491.

Pollack H.N. and Chapman D.S. (1977) On the regional variation of heat flow, geotherms, and lithospheric thickness. *Tectonophysics* **38,** 279-296.

Rudolph W.W., Fischer D. and Irmer G. (2006) Vibrational spectroscopic studies and density functional theory calculations of speciation in the CO_2-water system. *Appl. Spectrosc.* **60,** 130-144.

Runciman W.A. and Carter T. (1971) High resolution infra-red spectra of diamond. *Solid State Commun.* **9,** 315-317.

Schultz M.E.J., Chacko T., Heaman L.M., Sandeman H.A., Simonetti A. and Creaser R.A. (2007) Queen Maud block: A newly recognized Paleoproterozoic (2.4-2.5 Ga) terrane in northwest Laurentia. *Geology* **35,** 707-710.

Scott Smith B.H. (2008) Canadian kimberlites: Geological characteristics relevant to emplacement. *J. Volcanol. Geotherm. Res.* **174,** 9-19.

Skulski T., Sandeman H., Sanborn-Barrie M., MacHattie T., Young M., Carson C., Berman R., Brown J., Rayner N., Panagapko D., Byrne D. and Deyell C. (2003a) Bedrock geology of the Ellice Hills map area and new constraints on the regional geology of the Committee Bay area, Nunavut. *Geol. Surv. Can. Curr. Res.* **C22,** 1-11.

Skulski T., Sanborn-Barrie M. and Sandeman H. (2003b) Geology, Walker Lake and Arrowsmith River area, Nunavut. *Geol. Surv. Can. Open File*, **3777**.

Snyder D.B. and Grütter H.S. (2010) Lithoprobe's impact on the Canadian diamond-exploration industry. *Can. J. Earth Sci.* **47,** 783-800.

Sobolev E.V., Lenskaya S.V. and Lisoivan V.I. (1968) Lamellar formations in the structure of natural diamonds. (Engl. Transl.) *Jour. Struc. Chem.* **9,** 917-920.

Sobolev V.S. and Sobolev N.V. (1980) New proof on very deep subsidence of eclogitized crustal rocks. *Doklady Akad. Nauk SSSR* **250,** 683-685.

Stachel T. and Harris J.W. (1997) Syngenetic inclusions in diamond from the Birim field (Ghana) - a deep peridotitic profile with a history of depletion and re-enrichment. *Contrib. Mineral. Petrol.* **127,** 336-352.

Stachel T., Harris J.W. and Muehlenbachs K. (2009) Sources of carbon in inclusion bearing diamonds. *Lithos* **112,** 625-637.

Stornoway Diamond Corporation (2006) Slide 19 *in* Exploration update of December 21, 2006. (accessed September 2, 2010).

Stornoway Diamond Corporation (2009) http://www.stornowaydiamonds.com/ES1_HIstorical_Results_2.pdf (accessed, March 2, 2011).

Stornoway Diamond Corporation (2011) http://www.stornowaydiamonds.com/_resources/Aviat_Kimberlite_Pipes.pdf (accessed, June 2, 2011)

Taylor W.R., Jaques A.L. and Ridd M. (1990) Nitrogen-defect aggregation characteristics of some Australasian diamonds: Time-temperature constraints on the source regions of pipe and alluvial diamonds. *Am. Mineral.* **75,** 1290-1310.

Thongnopkun P. and Ekgasit S. (2005) FTIR Spectra of facted diamonds and diamond stimulants. *Diamond Relat. Mater.***14**, 1592-1599.

Woods G.S. (1986) Platelets and the Infrared-absorption of Type-Ia diamonds. *Proc. R. Soc. London, Ser. A* **407 (1832),** 219-238.

Chapter 4: Discussion and Conclusions

4.1. Introduction

Diamonds from the ES-1 kimberlite on the Aviat property have been examined and analyzed for their colour, morphology, carbon isotopic composition, nitrogen content and nitrogen aggregation state. This allows for some preliminary interpretations on the sources and residence history of diamonds in the lithospheric mantle beneath the northern Churchill Province.

The Churchill Province has been the locus of considerable diamond exploration activity in recent years, yet there has been little research completed in this area. Based on garnet compositional data provided by Stornoway Diamond Corporation (2011), Snyder and Grütter (2010) reported a “diamond friendly” conductive mantle geotherm of 38 mW/m^2. Garnets of both eclogitic and peridotitic paragenesis have been extracted from till samples on the Aviat property indicating that diamonds of both suites may be present (Besserer, 2008). While garnets provide valuable information about the area, addition of diamond derived information will further aid in the understanding and continued exploration of this region.

4.2. Aviat Samples

The most common color observed in Aviat diamonds is grey (39%) followed by colorless (28%) with the remainder exhibiting brown, yellow, and green coloration. The most prevalent morphology in the samples analyzed was irregular (51%) followed by dodecahedral (24%), octahedral (20%), and diamonds with shapes falling in between dodecahedral and octahedral end members (5%). No syngenetic inclusions were observed in the diamonds in this study, only graphite, likely formed during decompression, was present.

4.3. Diamond Sources and Mantle Residence at Aviat

Combining conventional bulk and SIMS point analyses of the carbon isotopic composition of Aviat diamonds results in a range of $\delta^{13}C$ values at Aviat of -29.7‰ to 0.7‰. Worldwide peridotitic diamonds have $\delta^{13}C$ values around -5‰, with the bulk of the values ranging from -10‰ to -1‰ (Galimov, 1991; Kirkley et al., 1991) and only 1.3% of inclusion bearing diamonds worldwide have $\delta^{13}C$ values falling below -10‰ (Stachel et al., 2009). Eclogitic and websteritic diamonds may display a much wider range of values (Sobolev and Sobolev, 1980). Therefore, a population with extremely negative $\delta^{13}C$ values (4 diamonds) at Aviat is indicative of an eclogitic diamond source paragenesis (Sobolev et al., 1979; Harris, 1987). In addition, a single diamondiferous eclogite has been found at Aviat, further confirming the presence of an eclogitic diamond population. The most likely explanation for the isotopically light $\delta^{13}C$ values at Aviat is a contribution of carbon derived from former organic matter transported into the mantle through subduction of oceanic crust (Sobolev and Sobolev, 1980; Milledge et al., 1983; Kirkley et al., 1991). The tectonic history around Aviat makes the contribution of a subducted component likely, as subduction occurred for example, in association with the 2.35 Ga Arrowsmith orogeny (Berman et al., 2005; Hartlaub et al., 2007) and the 1.9 Ga Trans-Hudson orogeny (Berman et al., 2005; Berman et al., 2010). In both cases, the subduction was directed towards the present day Melville Peninsula (where Aviat is located), thus both orogenies are feasible candidates, among other orogenic events in the area, for providing the crustal protoliths necessary to generate the eclogitic diamond sources beneath Aviat.

The remainder of the diamond carbon isotopic analyses cluster around -5‰, characteristic of either an eclogitic or peridotitic paragenesis. However, one diamond in this study of known eclogitic paragenesis (recovered from an eclogite xenolith) yielded a $\delta^{13}C$ value of -5‰, suggesting that diamonds around -5‰ are at least in part, eclogitic. Nevertheless, a peridotitic paragenesis cannot be ruled out for some Aviat diamonds. An inclusion study of diamonds from Aviat is necessary to get a more definitive picture of the diamond sources present in this region as well as their relative abundances.

FTIR analyses of the nitrogen content of Aviat diamonds yielded a range from 13 to 1467 at.ppm. Nitrogen contents obtained via SIMS point analyses, averaged to yield one value per diamond, are similar, ranging from 6 to 1353 at.ppm. Nitrogen aggregation of Aviat diamonds ranges from 0-98%B. The majority of Aviat diamonds are Type IaAB (62%) followed by Type IaA (37%) and a minor Type IaB population (1%). Examining the covariation of nitrogen content and %B component for Aviat diamonds reveals that the samples reflect a range in mantle residence temperatures. The complete suite of Aviat diamonds shows a spread in nitrogen based temperatures, assuming 1 Ga residence time, from ~1050-1300°C (calculated after Taylor et al. (1990) and Leahy and Taylor (1997)) with most samples clustering between ~1050 and 1150°C. This indicates that there was a range of source depths from ~170 to 200 km in the mantle for diamonds at Aviat.

FTIR spectroscopy demonstrated that Aviat diamonds have abundant hydrogen, typically displaying at least one of the peaks associated with the bending and stretching of the vinylidene group ($C=CH_2$): 3107 cm^{-1}, 2786 cm^{-1} and 1404 cm^{-1} (Charette, 1959; Runciman and Carter, 1971; Woods and Collins, 1983; Davies et al., 1984). Another hydrogen related peak belonging to a different C-H component at 3237 cm^{-1} was also present in some Aviat diamonds (Charette, 1959; Fritsch et al., 2007). Examining the covariation of the hydrogen related peak intensity at 3107 cm^{-1} (measured as peak area) and nitrogen content for Aviat diamonds reveals that many diamonds follow the same linear relationship previously noted by Iakoubovskii and Adriaenssens (2002) for Argyle diamonds which these authors interpret to indicate a source rich in NH_3 and NH_4^+. However, a subpopulation of Aviat diamonds does not follow this trend, exhibiting high nitrogen contents with low hydrogen peak intensities at 3107 cm^{-1} indicating a source rich in N_2 (Iakoubovskii and Adriaenssens, 2002). These data point toward fluids from multiple sources featuring distinct N speciation contributing to diamond formation at Aviat.

The CL patterns of most of the Aviat diamonds are the reverse of what is commonly observed, with dark areas featuring high nitrogen content and CL bright areas exhibiting low nitrogen contents. The hydrogen-rich nature of Aviat diamonds may provide an explanation for this phenomenon. In synthetic diamonds, hydrogen-terminated diamond surfaces (as opposed to oxygen-terminated surfaces) have been shown to suppress fluorescence of nitrogen vacancies, through a charge transformation from NV^- to NV^0 (Hauf et al., 2011). If this phenomenon applies to cathodoluminescence as well, then the reverse relationship of CL and nitrogen content may be explained.

Comparing the intensity of the integrated platelet peak (quantified as area in cm^{-2}) and the amount of nitrogen as B component (at.ppm) in Aviat diamonds revealed that most diamonds fall below the linear relationship observed for "regular diamonds" (Woods, 1986), i.e. the platelet peak intensity is not commensurate with the advanced level of nitrogen aggregation. This indicates that transient events and/or deformation during mantle residence caused catastrophic platelet degradation in Aviat diamonds (Woods, 1986; Evans et al., 1995).

4.4. Diamond Growth History

Combining cathodoluminescence images with SIMS carbon and nitrogen analyses, it becomes apparent that multiple diamond growth events must have taken place at Aviat. Some diamonds display core $\delta^{13}C$ values around -5‰ and much more negative rim values with evidence for diamond resorption in between the two layers. Others display the reverse trend; highly negative cores and rim $\delta^{13}C$ values around -5‰, again with evidence for resorption in between. The trends indicate that at least two diamond growth events must have occurred at Aviat.

Covariations of carbon isotopic compositions and nitrogen concentrations (SIMS point analyses) reveal an overall decrease in maximum nitrogen content with decreasing δ^{13}C; however, there is not a continuous trend. Comparing point analyses within single diamonds, there are large variations in carbon isotopic composition with little to no associated change in nitrogen content and vice versa. Again, this indicates that fluids from multiple sources likely contributed to diamond formation at Aviat and that closed system Rayleigh fractionation was not the dominant process.

4.5. Conclusions

The analysis of carbon isotopic compositions and nitrogen characteristics for Aviat diamonds has provided some insight into the mantle residence history and paragenesis of diamonds beneath the northern Churchill Province. The CL patterns exhibited by Aviat diamonds detail a complex growth history, with at least two periods of diamond growth punctuated by periods of diamond resorption. Nitrogen derived temperatures of mantle residence (1050-1100°C) indicate diamond growth occurred over a range of depths beneath Aviat. Variations within diamond growth zones of either δ^{13}C or nitrogen content without an associated change in the other chemical characteristic illustrate the independence of these two chemical attributes in Aviat diamonds. Thus, fluids from several sources must have contributed to diamond formation at Aviat.

An eclogitic subpopulation must be present at Aviat, due to low δ^{13}C values and the observation of a single diamond contained in a small eclogitic xenolith; however, a peridotitic subpopulation cannot be discounted based on the present data set. The graphitized organic matter needed to produce the ^{13}C depleted signatures observed among eclogitic diamonds at Aviat was likely transported to the mantle via subduction associated with orogenic events which occurred in the surrounding area.

Future work that could be done to further this study would be to obtain inclusion-bearing diamonds from Aviat, and subsequent electron microprobe analyses of these inclusions. This would determine whether there is a peridotitic source beneath Aviat, or whether the diamonds from this region are solely eclogitic in origin.

References

Berman R.G., Sanborn-Barrie M., Stern R.A. and Carson C.J. (2005) Tectonometamorphism at *ca*. 2.35 and 1.85 Ga in the Rae Domain, Western Churchill Prince, Nunavut, Canada: Insights from structural, metamorphic and *in situ* geochronological analysis of the southwestern Committee Bay Belt. *Can. Mineral.* **43,** 409-442.

Berman R.G., Sanborn-Barrie M., Rayner N., Carson C., Sandeman H.A. and Skulski T. (2010) Petrological and *in situ* SHRIMP geochronological constraints on the tectonometamorphic evolution of the Committee Bay belt, Rae Province, Nunavut. *Precamb. Res.* **181,** 1-20.

Besserer, D.J. (2008) Technical report for the Aviat property Melville Peninsula, Nunavut, Canada. 1-61.

Charette J.J. (1959) Le Spectre Infra-rouge a grande dispersion des trois types de diamants et ses variations en fonction de la temperature. (in French) *Physica* **25,** 1303-1312.

Davies G., Collins A.T. and Spear P. (1984) Sharp infra-red absorption lines in diamond. *Solid State Commun.* **49,** 433-436.

Evans T., Kiflawi, I., Luyten, W., Vantendeloo G. and Woods G.S. (1995) Conversion of platelets into dislocation loops and voidite formation in Type IaB diamonds. *Proc. R. Soc. London, Ser. A* **449 (1936),** 295-313.

Fritsch E., Hainschwang T., Massi L. and Rondeau B. (2007) Hydrogen-related optical centers in natural diamond: An update. *New Diamond and Front. Carbon Technol.* **17,** 63-89.

Galimov E.M. (1991) Isotope fractionation related to kimberlite magmatism and diamond formation. *Geochim. Cosmochim. Acta* **55,** 1697-1708.

Harris J.W. (1987) Recent physical, chemical, and isotopic research of diamond. *In* Mantle Xenoliths (ed. P. H. Nixon). John Wiley & Sons Ltd., pp. 477-500.

Hartlaub R.P., Heaman L.M., Chacko T. and Ashton K.E. (2007) Circa 2.3-Ga Magmatism of the Arrowsmith Orogeny, Uranium City Region, Western Churchill craton, Canada. *J. Geol.* **115,** 181-195.

Hauf, M.V., Grotz, B., Naydenov, B., Dankerl, M., Pezzagna, S., Meijer, J., Jelezko, F., Wrachtrup, J., Stutzmann, M., Reinhard, F., and Garrido, J.A. (2011) Chemical control of the charge state of nitrogen-vacancy centers in diamond *Phys. Rev. B* **83**, 081304(R).

Iakoubovskii K. and Adriaenssens G.J. (2002) Optical characterization of natural Argyle diamonds. *Diamond Relat. Mater.* **11***,* 125-131.

Kirkley M.B., Gurney J.J., Otter M.L., Hill S.J. and Daniels L.R. (1991) The application of C isotopes measurements to the identification of the sources of C in diamonds: a review. *Appl. Geochem.* **6,** 477-494.

Leahy K. and Taylor W. R. (1997) The influence of the Glennie domain deep structure on the diamonds in Saskatchewan kimberlites. *Russ. Geol. Geophys.* **38,** 481-491.

Milledge H.J., Mendelssohn M.J., Seal M., Rouse J.E., Swart P.K. and Pillinger C.T. (1983) Carbon isotopic variation in spectral type II diamonds. *Nature* **303,** 791-792.

Runciman W.A. and Carter T. (1971) High resolution infra-red spectra of diamond. *Solid State Commun.* **9,** 315-317.

Snyder D.B. and Grütter H.S. (2010) Lithoprobe's impact on the Canadian diamond-exploration industry. *Can. J. Earth Sci.* **47,** 783-800.

Sobolev V.S. and Sobolev N.V. (1980) New proof on very deep subsidence of eclogitized crustal rocks. *Doklady Akad. Nauk SSSR* **250,** 683-685.

Sobolev N.V., Galimov E.M., Ivanovskaia I.N. and Yefimova E.S. (1979) Isotopic composition of carbon from diamonds containing crystalline inclusions (in Russian). *Doklady Akad. Nauk SSSR* **5,** 1217-1220.

Stachel T., Harris J.W. and Muehlenbachs K. (2009) Sources of carbon in inclusion bearing diamonds. *Lithos* **112,** 625-637.

Stornoway Diamond Corporation (2011) http://www.stornowaydiamonds.com/advanced/aviat (accessed February 1, 2011).

Taylor W.R., Jaques A.L. and Ridd M. (1990) Nitrogen-defect aggregation characteristics of some Australasian diamonds: Time-temperature constraints on the source regions of pipe and alluvial diamonds. *Am. Mineral.***75,** 1290-1310.

Woods G.S. (1986) Platelets and the infrared-absorption of Type-Ia diamonds. *Proc. R. Soc. London, Ser. A* **407 (1832),** 219-238.

Woods G.S. and Collins A.T. (1983) Infrared absorption spectra of hydrogen complexes in Type I diamonds. *J. Phys. Chem. Solids* **44,** 471-475.

Appendices

Appendix A: Analytical Methods

A.1. Diamond Cleaning

The diamonds were placed in beakers which were subsequently filled with nitric acid and placed on a hot plate heated to about 70°C for approximately three hours. As this did not fully remove traces of silicates adhered to the diamonds, the diamonds were then cleaned in the same manner this time using Teflon containers and hydrofluoric acid. Next, before analyses were carried out, the diamonds were cleaned in petrol-ether using an ultrasonic bath for approximately five minutes. Diamonds which yielded “noisy” FTIR spectra, or showed unusual peaks were cleaned once more using eucalyptus oil to remove possible organic contaminants (e.g. resin derived from sticky tape).

A.2. Fourier Transform Infrared Spectroscopy

A.2.1. Introduction

Fourier Transform Infrared (FTIR) Spectrometry was used to measure the nitrogen content and aggregation state of Aviat diamonds. Nitrogen, due to its similar size and valence, is the most common impurity found in diamond. Diamonds which contain aggregated nitrogen are classified into different types based upon the amount of B centre they contain: Type IaA = 0-10 %B, Type IaAB = 10-90 %B, Type IaB = 90-100 %B. Hydrogen, another common impurity in diamond, also shows characteristic spectral peaks in FTIR.

A.2.2. Sample Preparation

After cleaning in petrol-ether, the diamonds were mounted on the side of a glass side with double sided sticky tape; about five to eight diamonds mounted on each slide. This slide could then easily be maneuvered under the infrared microscope to analyze each diamond quickly and efficiently.

A.2.3. Analytical Settings

FTIR analyses were conducted at the University of Alberta using a Thermo-Nicolet Nexus 470 FTIR spectrometer connected with a Continuum IR microscope outfitted with a KBr beam splitter. In order to ensure a stable environment for analysis, the instrument was purged with a dry nitrogen-oxygen mixture. A background measurement was taken before analysis, and a new background was taken every 30-60 minutes. Spectra were collected for each sample from 4000-650 cm^{-1}, with a collection time of 200 cycles. After collection, the spectra were base line corrected and normalized to 1 cm sample thickness, thereby converting them to absorption coefficient. Nitrogen content and aggregation state were determined through spectral deconvolution using the Caxbd97 software of David Fisher (Research Laboratories of the Diamond Trading Company, Maidenhead UK). The lower detection limit of this method ranges from 5-15 at.ppm with errors typically ranging from 5-10% of the total nitrogen concentration. The exact values of the aforementioned parameters strongly depend upon the quality of the samples.

Using the Thermo-Nicolet OMNIC software, the intensity of platelet and/or hydrogen (at 3107cm^{-1}) related peaks, when observed, was quantified by measuring the area underneath of the peaks. The peak area measurements taken after the spectra were normalized to 1 cm sample thickness, and a specific background (fitted by the OMNIC software to the peaks) was subtracted in order to remove diamond related absorbance.

A.3. Conventional Carbon Isotopic Analysis

A.3.1. Introduction

Ten diamonds with masses >0.5 mg were analyzed for their $\delta^{13}C$ values using conventional sealed tube combustion and mass spectrometry. The $\delta^{13}C$ value is obtained using the equation:

$$\delta^{13}\text{Csample} = \left[\frac{13\text{C}/12\text{Csample} - 13\text{C}/12\text{Cstandard}}{13\text{C}/12\text{Cstandard}}\right] \text{x } 1000$$

and is reported relative to the VPDB (Vienna Pee Dee Belemnite) standard in per mille (‰).

A.3.2. Sample Preparation

Each diamond (ranging in mass from 1.1 to 2.4 mg) was placed in a silica glass tube which was filled with 1-2 g of copper oxide acting as an oxygen donor. These tubes were loaded onto a vacuum line for three hours and sealed with a blowtorch to preserve the vacuum. The sealed tubes were placed in an oven set at 980°C overnight in order to combust the diamonds, yielding CO_2 gas. The tubes were allowed to cool for about three hours and then were broken under vacuum allowing the extraction of the CO_2 from the sample tubes using liquid nitrogen traps.

A.3.3. Sample Analysis

The CO_2 produced by the diamonds was analyzed using a Finnigan Mat 252 dual inlet mass spectrometer. Six analytical cycles were run for each sample to ensure accuracy. For calibration, analysis of a laboratory-standard CO_2 gas was performed simultaneously. Donnelly (2006) established the analytical precision of the entire process to be better than ±0.1‰ based on repeat analyses of multiple fragments of a single diamond. Figure A-1 displays a sample FTIR spectra for reference.

A.4. Secondary Ion Mass Spectrometry (SIMS)

A.4.1. Introduction

The underlying principle of SIMS involves the bombardment of a sample with an ion beam causing secondary ions to sputter off of the sample. Subsequently the isotopic composition of the ions can then be measured by a mass spectrometer.

A.4.2. Sample Preparation

Samples were mounted in epoxy and polished using a two step process with 15 micron and 6 micron diamond grit embedded in metal plates. The samples were analyzed for their cathodoluminescence (CL) patterns after this step. Subsequently, the epoxy plugs were drilled out and cut, generating disks of embedded diamonds less than 0.5 cm in diameter and approximately 3 mm in thickness. These epoxy disks were pressed into indium around a diamond standard with <1 cm in distance between the standard and farthest samples. The indium mounts were then coated with a 3 nm layer of gold to ensure conductivity for analysis.

A.4.3. Sample Analysis

Samples were analyzed for their CL patterns using a Zeiss EVO 15 scanning electron microscope equipped with both Gatan Chroma and Robinson wide spectrum CL detectors at the Canadian Centre for Isotopic Microanalysis (CCIM) at the University of Alberta. SIMS analysis for both carbon isotopic composition and nitrogen content were carried out using a Cameca IMS1280 ion microprobe, also available at the CCIM.

For both $\delta^{13}C$ and nitrogen analyses performed by SIMS, a Cs^+ ion beam was focused onto the samples, resulting in the sputtering of ions off the sample surface. These secondary ions were focused into a mass spectrometer, divided by mass, and counted by either Faraday cups or an electron multiplier. The electron multiplier was used for nitrogen analysis of samples yielding low count rates, ($<5x10^4$ cts/sec). Pre-sputtering for 60 seconds was necessary to remove the gold coat for each analytical spot. The Cs^+ of the primary beam were accelerated to an impact energy of 20 kV. Mass resolutions of approximately 2300 and 7000 were used for carbon and nitrogen analyses, respectively. The higher mass resolution for nitrogen was necessary in order to distinguish the interference of the molecular species $^{26}C_2^-$ and $^{12}C^{13}C^{1}H^-$ from the desired nitrogen bearing compound ($^{12}C^{14}N^-$). For $\delta^{13}C$ analyses, the standard was re-analyzed after a maximum of every five unknown analyses and values of the unknowns were corrected for instrumental drift. For nitrogen analyses, the unknowns were quantified based on the standard’s nitrogen content (470 at.ppm), which was determined in house using FTIR. Further analytical conditions for analysis are provided in Table A.1.

A.5. Electron-Probe Microanalysis (EPMA)

A.5.1. Sample Preparation

Garnets from a small eclogite xenolith sample were embedded in Araldite® epoxy resin within 5 mm brass rings and polished for analysis. The garnets were subsequently carbon coated for analysis.

A.5.2. Sample Analysis

Major element compositions were obtained for the garnets using wavelength dispersive spectrometry (WDS) on a Cameca SX100 electron microprobe at the University of Alberta. The instrument operated at an accelerating voltage of 20 kV and beam current of 20 nA. Silicate, oxide and metal standards were used for analysis, with peak count times ranging from 30-60 seconds, with half that amount of time utilized for background measurements on each peak side. Each garnet was analyzed at two points, one towards the centre, and one towards the rim of each grain.

References

Donnelly C. (2006) The characterization of diamonds and their mineral inclusions from the Diavik diamond mine, Lac de Gras, Northwest Territories, Canada. MSc. thesis, University of Alberta, Edmonton, Alberta pp. 1-187.

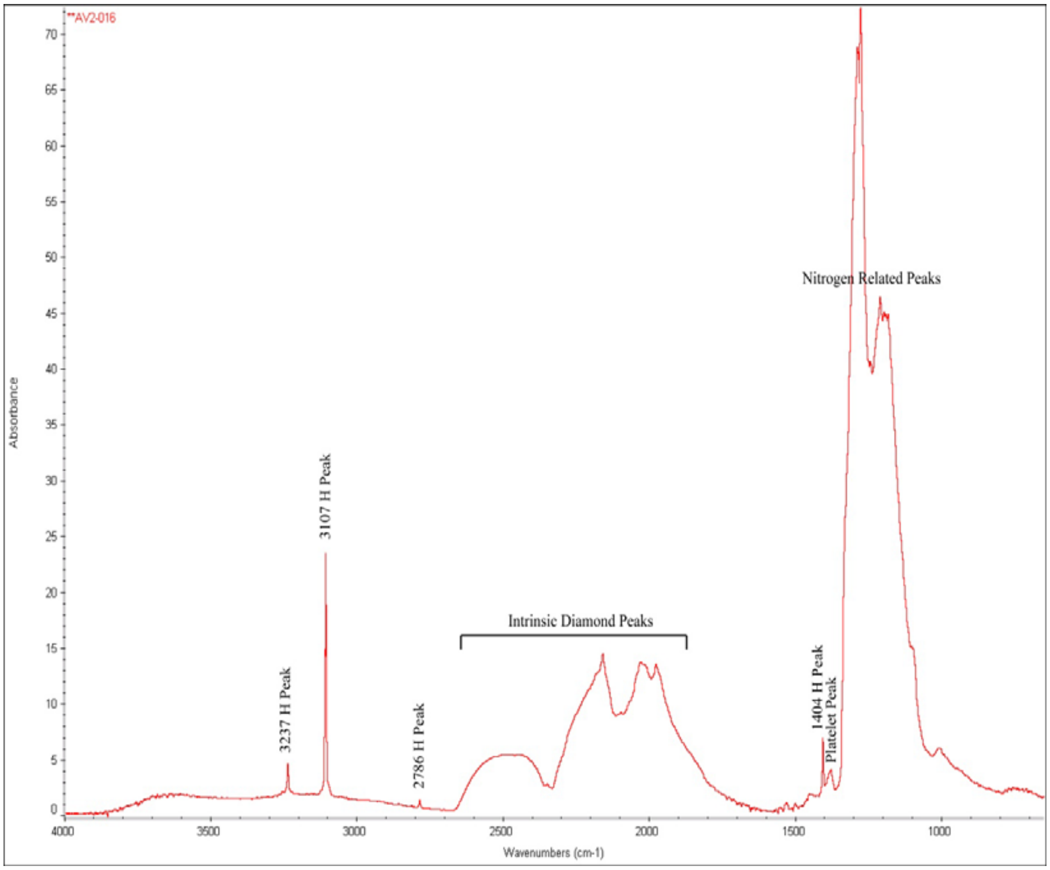

Figure A-1. Sample FTIR spectra for AV2-016 annotated to show the major intrinsic diamond, nitrogen related, and hydrogen related peaks.

Table A-1. SIMS Analytical Settings

Parameter	$\delta^{13}C$	Nitrogen Content
Primary Beam	$^{133}Cs^+$	$^{133}Cs^+$
Primary Beam Diameter	15 µm	15 µm
Electron Charge Neutralization	no	no
Primary Beam Current	4 nA	1 nA
Primary Beam Impact Energy	20 keV	20 keV
Field Aperature	5000 µm	2000 µm
Entrance Slit	122 µm	45 µm
Exit Slit (s)	1418 µm	500 µm, 140 µm
Energy Slit	40 µm	40 µm
Contrast Aperture	400 µm	400 µm
Image Magnification at FA	100X	100X
Pre-sputter	60s	60s
Seconday Ions	$^{13}C^-$ and $^{12}C^-$	$^{12}C^{12}C^-$ and $^{12}C^{14}N^-$
Secondary Extraction Potential	10kV	10kV
Counting Mode	multi-collection	multi-collection
Counter	simultaneous counting on Faraday cups	counting on Faraday cups or electron multiplier
Counting	5s count time for both $^{13}C^-$ and $^{12}C^-$ for 20 cycles	5s count time for both $^{12}C^{12}C^-$ and $^{12}C^{14}N^-$, 10 cycles
Mass Resolution	$^{13}C^-$ ~2300	$^{12}C^{14}N^-$ ~ 7000

Appendix B: Diamond Photographs

B.1. Morphologies

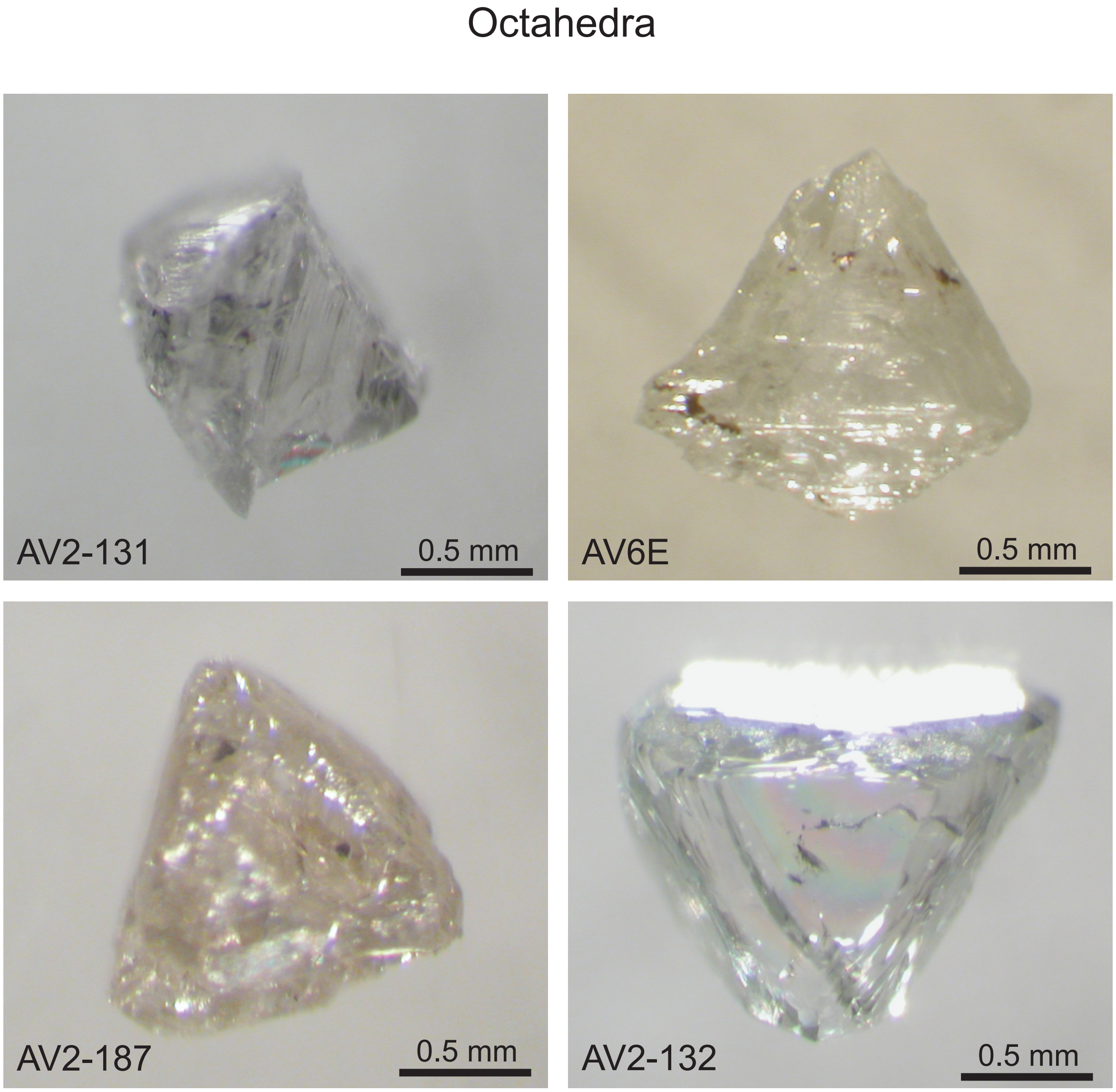

Figure B.1. Examples of the octahedral morphologies observed in the Aviat sample set.

Dodecahedra

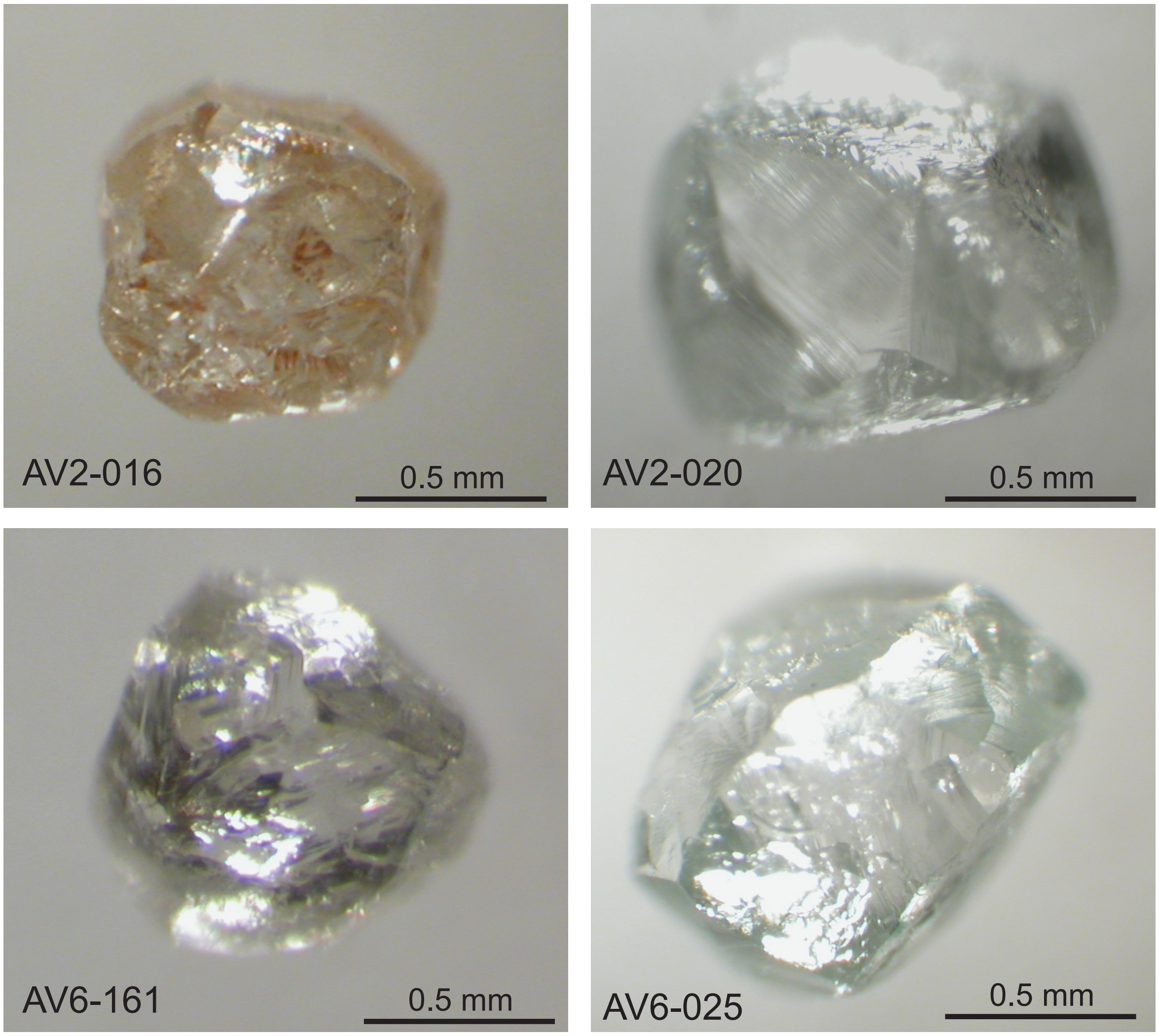

Figure B.2. Examples of dodecahedroids from the Aviat sample set.

Irregular

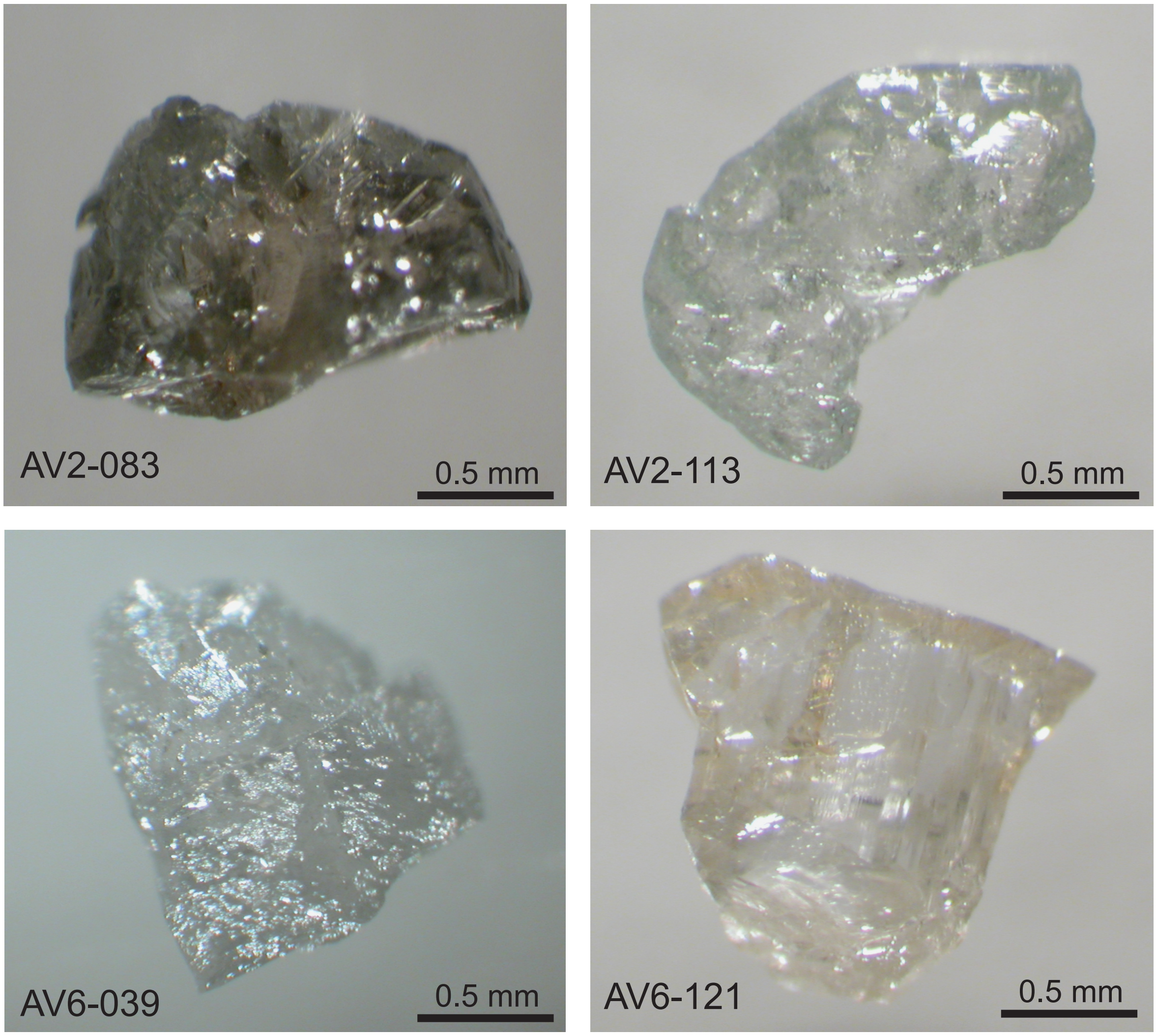

Figure B.3. Examples of Aviat diamonds classified into the irregular morphology.

Aggregates

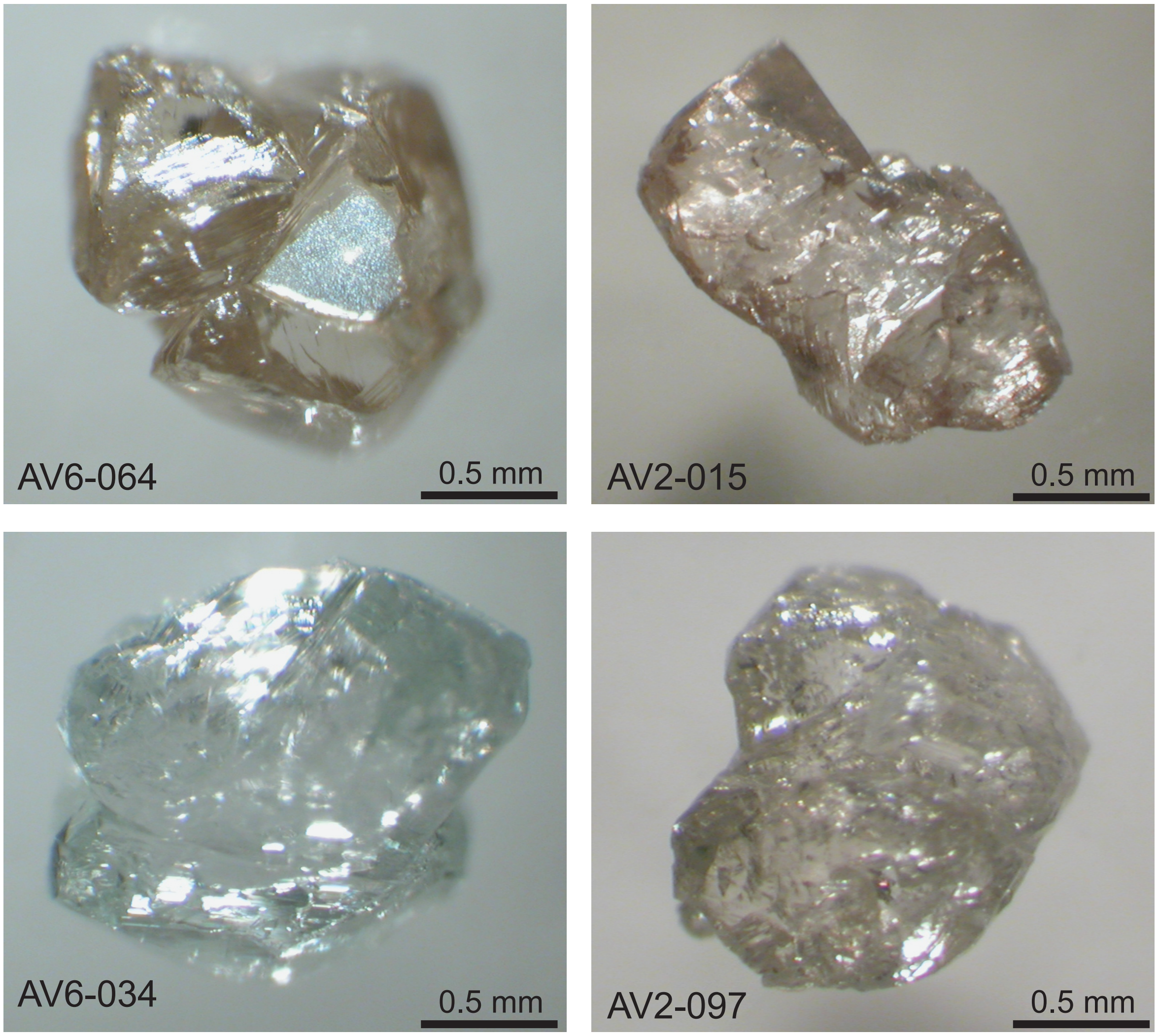

Figure B.4. Examples of Aviat diamonds which are aggregates of a minimum of two separate diamonds.

Fragments

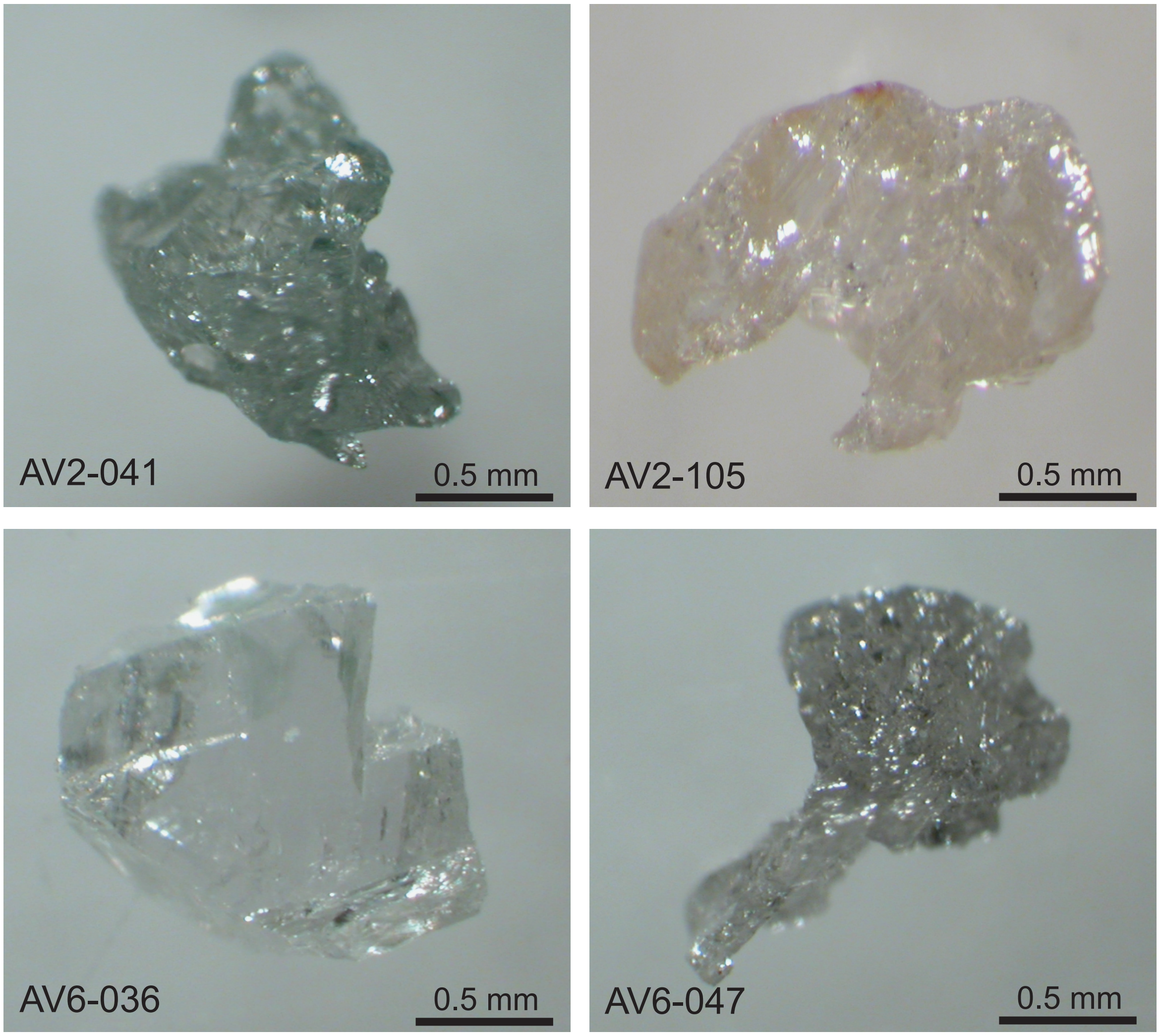

Figure B.5. Examples of Aviat diamonds which have been fragmented.

B.2. Colours

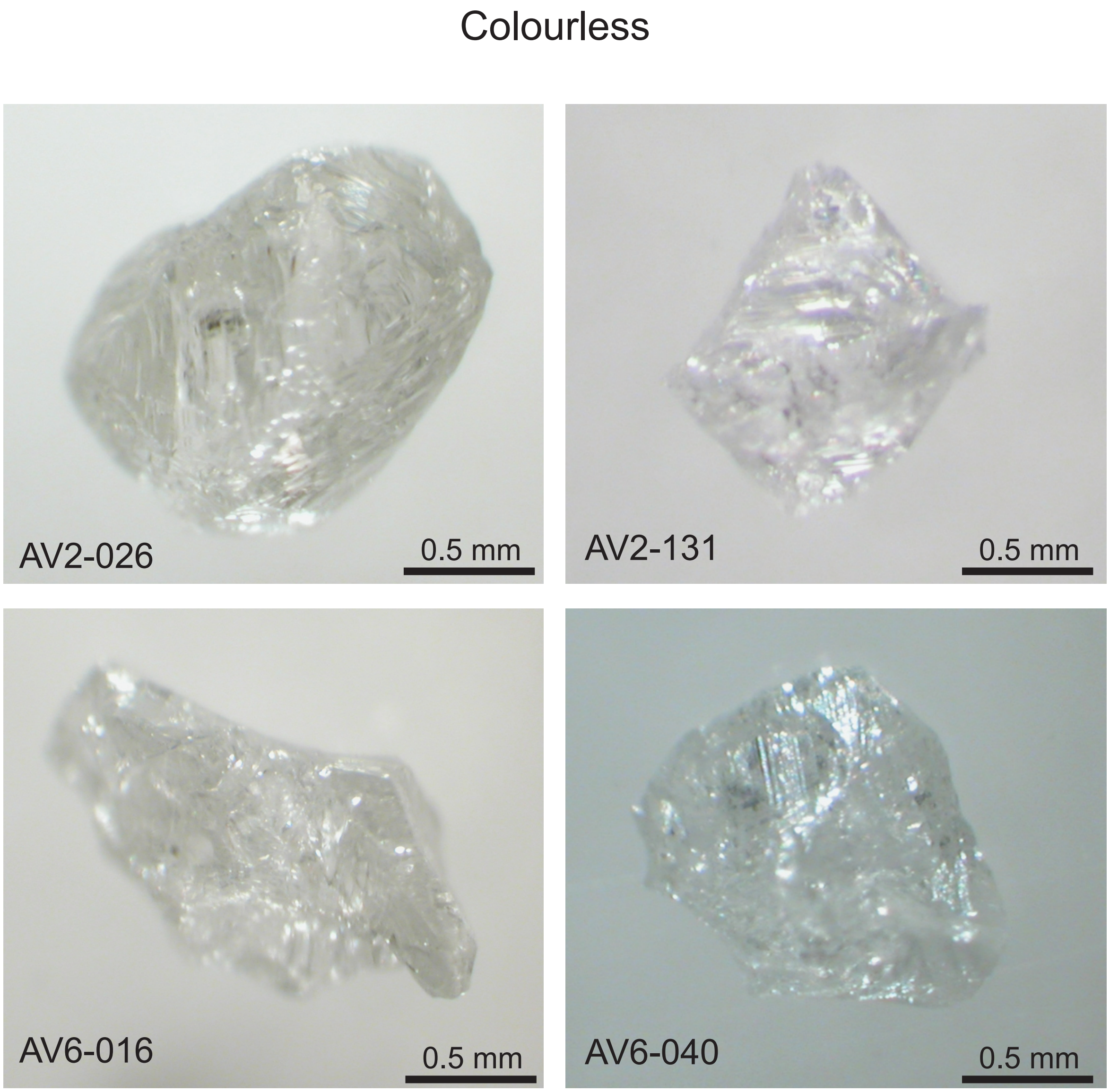
Colourless

Figure B.6. Examples of colourless Aviat diamonds.

Green

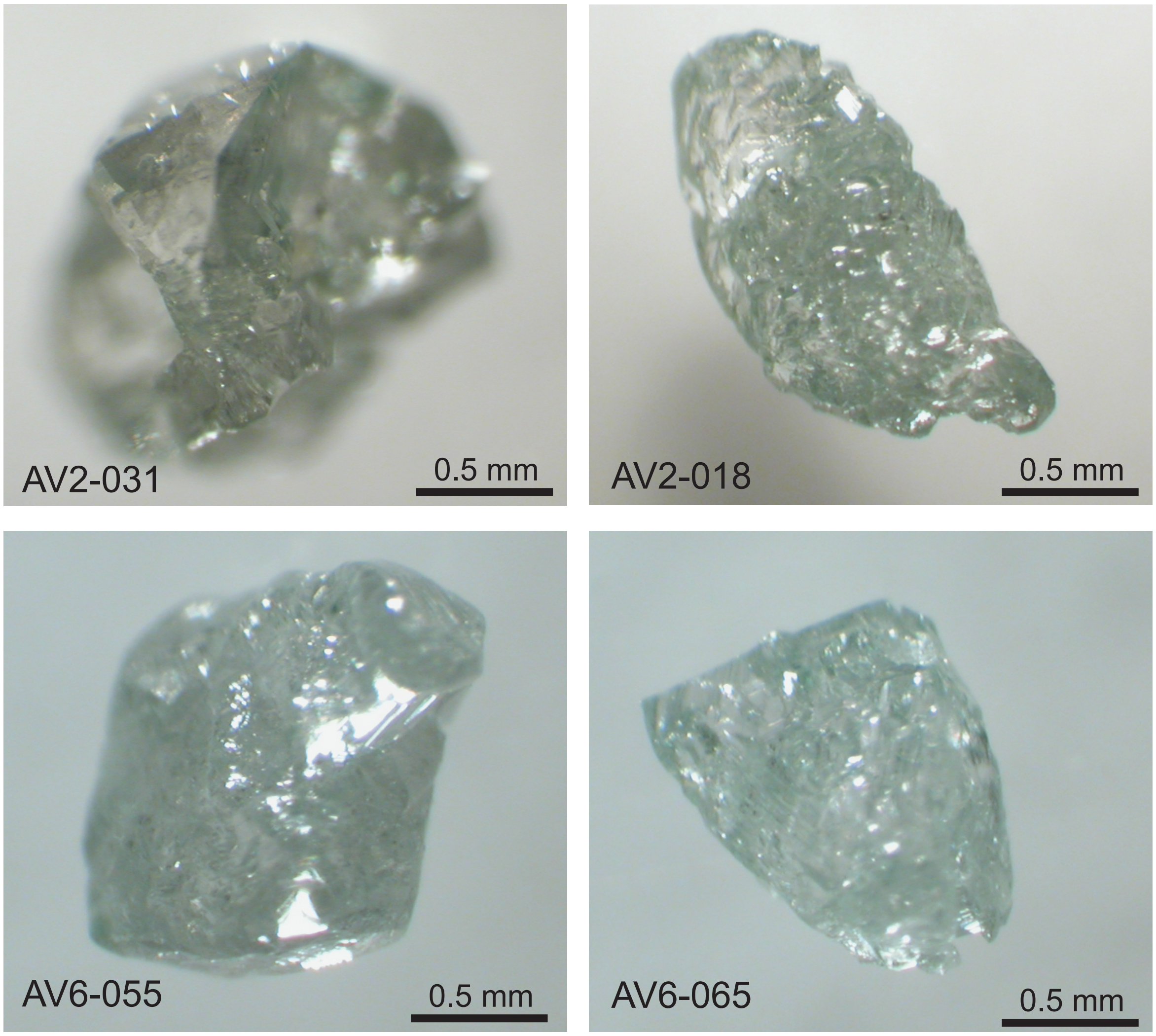

Figure B.7. Examples of green diamonds from Aviat.

Grey

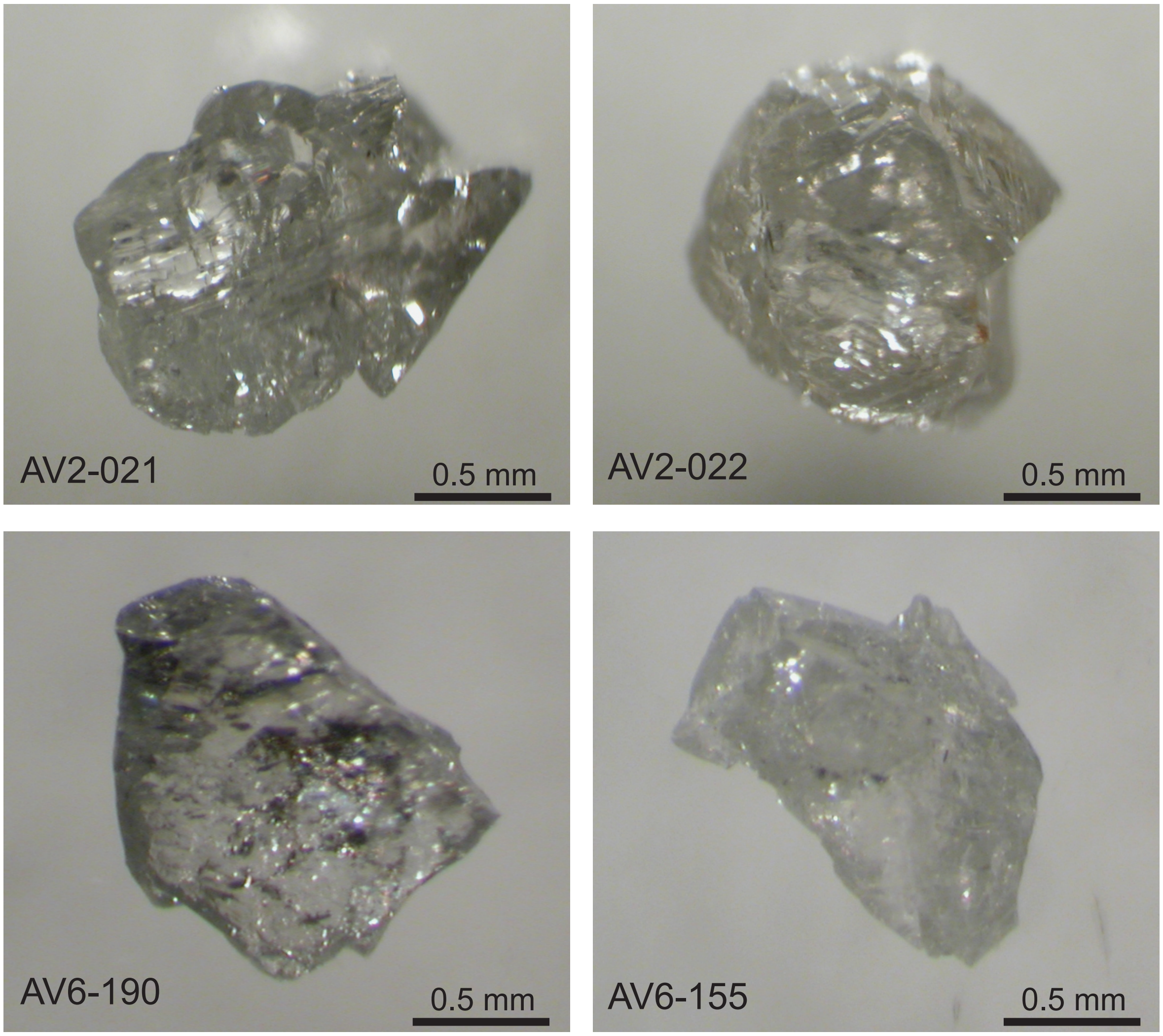

Figure B.8. Grey diamonds from Aviat.

Brown

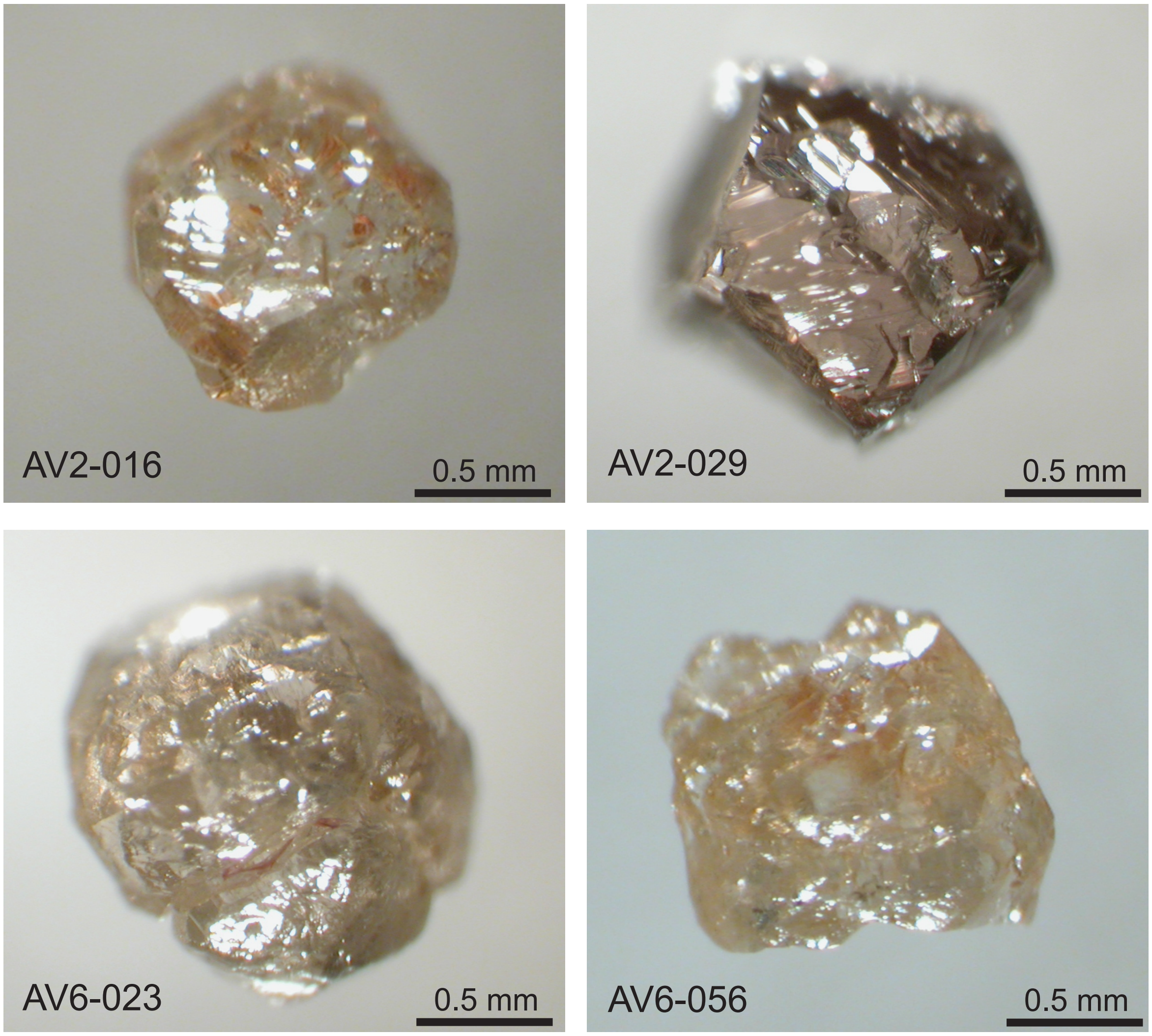

Figure B.9. Brown diamonds from Aviat.

B.3. Surface Features

Stacked Growth Layering

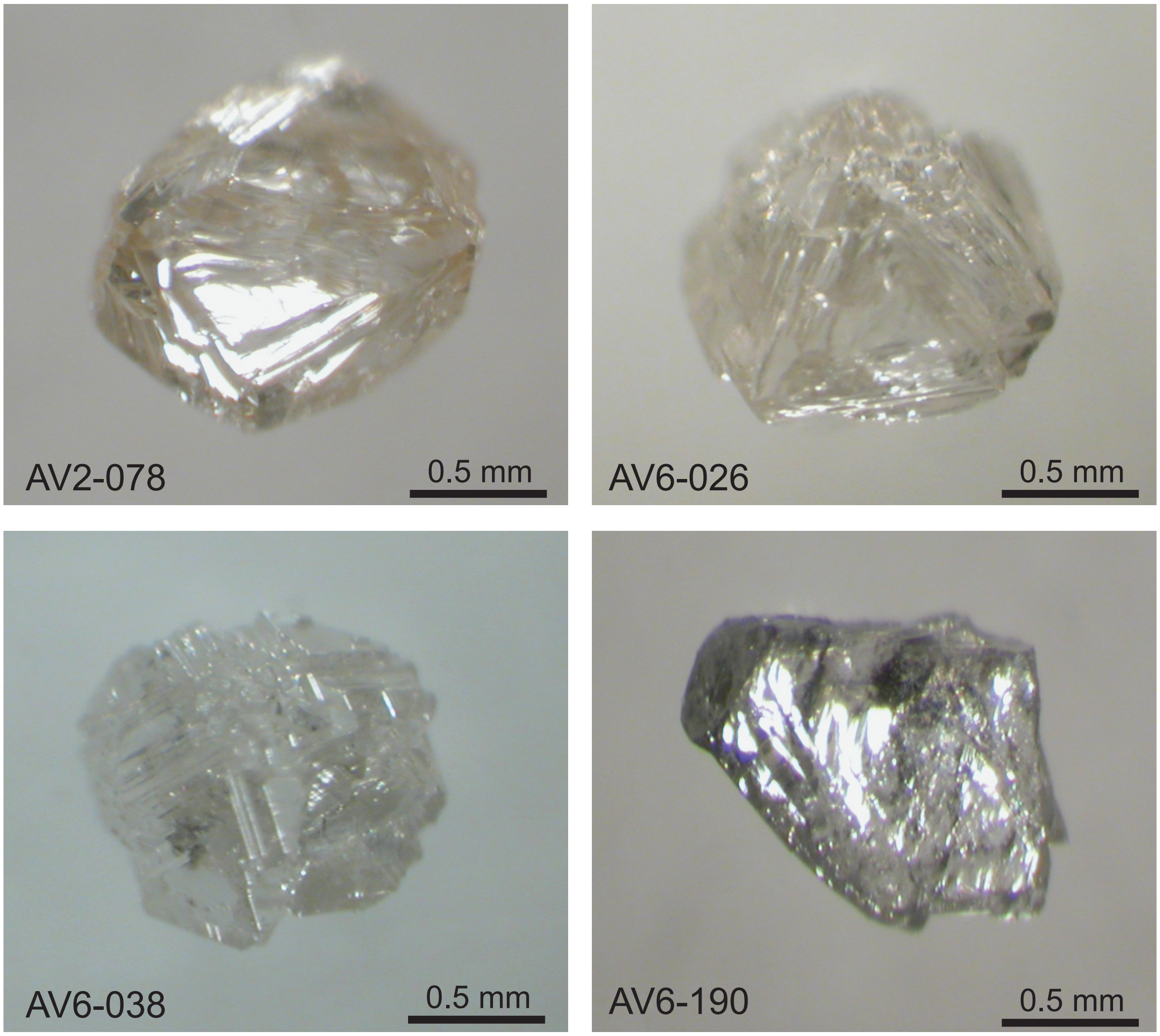

Figure B.10. Stacked growth layering, parallel to octahedral growth planes.

Trigons

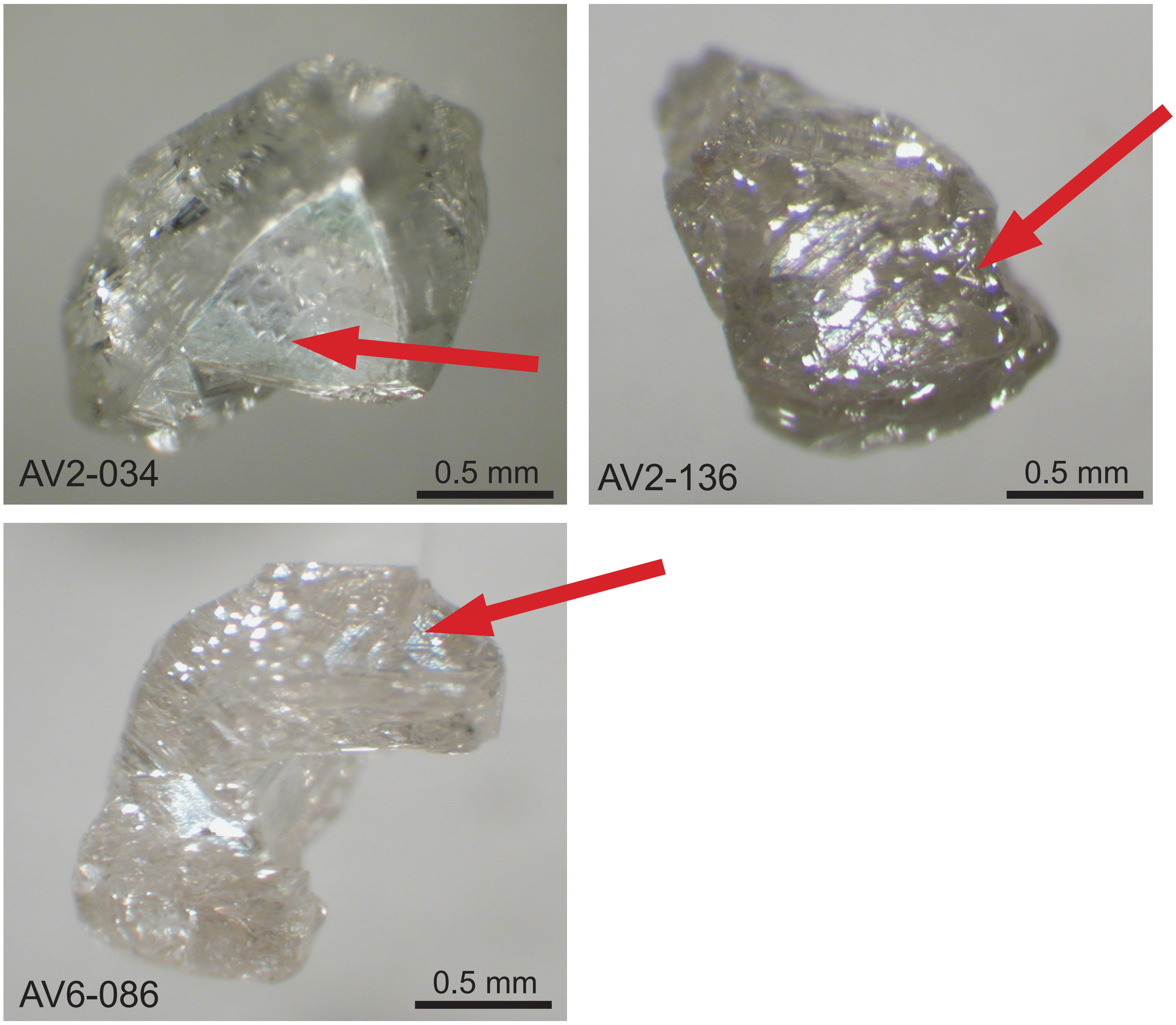

Figure B.11. Trigonal etch pits are pointed out by the red arrows. In the diamond AV2-034, the trigons are in a negative orientation, in the other two diamonds, the orientation is not discernable due to resorption of the diamond faces.

Graphite Flakes

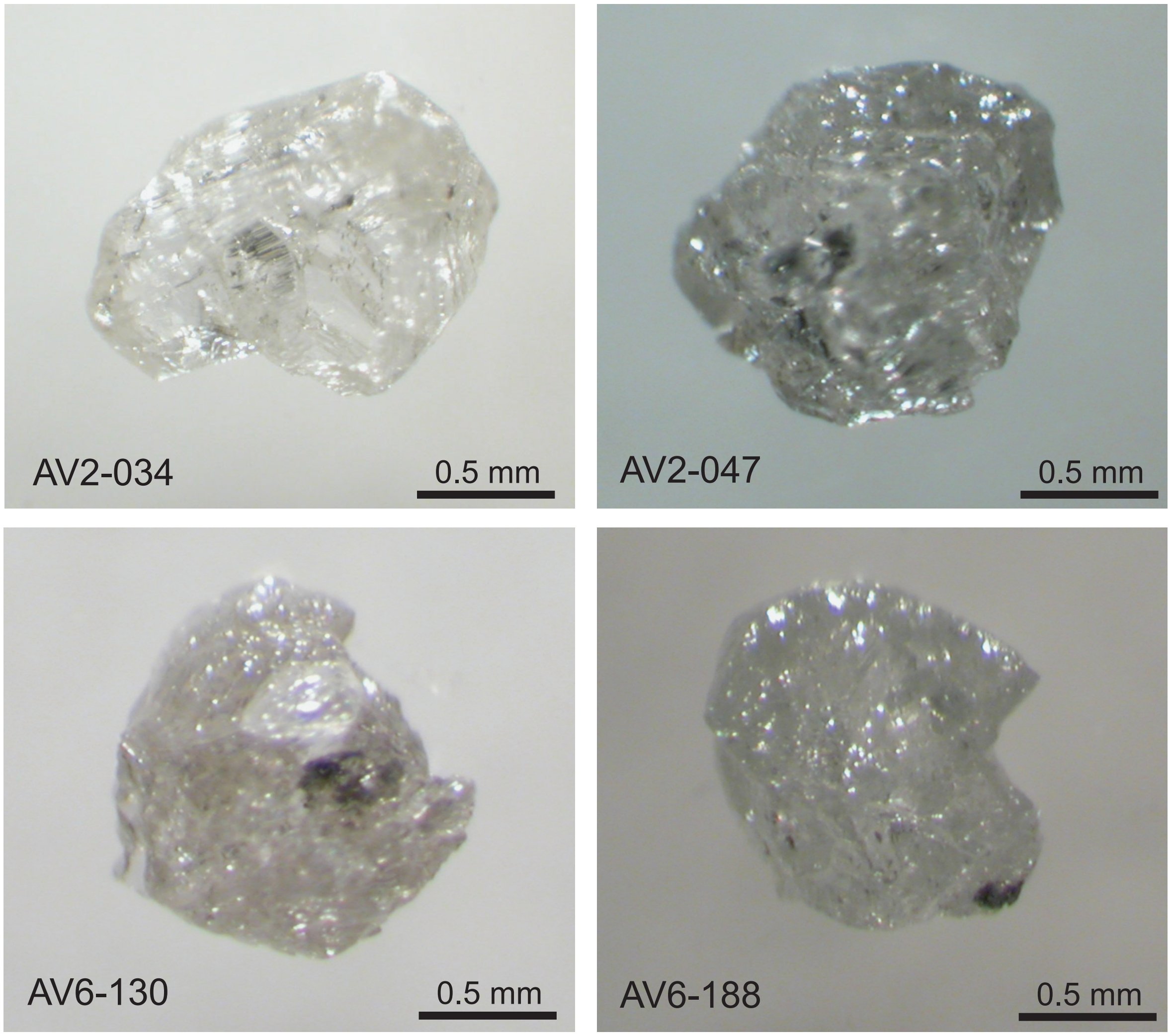

Figure B.12. Graphite flakes, (dark spots) likely formed by decompression.

Appendix C: Supplementary Data

C.1. Annotated Cathodoluminescence Images

The following cathodoluminescence images display SIMS analysis points (red circles). Beside each circle, the $\delta^{13}C$ value (in per mille) above the nitrogen content (in at.ppm) is displayed.

Figure C.1-1. Annotated Cathodoluminescence Images

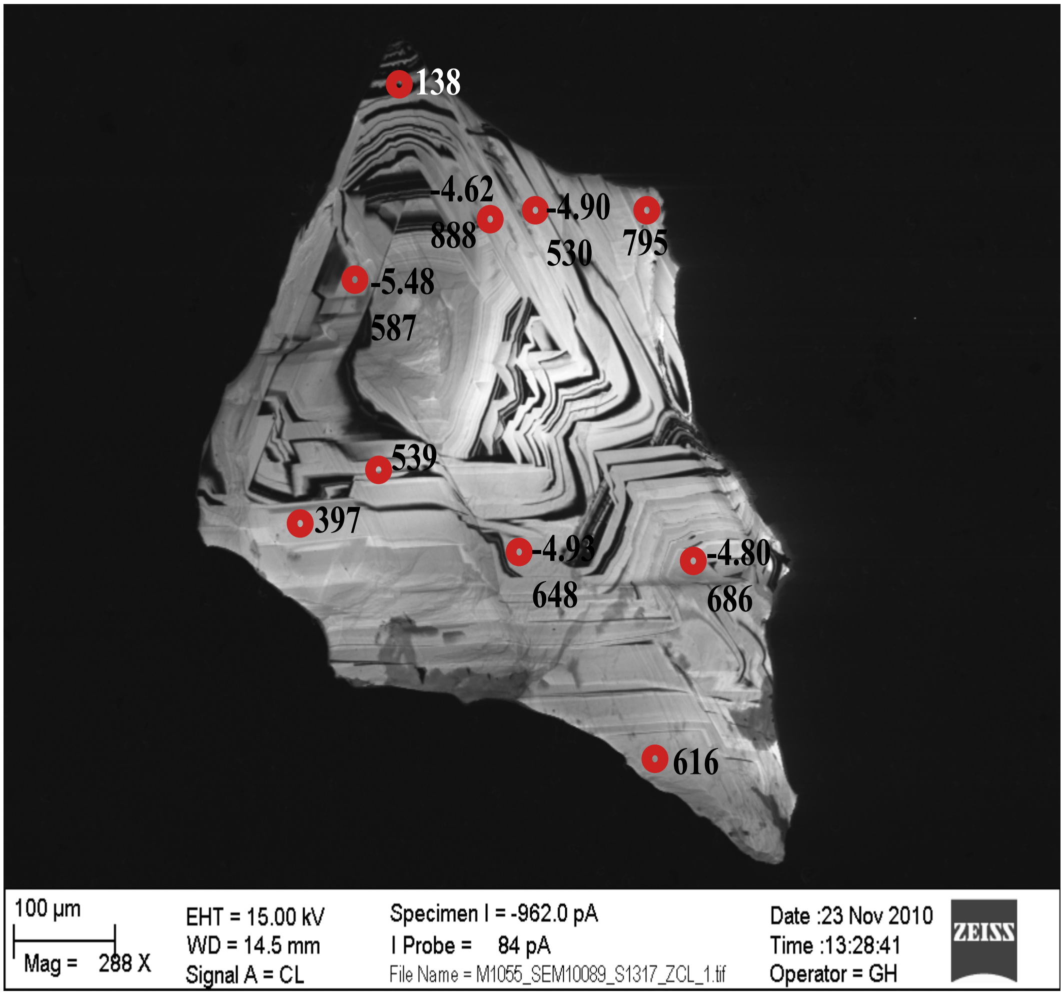

P1001_M1055_IP10144_13C12C_S1317

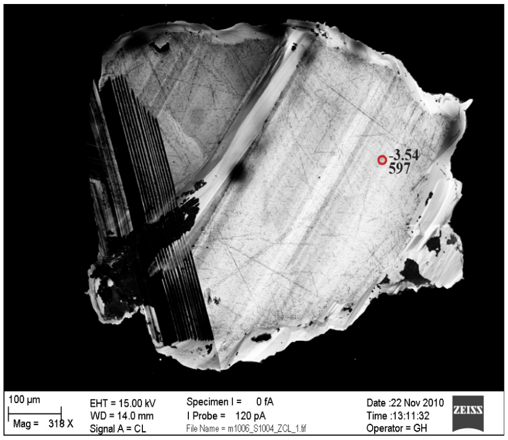

P1001B_M1053_m1006_SEM10087_S1004_ZCL_1

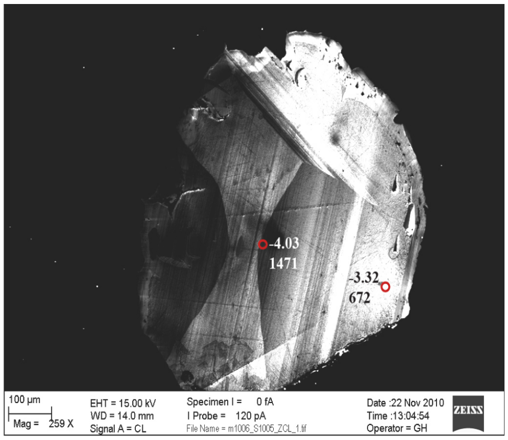

P1001B_M1053_m1006_SEM10087_S1005_ZCL_1

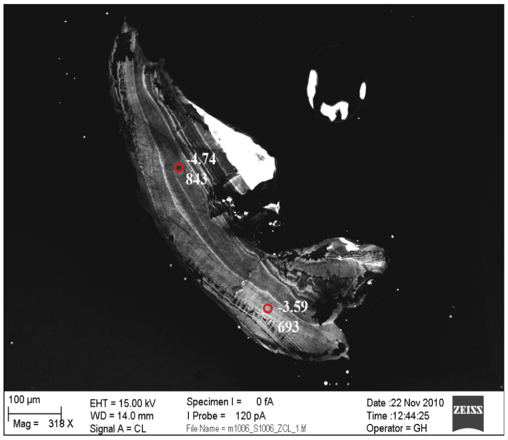

P1001B_M1053_m1006_SEM10087_S1006_ZCL_1

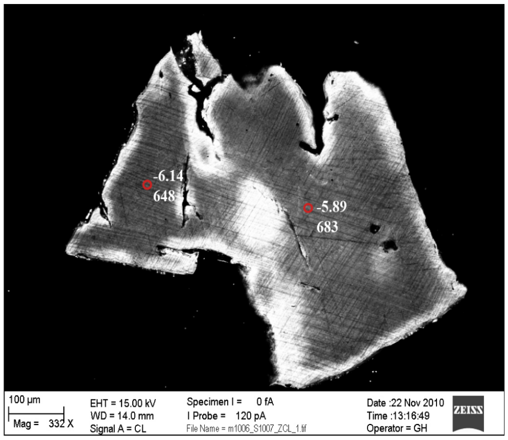

P1001B_M1053_m1006_SEM10087_S1007_ZCL_1

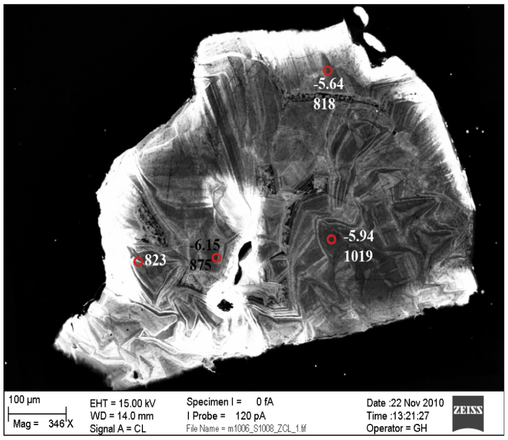

P1001B_M1053_m1006_SEM10087_S1008_ZCL_1

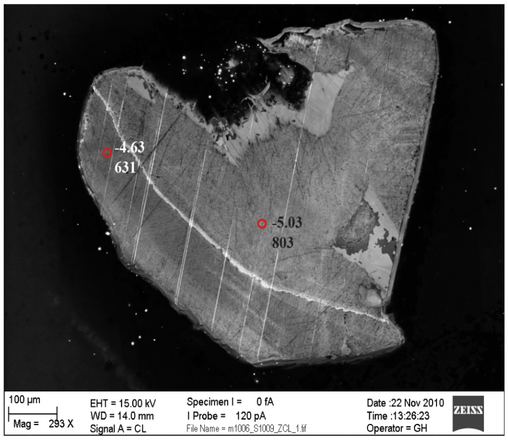

P1001B_M1053_m1006_SEM10087_S1009_ZCL_1

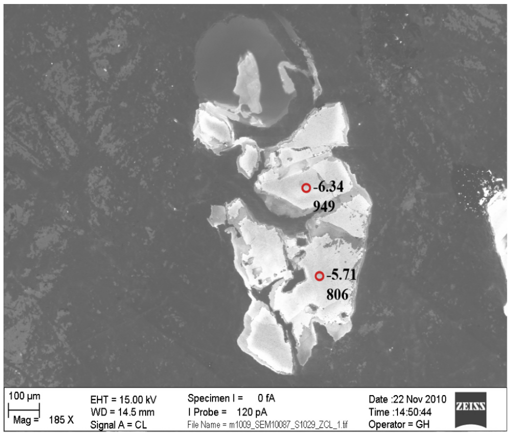

P1001B_M1053_m1009_SEM10087_S1029_ZCL_1

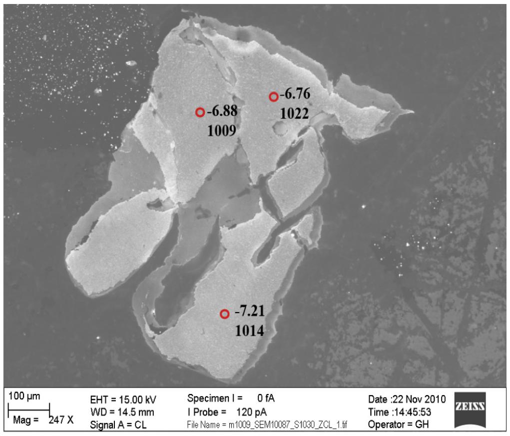

P1001B_M1053_m1009_SEM10087_S1030_ZCL_1

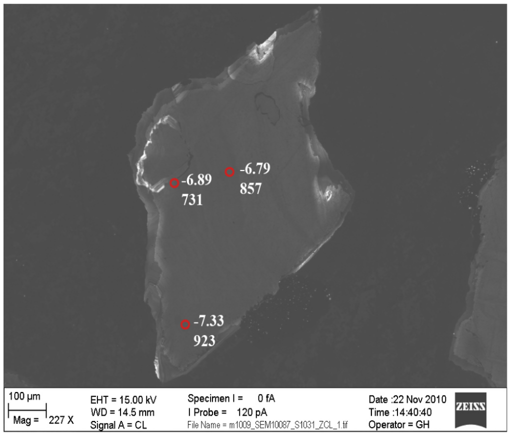

P1001B_M1053_m1009_SEM10087_S1031_ZCL_1

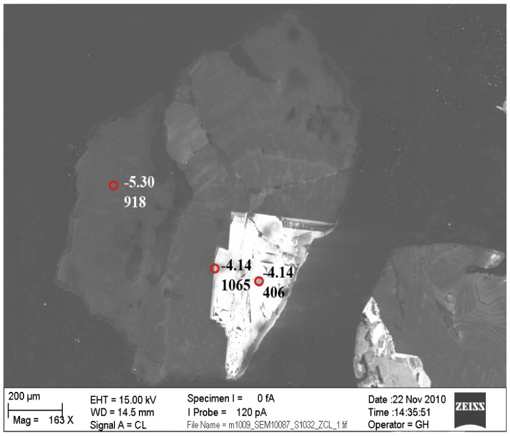

P1001B_M1053_m1009_SEM10087_S1032_ZCL_1

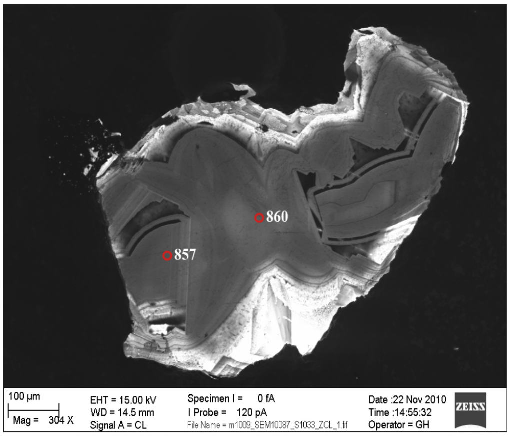

P1001B_M1053_m1009_SEM10087_S1033_ZCL_1

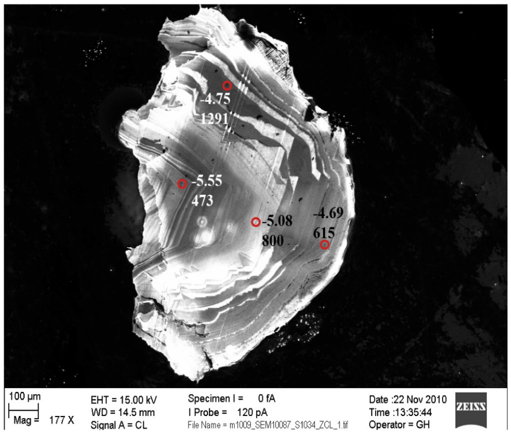

P1001B_M1053_m1009_SEM10087_S1034_ZCL_1

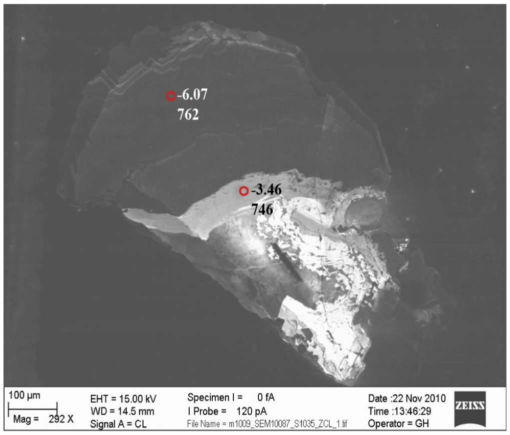

P1001B_M1053_m1009_SEM10087_S1035_ZCL_1

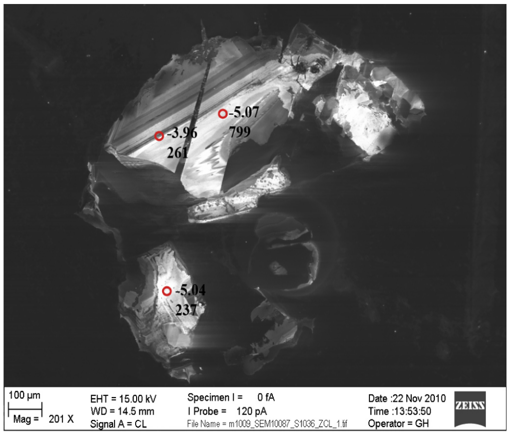

P1001B_M1053_m1009_SEM10087_S1036_ZCL_1

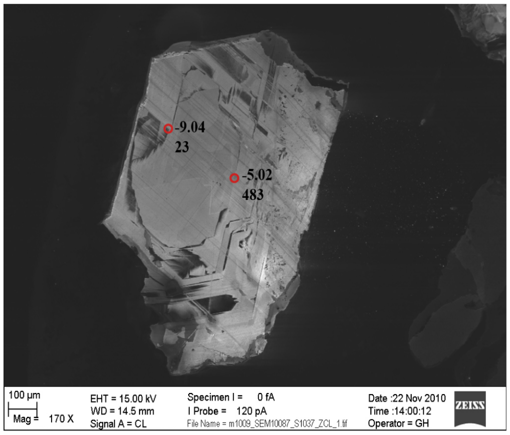

P1001B_M1053_m1009_SEM10087_S1037_ZCL_1

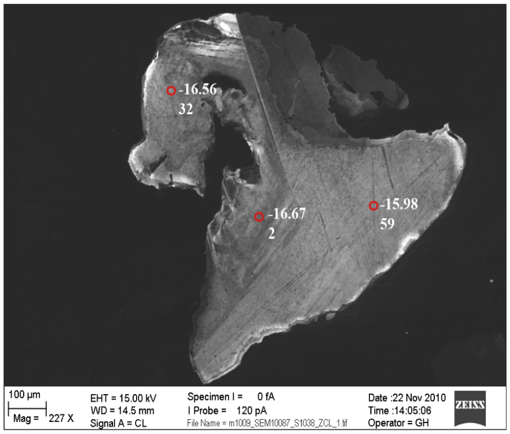

P1001B_M1053_m1009_SEM10087_S1038_ZCL_1

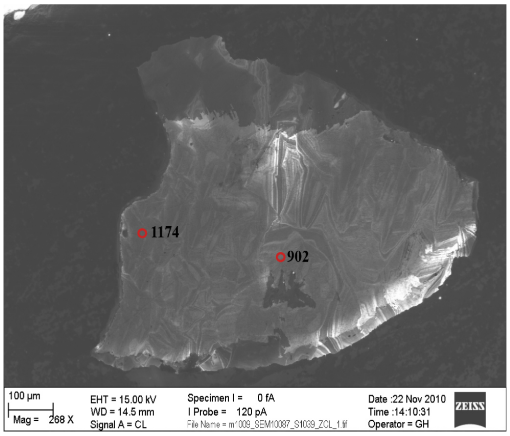

P1001B_M1053_m1009_SEM10087_S1039_ZCL_1

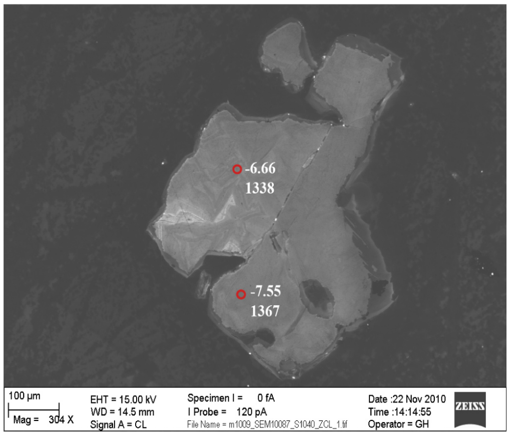

P1001B_M1053_m1009_SEM10087_S1040_ZCL_1

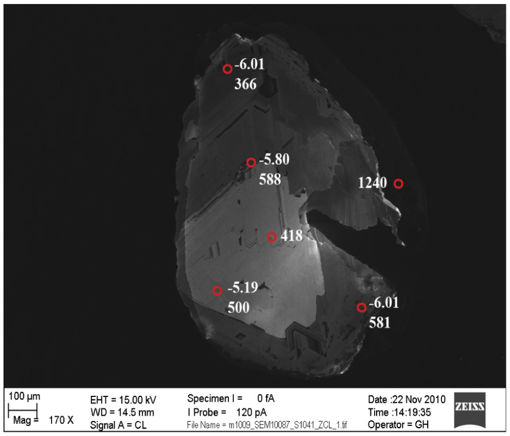

P1001B_M1053_m1009_SEM10087_S1041_ZCL_1

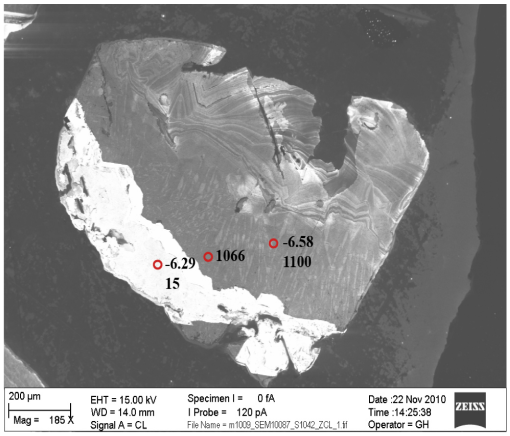

P1001B_M1053_m1009_SEM10087_S1042_ZCL_1

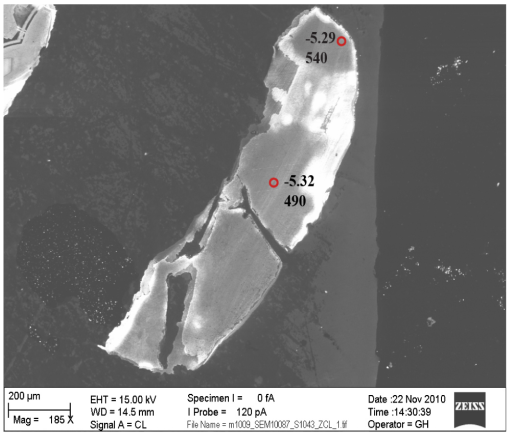

P1001B_M1053_m1009_SEM10087_S1043_ZCL_1

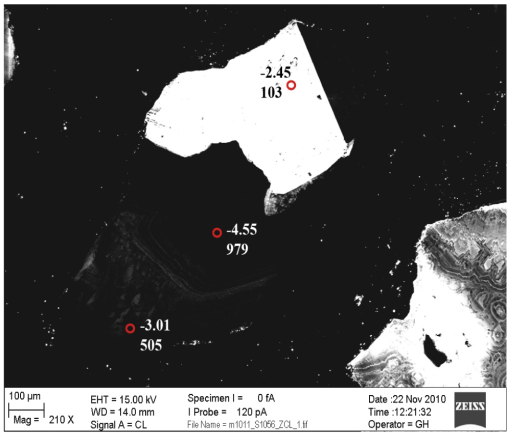

P1001B_M1053_m1011_SEM10087_S1056_ZCL_1

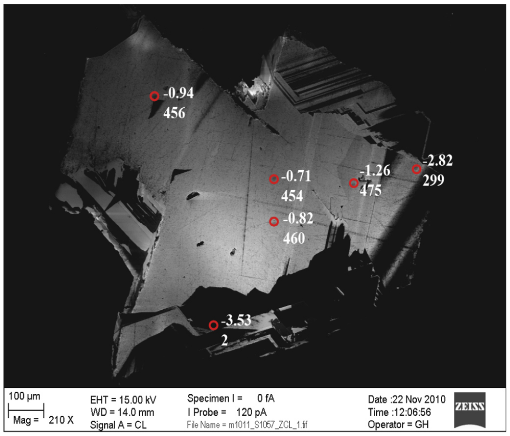

P1001B_M1053_m1011_SEM10087_S1057_ZCL_1

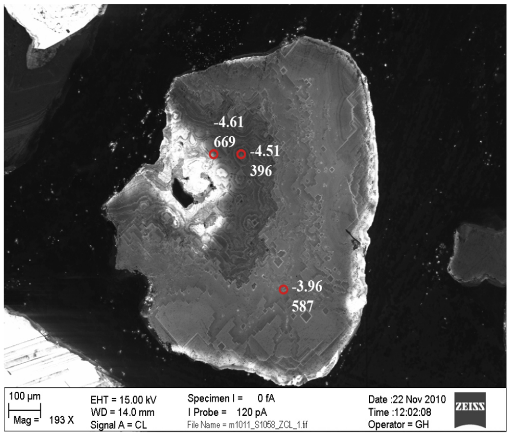

P1001B_M1053_m1011_SEM10087_S1058_ZCL_1

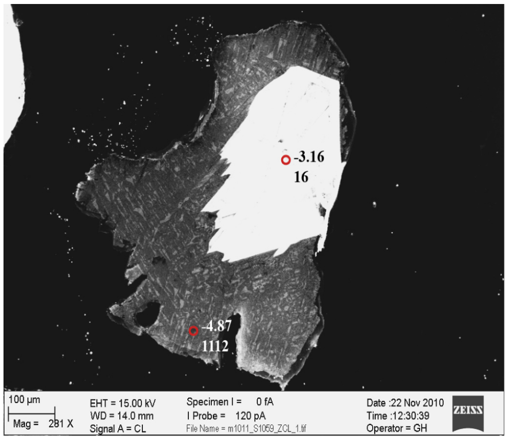

P1001B_M1053_m1011_SEM10087_S1059_ZCL_1

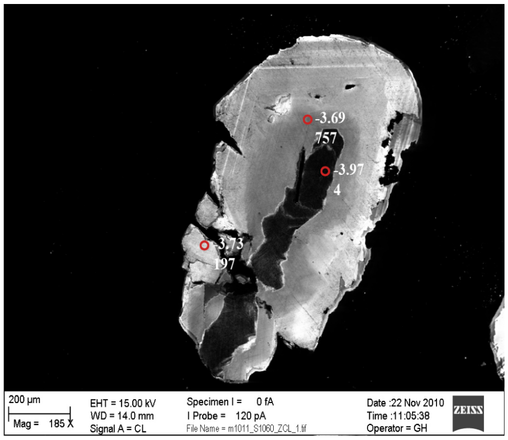

P1001B_M1053_m1011_SEM10087_S1060_ZCL_1

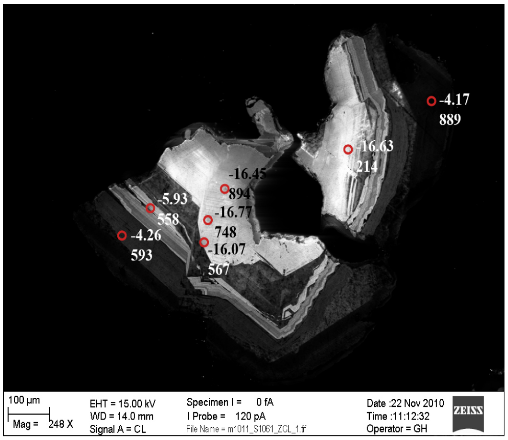

P1001B_M1053_m1011_SEM10087_S1061_ZCL_1

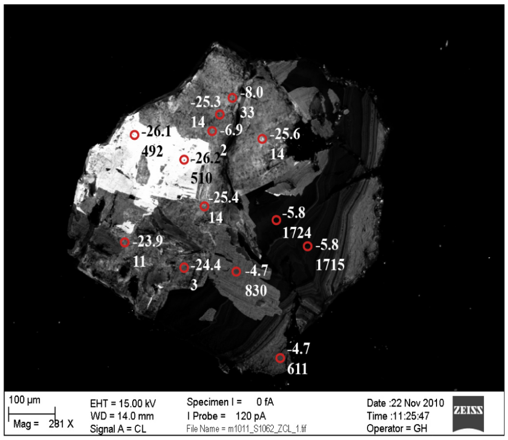

P1001B_M1053_m1011_SEM10087_S1062_ZCL_1

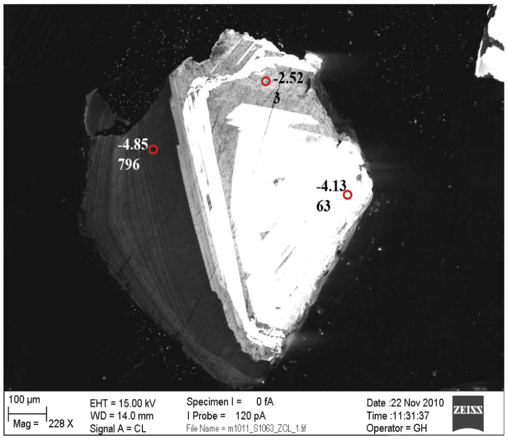

P1001B_M1053_m1011_SEM10087_S1063_ZCL_1

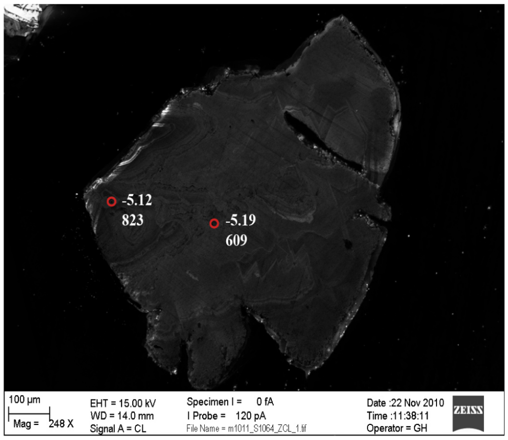

P1001B_M1053_m1011_SEM10087_S1064_ZCL_1

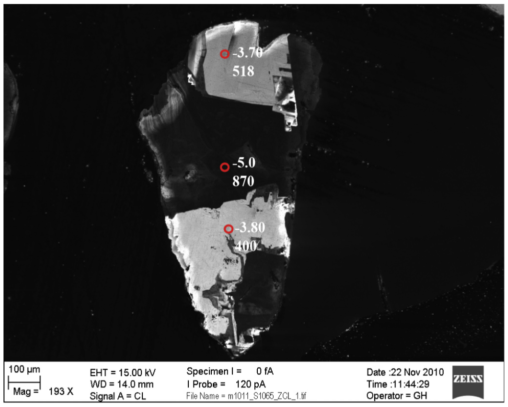

P1001B_M1053_m1011_SEM10087_S1065_ZCL_1

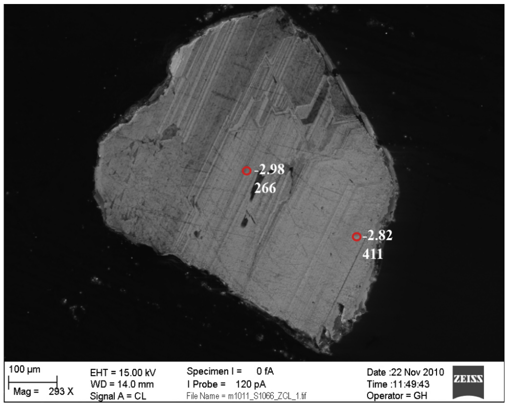

P1001B_M1053_m1011_SEM10087_S1066_ZCL_1

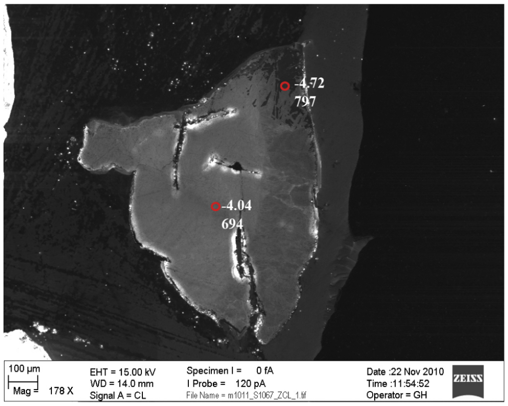

P1001B_M1053_m1011_SEM10087_S1067_ZCL_1

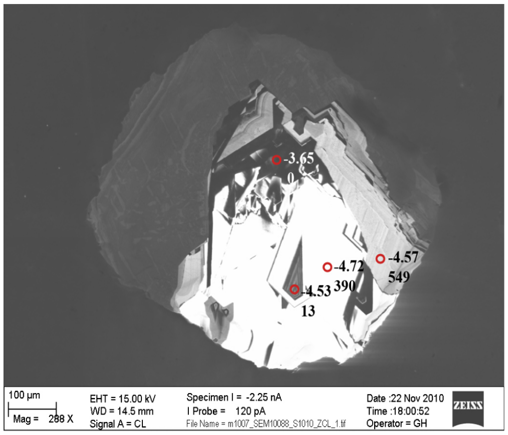

m1007_SEM10088_S1010_ZCL_1

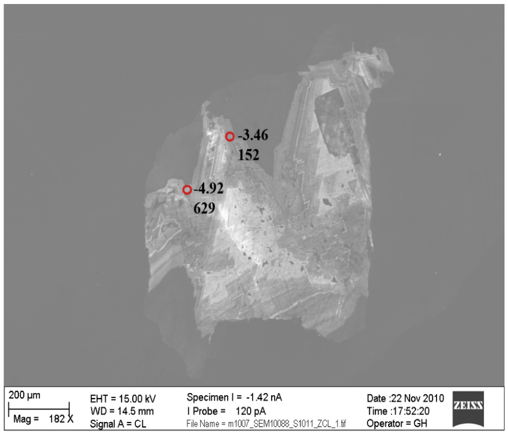

m1007_SEM10088_S1011_ZCL_1

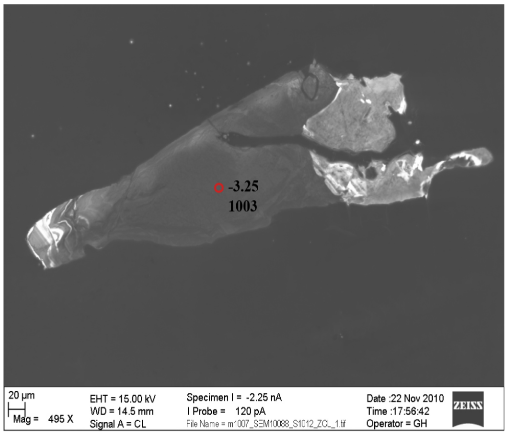

m1007_SEM10088_S1012_ZCL_1

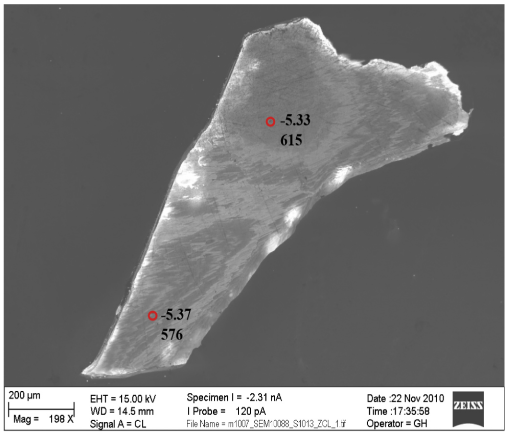

m1007_SEM10088_S1013_ZCL_1

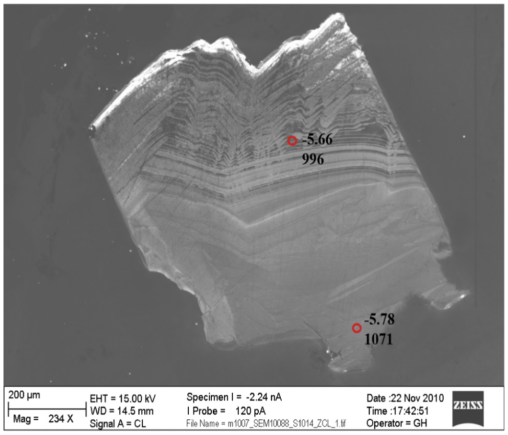

m1007_SEM10088_S1014_ZCL_1

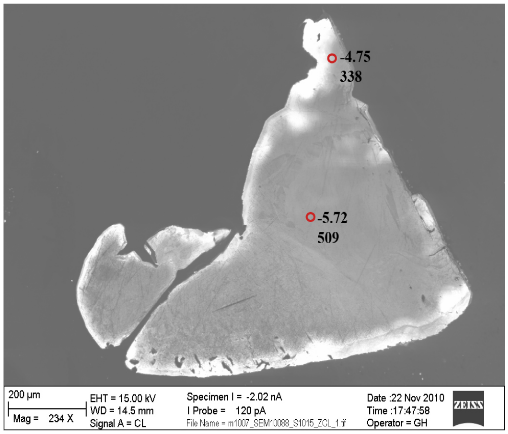

m1007_SEM10088_S1015_ZCL_1

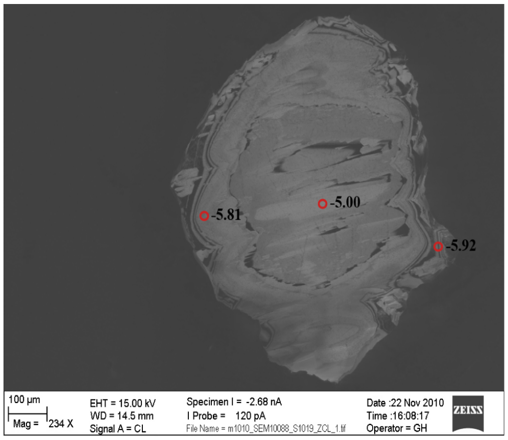

m1010_SEM10088_S1019_ZCL_1

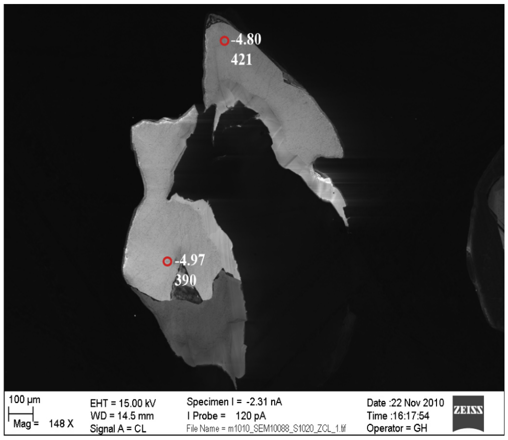

m1010_SEM10088_S1020_ZCL_1

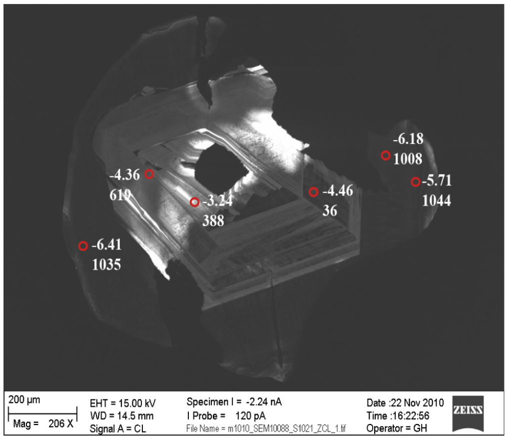

m1010_SEM10088_S1021_ZCL_1

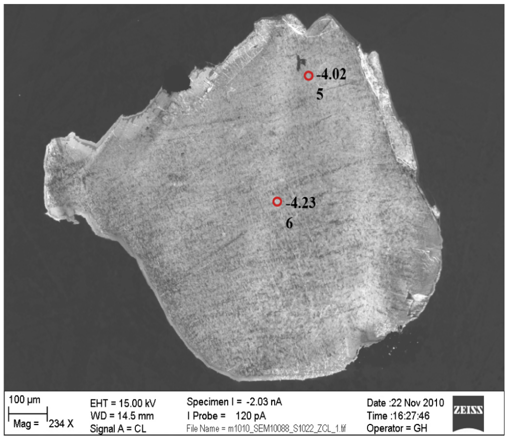

m1010_SEM10088_S1022_ZCL_1

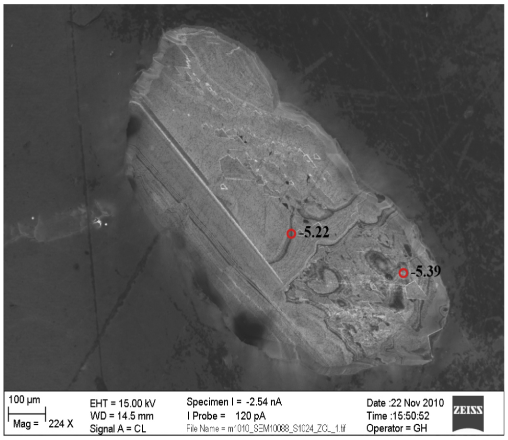

m1010_SEM10088_S1024_ZCL_1

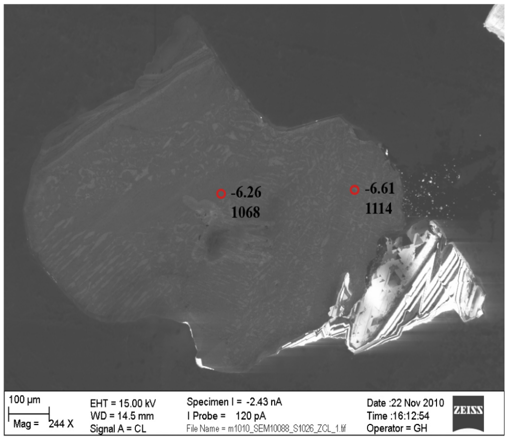

m1010_SEM10088_S1026_ZCL_1

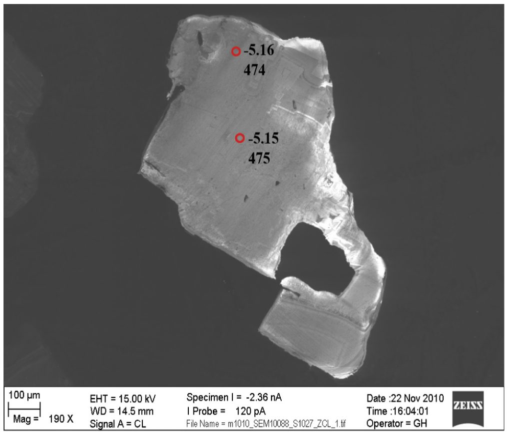

m1010_SEM10088_S1027_ZCL_1

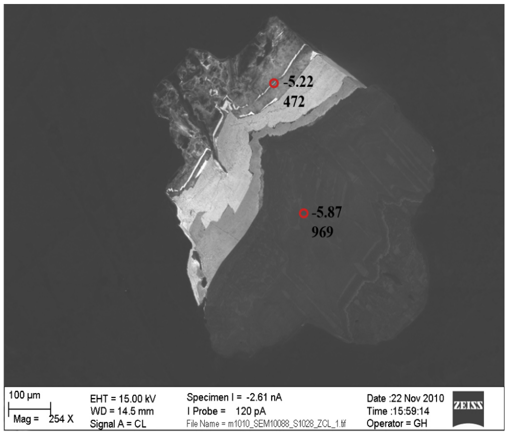

m1010_SEM10088_S1028_ZCL_1

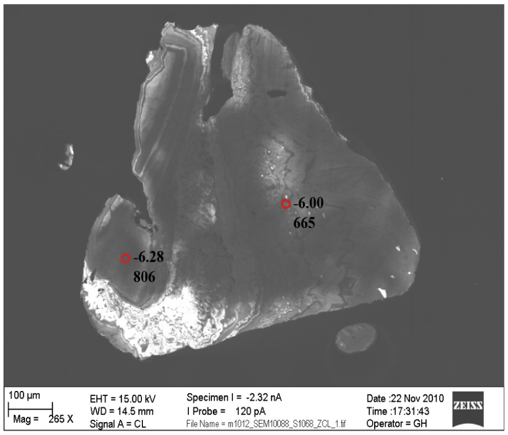

m1012_SEM10088_S1068_ZCL_1

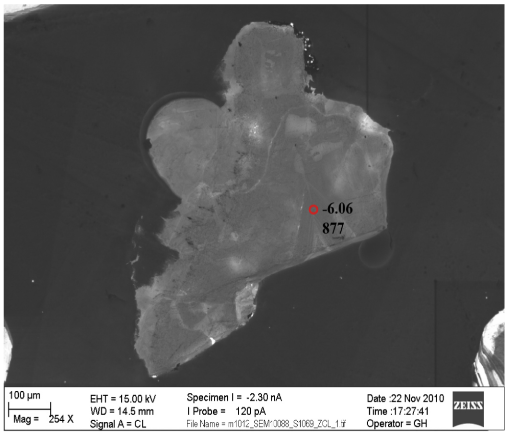

m1012_SEM10088_S1069_ZCL_1

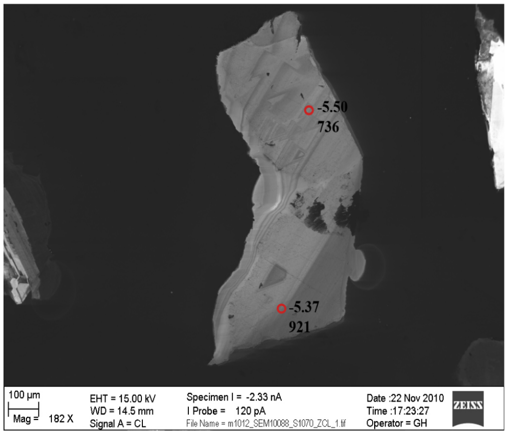

m1012_SEM10088_S1070_ZCL_1

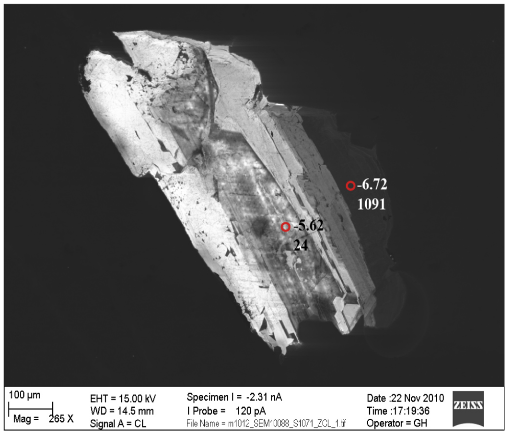

m1012_SEM10088_S1071_ZCL_1

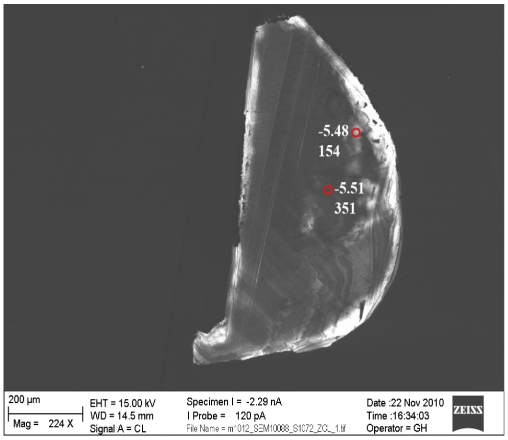

m1012_SEM10088_S1072_ZCL_1

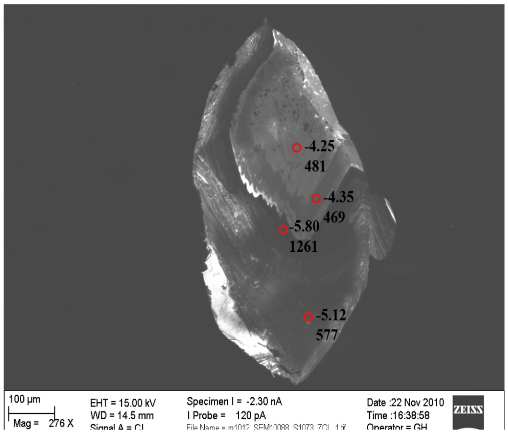

m1012_SEM10088_S1073_ZCL_1

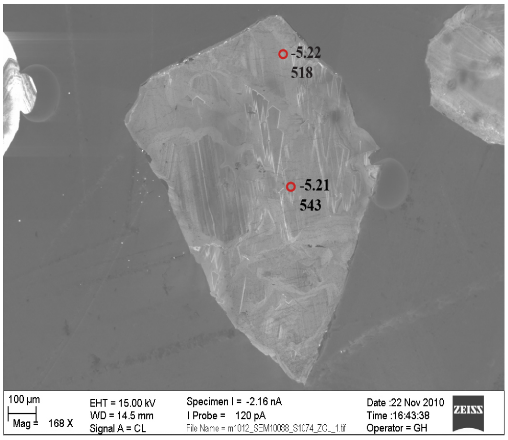

m1012_SEM10088_S1074_ZCL_1

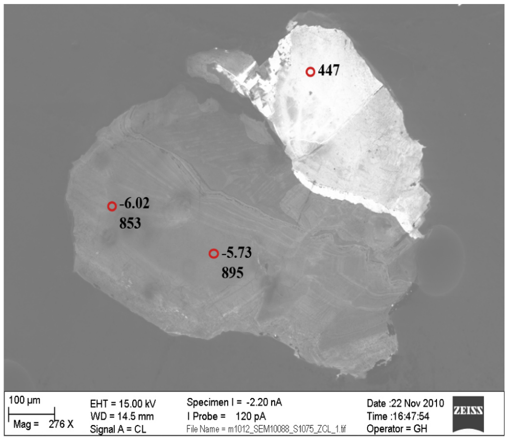

m1012_SEM10088_S1075_ZCL_1

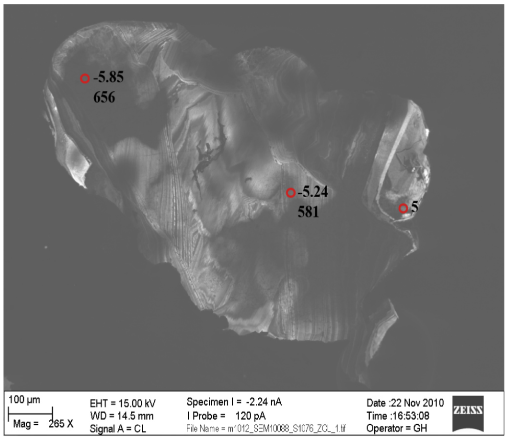

m1012_SEM10088_S1076_ZCL_1

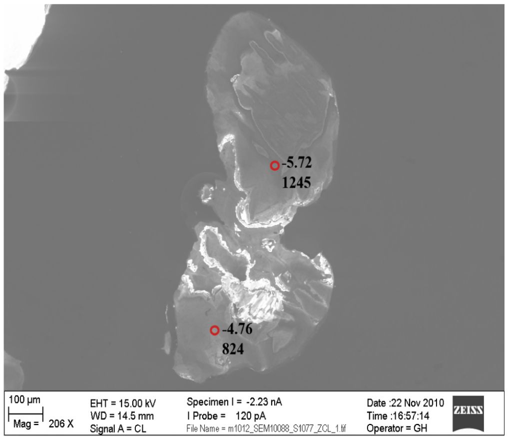

m1012_SEM10088_S1077_ZCL_1

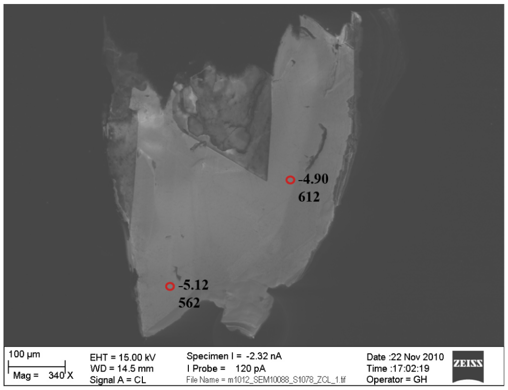

m1012_SEM10088_S1078_ZCL_1

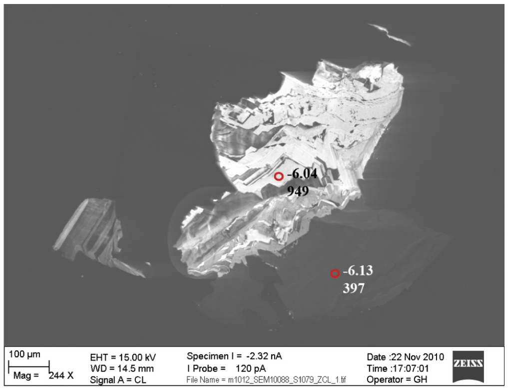

m1012_SEM10088_S1079_ZCL_1

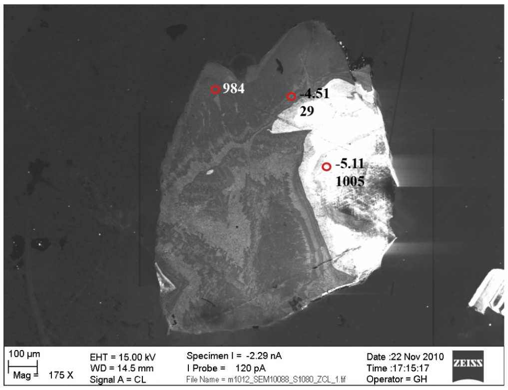

m1012_SEM10088_S1080_ZCL_1

M1054B_m1010_SEM10088_S1025_ZCL_1

Table C-2. CCIM and Corresponding Aviat Sample Numbers	
CCIM #	**Aviat #**
S1004	AV2-026
S1005	AV2-029
S1006	AV2-031
S1007	AV2-050
S1008	AV2-072
S1009	AV2-131
S1010	AV6-024
S1011	AV6-032
S1012	AV6-054
S1013	AV6-171
S1014	AV6-177
S1015	AV6-183
S1019	AV2-017
S1020	AV2-021
S1021	AV2-022
S1022	AV2-023
S1023	AV2-024
S1024	AV2-027
S1025	AV2-028
S1026	AV2-193
S1027	AV2-194
S1028	AV2-196
S1029	AV2-033
S1030	AV2-044
S1031	AV2-084
S1032	AV2-093
S1033	AV2-105
S1034	AV2-107
S1035	AV2-111
S1036	AV2-117
S1037	AV2-144
S1038	AV2-155
S1039	AV2-158
S1040	AV2-168
S1041	AV2-179
S1042	AV2-180
S1043	AV2-189
S1056	AV6-004
S1057	AV6-036
S1058	AV6-040

S1059	AV6-068
S1060	AV6-107
S1061	AV6-111
S1062	AV6-115
S1063	AV6-124
S1064	AV6-131
S1065	AV6-133
S1066	AV6-134
S1067	AV6-136
S1068	AV6-138
S1069	AV6-142
S1070	AV6-148
S1071	AV6-155
S1072	AV6-168
S1073	AV6-169
S1074	AV6-170
S1075	AV6-172
S1076	AV6-173
S1077	AV6-175
S1078	AV6-176
S1079	AV6-181
S1080	AV6-190
S1317	AV6E

Table C-3. SIMS Carbon Results

Spot (CCIM Sample Number)	$^{13}C/^{12}C$	(PDB, ‰)	Error (‰, 2σ)
IP10053_M1015_M1007_S1011_1	0.0111413	-3.46	0.1
IP10053_M1015_M1007_S1011_2	0.0111250	-4.92	0.1
IP10053_M1015_M1007_S1012_1	0.0111436	-3.25	0.1
IP10053_M1015_M1007_S1013_1	0.0111204	-5.33	0.1
IP10053_M1015_M1007_S1013_2	0.0111199	-5.37	0.1
IP10053_M1015_M1007_S1014_1	0.0111167	-5.66	0.1
IP10053_M1015_M1007_S1014_2	0.0111154	-5.78	0.1
IP10053_M1015_M1007_S1015_1	0.0111160	-5.72	0.1
IP10053_M1015_M1007_S1015_2	0.0111269	-4.75	0.1
IP10053_M1015_M1010_S1020_1	0.0111244	-4.97	0.1
IP10053_M1015_M1010_S1020_2	0.0111263	-4.80	0.1
IP10053_M1015_M1010_S1021_1	0.0111438	-3.24	0.1
IP10053_M1015_M1010_S1021_2	0.0111313	-4.36	0.1
IP10053_M1015_M1010_S1021_3	0.0111302	-4.46	0.1
IP10053_M1015_M1010_S1021_4	0.0111083	-6.41	0.1
IP10053_M1015_M1010_S1021_5	0.0111109	-6.18	0.1
IP10053_M1015_M1010_S1021_6	0.0111161	-5.71	0.1
IP10053_M1015_M1010_S1022_1	0.0111327	-4.23	0.1
IP10053_M1015_M1010_S1022_2	0.0111350	-4.02	0.1
IP10053_M1015_M1010_S1023_1	0.0111290	-4.57	0.1
IP10053_M1015_M1010_S1023_2	0.0111254	-4.89	0.1
IP10053_M1015_M1010_S1024_1	0.0111217	-5.22	0.1
IP10053_M1015_M1010_S1024_2	0.0111197	-5.39	0.1
IP10053_M1015_M1010_S1025_1	0.0111237	-5.03	0.1
IP10053_M1015_M1010_S1025_2	0.0111122	-6.06	0.1
IP10053_M1015_M1010_S1026_1	0.0111100	-6.26	0.1
IP10053_M1015_M1010_S1026_2	0.0111061	-6.61	0.1
IP10053_M1015_M1010_S1027_1	0.0111224	-5.15	0.1
IP10053_M1015_M1010_S1027_2	0.0111223	-5.16	0.1
IP10053_M1015_M1010_S1028_1	0.0111144	-5.87	0.1
IP10053_M1015_M1010_S1028_2	0.0111216	-5.22	0.1
IP10053_M1015_M1012_S1068_1	0.0111130	-6.00	0.1
IP10053_M1015_M1012_S1068_2	0.0111098	-6.28	0.1
IP10053_M1015_M1012_S1069_1	0.0111122	-6.06	0.1
IP10053_M1015_M1012_S1070_1	0.0111200	-5.37	0.1
IP10053_M1015_M1012_S1070_2	0.0111185	-5.50	0.1
IP10053_M1015_M1012_S1071_1	0.0111171	-5.62	0.1
IP10053_M1015_M1012_S1071_2	0.0111049	-6.72	0.1
IP10053_M1015_M1012_S1072_1	0.0111184	-5.51	0.1
IP10053_M1015_M1012_S1072_2	0.0111187	-5.48	0.1

IP10053_M1015_M1012_S1073_1	0.0111325	-4.25	0.1
IP10053_M1015_M1012_S1073_2	0.0111313	-4.35	0.1
IP10053_M1015_M1012_S1073_3	0.0111152	-5.80	0.1
IP10053_M1015_M1012_S1073_4	0.0111227	-5.12	0.1
IP10053_M1015_M1012_S1074_1	0.0111217	-5.21	0.1
IP10053_M1015_M1012_S1074_2	0.0111216	-5.22	0.1
IP10053_M1015_M1012_S1075_1	0.0111159	-5.73	0.1
IP10053_M1015_M1012_S1075_2	0.0111127	-6.02	0.1
IP10053_M1015_M1012_S1076_1	0.0111215	-5.24	0.1
IP10053_M1015_M1012_S1076_2	0.0111146	-5.85	0.1
IP10053_M1015_M1012_S1077_1	0.0111268	-4.76	0.1
IP10053_M1015_M1012_S1077_2	0.0111160	-5.72	0.1
IP10053_M1015_M1012_S1078_1	0.0111252	-4.90	0.1
IP10053_M1015_M1012_S1078_2	0.0111227	-5.12	0.1
IP10053_M1015_M1012_S1079_1	0.0111125	-6.04	0.1
IP10053_M1015_M1012_S1079_2	0.0111115	-6.13	0.1
IP10053_M1015_M1012_S1080_1	0.0111228	-5.11	0.1
IP10053_M1015_M1012_S1080_2	0.0111295	-4.51	0.1
IP10053_M1015_M1007_S1010_1	0.0111289	-4.57	0.1
IP10053_M1015_M1007_S1010_2	0.0111273	-4.72	0.1
IP10053_M1015_M1007_S1010_3	0.0111392	-3.65	0.1
IP10053_M1015_M1007_S1010_4	0.0111294	-4.53	0.1
IP10053_M1015_M1010_S1019_1	0.0111241	-5.00	0.1
IP10053_M1015_M1010_S1019_2	0.0111150	-5.81	0.1
IP10053_M1015_M1010_S1019_3	0.0111138	-5.92	0.1
IP10054_M1016_M1006_S1004_1	0.0111404	-3.54	0.1
IP10054_M1016_M1006_S1008_1	0.0111136	-5.94	0.1
IP10054_M1016_M1006_S1008_2	0.0111170	-5.64	0.1
IP10054_M1016_M1006_S1008_3	0.0111113	-6.15	0.1
IP10054_M1016_M1009_S1035_1	0.0111413	-3.46	0.1
IP10054_M1016_M1009_S1035_2	0.0111121	-6.07	0.1
IP10054_M1016_M1009_S1043_1	0.0111206	-5.32	0.1
IP10054_M1016_M1009_S1043_2	0.0111209	-5.29	0.1
IP10054_M1016_M1011_S1060_1	0.0111356	-3.97	0.1
IP10054_M1016_M1011_S1060_2	0.0111388	-3.69	0.1
IP10054_M1016_M1011_S1060_3	0.0111383	-3.73	0.1
IP10054_M1016_M1011_S1061_1	0.0109961	-16.45	0.1
IP10054_M1016_M1011_S1061_2	0.0111137	-5.93	0.1
IP10054_M1016_M1011_S1061_3	0.0111323	-4.26	0.1
IP10054_M1016_M1011_S1061_4	0.0111334	-4.17	0.1
IP10054_M1016_M1011_S1063_1	0.0111339	-4.13	0.1
IP10054_M1016_M1006_S1005_1	0.0111349	-4.03	0.1
IP10054_M1016_M1006_S1005_2	0.0111429	-3.32	0.1

IP10054_M1016_M1006_S1006_1	0.0111399	-3.59	0.1
IP10054_M1016_M1006_S1006_2	0.0111270	-4.74	0.1
IP10054_M1016_M1006_S1007_1	0.0111141	-5.89	0.1
IP10054_M1016_M1006_S1007_2	0.0111114	-6.14	0.1
IP10054_M1016_M1006_S1009_1	0.0111238	-5.03	0.1
IP10054_M1016_M1006_S1009_2	0.0111282	-4.63	0.1
IP10054_M1016_M1011_S1056_1	0.0111292	-4.55	0.1
IP10054_M1016_M1011_S1056_2	0.0111464	-3.01	0.1
IP10054_M1016_M1011_S1056_3	0.0111526	-2.45	0.1
IP10054_M1016_M1011_S1057_1	0.0111721	-0.71	0.1
IP10054_M1016_M1011_S1057_2	0.0111485	-2.82	0.1
IP10054_M1016_M1011_S1058_1	0.0111357	-3.96	0.1
IP10054_M1016_M1011_S1058_2	0.0111285	-4.61	0.1
IP10054_M1016_M1011_S1059_1	0.0111446	-3.16	0.1
IP10054_M1016_M1011_S1059_2	0.0111255	-4.87	0.1
IP10054_M1016_M1011_S1062_1	0.0108958	-25.42	0.1
IP10054_M1016_M1011_S1062_2	0.0108885	-26.07	0.1
IP10054_M1016_M1011_S1063_2	0.0111257	-4.85	0.1
IP10054_M1016_M1011_S1063_3	0.0111518	-2.52	0.1
IP10054_M1016_M1011_S1064_1	0.0111219	-5.19	0.1
IP10054_M1016_M1011_S1064_2	0.0111228	-5.12	0.1
IP10054_M1016_M1011_S1065_1	0.0111375	-3.80	0.1
IP10054_M1016_M1011_S1065_2	0.0111238	-5.03	0.1
IP10054_M1016_M1011_S1065_3	0.0111386	-3.70	0.1
IP10054_M1016_M1011_S1066_1	0.0111467	-2.98	0.1
IP10054_M1016_M1011_S1066_2	0.0111484	-2.82	0.1
IP10054_M1016_M1011_S1067_1	0.0111348	-4.04	0.1
IP10054_M1016_M1011_S1067_2	0.0111272	-4.72	0.1
IP10055_M1016_M1011_S1057_3	0.0111708	-0.82	0.1
IP10055_M1016_M1011_S1057_4	0.0111405	-3.53	0.1
IP10055_M1016_M1011_S1057_5	0.0111695	-0.94	0.1
IP10055_M1016_M1011_S1057_6	0.0111660	-1.26	0.1
IP10055_M1016_M1011_S1058_3	0.0111296	-4.51	0.1
IP10055_M1016_M1011_S1061_5	0.0109925	-16.77	0.1
IP10055_M1016_M1011_S1061_6	0.0109941	-16.63	0.1
IP10055_M1016_M1011_S1061_7	0.0110003	-16.07	0.1
IP10055_M1016_M1011_S1062_3	0.0111270	-4.74	0.1
IP10055_M1016_M1011_S1062_4	0.0111152	-5.80	0.1
IP10055_M1016_M1011_S1062_5	0.0108941	-25.57	0.1
IP10055_M1016_M1011_S1062_6	0.0111275	-4.69	0.1
IP10055_M1016_M1011_S1062_7	0.0111152	-5.79	0.1
IP10055_M1016_M1011_S1062_8	0.0108875	-26.16	0.1
IP10055_M1016_M1011_S1062_9	0.0109075	-24.38	0.1

IP10055_M1016_M1011_S1062_10	0.0109132	-23.87	0.1
IP10055_M1016_M1011_S1062_11	0.0110907	-7.99	0.1
IP10055_M1016_M1011_S1062_12	0.0108974	-25.28	0.1
IP10055_M1016_M1011_S1062_13	0.0111034	-6.85	0.1
IP10056_M1016_M1009_S1029_1	0.0111091	-6.34	0.2
IP10056_M1016_M1009_S1029_2	0.0111162	-5.71	0.2
IP10056_M1016_M1009_S1030_1	0.0111031	-6.88	0.2
IP10056_M1016_M1009_S1030_2	0.0111045	-6.76	0.2
IP10056_M1016_M1009_S1030_3	0.0110994	-7.21	0.2
IP10056_M1016_M1009_S1031_1	0.0111041	-6.79	0.2
IP10056_M1016_M1009_S1031_2	0.0111030	-6.89	0.2
IP10056_M1016_M1009_S1031_3	0.0110980	-7.33	0.2
IP10056_M1016_M1009_S1032_1	0.0111337	-4.14	0.2
IP10056_M1016_M1009_S1032_2	0.0111337	-4.14	0.2
IP10056_M1016_M1009_S1032_3	0.0111207	-5.30	0.2
IP10056_M1016_M1009_S1034_1	0.0111179	-5.55	0.2
IP10056_M1016_M1009_S1034_2	0.0111269	-4.75	0.2
IP10056_M1016_M1009_S1034_3	0.0111275	-4.69	0.2
IP10056_M1016_M1009_S1034_4	0.0111232	-5.08	0.2
IP10056_M1016_M1009_S1036_1	0.0111237	-5.04	0.2
IP10056_M1016_M1009_S1036_2	0.0111357	-3.96	0.2
IP10056_M1016_M1009_S1036_3	0.0111234	-5.07	0.2
IP10056_M1016_M1009_S1037_1	0.0111239	-5.02	0.2
IP10056_M1016_M1009_S1037_2	0.0110790	-9.04	0.2
IP10056_M1016_M1009_S1038_1	0.0109937	-16.67	0.2
IP10056_M1016_M1009_S1038_2	0.0110014	-15.98	0.2
IP10056_M1016_M1009_S1038_3	0.0109948	-16.56	0.2
IP10056_M1016_M1009_S1040_1	0.0110956	-7.55	0.2
IP10056_M1016_M1009_S1040_2	0.0111055	-6.66	0.2
IP10056_M1016_M1009_S1041_1	0.0111219	-5.19	0.2
IP10056_M1016_M1009_S1041_2	0.0111128	-6.01	0.2
IP10056_M1016_M1009_S1041_3	0.0111151	-5.80	0.2
IP10056_M1016_M1009_S1041_4	0.0111128	-6.01	0.2
IP10056_M1016_M1009_S1042_1	0.0111096	-6.29	0.2
IP10056_M1016_M1009_S1042_2	0.0111064	-6.58	0.2
P1001_M1055_IP10144_13C12C_S1317_1	0.0111264	-4.80	0.3
P1001_M1055_IP10144_13C12C_S1317_2	0.0111248	-4.93	0.3
P1001_M1055_IP10144_13C12C_S1317_3	0.0111187	-5.48	0.3
P1001_M1055_IP10144_13C12C_S1317_4	0.0111283	-4.62	0.3
P1001_M1055_IP10144_13C12C_S1317_5	0.0111252	-4.90	0.3

Table C-4. SIMS Nitrogen Results

Spot with CCIM Sample Number	**N (at. ppm)**	**Internal +/-**	**External +/-**
		95% cl[1]	**95% cl[2]**
P1001B_M1053_m1006_IP10142_24C26CN_L'2FC2_S1005_2_2@1	672	1.7	68
P1001B_M1053_m1006_IP10142_24C26CN_L'2FC2_S1006_1_2@1	693	2.4	71
P1001B_M1053_m1006_IP10142_24C26CN_L'2FC2_S1006_2_2@1	843	3.1	88
P1001B_M1053_m1006_IP10142_24C26CN_L'2FC2_S1007_1_2@1	683	1.7	69
P1001B_M1053_m1006_IP10142_24C26CN_L'2FC2_S1007_2_2@1	648	1.0	65
P1001B_M1053_m1006_IP10142_24C26CN_L'2FC2_S1008_1_2@2	1019	1.5	103
P1001B_M1053_m1006_IP10142_24C26CN_L'2FC2_S1008_2_2@2	818	3.2	86
P1001B_M1053_m1006_IP10142_24C26CN_L'2FC2_S1008_3_2@2	875	4.0	94
P1001B_M1053_m1006_IP10142_24C26CN_L'2FC2_S1008_4_1@2	870	1.0	87
P1001B_M1053_m1006_IP10142_24C26CN_L'2FC2_S1008_4_1@3	777	2.0	79
P1001B_M1053_m1006_IP10142_24C26CN_L'2FC2_S1009_1_2@3	803	1.3	81
P1001B_M1053_m1006_IP10142_24C26CN_L'2FC2_S1009_2_2@3	631	2.3	65
P1001B_M1053_m1006_IP10142_24C26CN_L'2FC2_S1004_1_2	593	2.3	61
P1001B_M1053_m1006_IP10142_24C26CN_L'2FC2_S1004_1_3	602	0.9	60
P1001B_M1053_m1006_IP10142_24C26CN_L'2FC2_S1005_1_2	1471	2.9	153
P1001B_M1053_m1009_IP10142_24C26CN_L'2FC2_S1041_1_2@3	503	1.8	51
P1001B_M1053_m1009_IP10142_24C26CN_L'2FC2_S1041_2_2@3	581	2.0	59
P1001B_M1053_m1009_IP10142_24C26CN_L'2FC2_S1041_3_2@3	588	2.1	60
P1001B_M1053_m1009_IP10142_24C26CN_L'2FC2_S1041_4_2@3	359	0.6	36
P1001B_M1053_m1009_IP10142_24C26CN_L'2FC2_S1042_1_2@3	15	0.2	1
P1001B_M1053_m1009_IP10142_24C26CN_L'2FC2_S1042_1_3@3	16	0.2	2
P1001B_M1053_m1009_IP10142_24C26CN_L'2FC2_S1042_2_2@3	1100	3.8	118
P1001B_M1053_m1009_IP10142_24C26CN_L'2FC2_S1042_3_1@3	1066	4.0	115
P1001B_M1053_m1009_IP10142_24C26CN_L'2FC2_S1041_1_3	496	1.6	50
P1001B_M1053_m1009_IP10142_24C26CN_L'2FC2_S1041_6_2	418	1.0	42
P1001B_M1053_m1009_IP10142_24C26CN_L'2FC2_S1041_5_2	1240	4.3	135
P1001B_M1053_m1009_IP10142_24C26CN_L'2FC2_S1041_4_3	372	0.2	37
P1001B_M1053_m1009_IP10142_24C26CN_L'2FC2_S1042_1_4	15	0.1	1
P1001B_M1053_m1009_IP10142_24C26CN_L'2FC2_S1029_1_2	949	1.9	97
P1001B_M1053_m1009_IP10142_24C26CN_L'2FC2_S1043_2_2	540	1.3	54
P1001B_M1053_m1009_IP10142_24C26CN_L'2FC2_S1043_1_2	490	2.4	50
P1001B_M1053_m1009_IP10142_24C26CN_L'2FC2_S1033_2_1	857	3.3	90
P1001B_M1053_m1009_IP10142_24C26CN_L'2FC2_S1033_1_1	860	3.0	90
P1001B_M1053_m1009_IP10142_24C26CN_L'2FC2_S1032_3_2	918	2.4	95
P1001B_M1053_m1009_IP10142_24C26CN_L'2FC2_S1032_2_2	406	1.6	41
P1001B_M1053_m1009_IP10142_24C26CN_L'2FC2_S1032_1_2	1065	3.1	112
P1001B_M1053_m1009_IP10142_24C26CN_L'2FC2_S1029_2_2	806	3.5	85
P1001B_M1053_m1009_IP10142_24C26CN_L'2FC2_S1040_2_2	1338	3.1	140
P1001B_M1053_m1009_IP10142_24C26CN_L'2FC2_S1040_1_2	1367	2.9	142
P1001B_M1053_m1009_IP10142_24C26CN_L'2FC2_S1039_2_1	1174	4.0	126
P1001B_M1053_m1009_IP10142_24C26CN_L'2FC2_S1039_1_1	902	3.5	96
P1001B_M1053_m1009_IP10142_24C26CN_L'2EM_S1038_3_5	32	0.2	3
P1001B_M1053_m1009_IP10142_24C26CN_L'2FC2_S1038_2_2	59	0.5	6
P1001B_M1053_m1009_IP10142_24C26CN_L'2EM_S1038_1_7	2	0.0	0
P1001B_M1053_m1009_IP10142_24C26CN_L'2FC2_S1037_2_2	23	0.2	2
P1001B_M1053_m1009_IP10142_24C26CN_L'2FC2_S1037_1_2	483	1.4	49
P1001B_M1053_m1009_IP10142_24C26CN_L'2FC2_S1036_3_2	799	4.6	88
P1001B_M1053_m1009_IP10142_24C26CN_L'2FC2_S1036_2_2	260	6.2	31
P1001B_M1053_m1009_IP10142_24C26CN_L'2FC2_S1036_1_2	237	2.1	24
P1001B_M1053_m1009_IP10142_24C26CN_L'2FC2_S1035_4_2	800	1.7	81
P1001B_M1053_m1009_IP10142_24C26CN_L'2FC2_S1035_3_2	615	1.9	63
P1001B_M1053_m1009_IP10142_24C26CN_L'2FC2_S1035_2_2	1291	5.4	147
P1001B_M1053_m1009_IP10142_24C26CN_L'2FC2_S1035_1_2	473	2.1	48
P1001B_M1053_m1009_IP10142_24C26CN_L'2FC2_S1034_2_2	762	2.0	78
P1001B_M1053_m1009_IP10142_24C26CN_L'2FC2_S1034_1_2	746	1.5	76
P1001B_M1053_m1009_IP10142_24C26CN_L'2FC2_S1031_3_2	923	2.6	95
P1001B_M1053_m1009_IP10142_24C26CN_L'2FC2_S1031_2_2	731	1.2	74
P1001B_M1053_m1009_IP10142_24C26CN_L'2FC2_S1031_1_2	857	3.2	90
P1001B_M1053_m1009_IP10142_24C26CN_L'2FC2_S1030_3_2	1014	3.9	109
P1001B_M1053_m1009_IP10142_24C26CN_L'2FC2_S1030_2_2	1022	3.5	108
P1001B_M1053_m1009_IP10142_24C26CN_L'2FC2_S1030_1_2	1009	3.9	108

P1001B_M1053_m1011_IP10142_24C26CN_L'2FC2_S1067_2_2	796	2.2	82
P1001B_M1053_m1011_IP10142_24C26CN_L'2FC2_S1067_1_2	694	2.8	72
P1001B_M1053_m1011_IP10142_24C26CN_L'2FC2_S1066_2_2	411	1.0	41
P1001B_M1053_m1011_IP10142_24C26CN_L'2FC2_S1066_1_2	266	4.2	29
P1001B_M1053_m1011_IP10142_24C26CN_L'2FC2_S1065_3_2	518	2.8	54
P1001B_M1053_m1011_IP10142_24C26CN_L'2FC2_S1065_2_2	870	4.9	97
P1001B_M1053_m1011_IP10142_24C26CN_L'2FC2_S1065_1_2	400	1.0	40
P1001B_M1053_m1011_IP10142_24C26CN_L'2FC2_S1064_2_2	822	3.4	87
P1001B_M1053_m1011_IP10142_24C26CN_L'2FC2_S1064_1_2	609	4.9	68
P1001B_M1053_m1011_IP10142_24C26CN_L'2EM_S1063_3_3	3	0.0	0
P1001B_M1053_m1011_IP10142_24C26CN_L'2FC2_S1063_2_2	796	2.5	82
P1001B_M1053_m1011_IP10142_24C26CN_L'2EM_S1063_1_3	62	0.4	6
P1001B_M1053_m1011_IP10142_24C26CN_L'2EM_S1062_13_3	2	0.0	0
P1001B_M1053_m1011_IP10142_24C26CN_L'2FC2_S1062_12_2	14	0.2	1
P1001B_M1053_m1011_IP10142_24C26CN_L'2FC2_S1062_11_2	33	0.1	3
P1001B_M1053_m1011_IP10142_24C26CN_L'2FC2_S1062_10_2	11	0.2	1
P1001B_M1053_m1011_IP10142_24C26CN_L'2EM_S1062_9_3	3	0.0	0
P1001B_M1053_m1011_IP10142_24C26CN_L'2FC2_S1062_8_2	511	2.5	53
P1001B_M1053_m1011_IP10142_24C26CN_L'2FC2_S1062_7_2	1715	5.5	196
P1001B_M1053_m1011_IP10142_24C26CN_L'2FC2_S1062_6_2	611	5.1	69
P1001B_M1053_m1011_IP10142_24C26CN_L'2FC2_S1062_5_2	14	0.2	1
P1001B_M1053_m1011_IP10142_24C26CN_L'2FC2_S1062_4_2	1724	3.9	185
P1001B_M1053_m1011_IP10142_24C26CN_L'2FC2_S1062_3_2	830	1.3	84
P1001B_M1053_m1011_IP10142_24C26CN_L'2FC2_S1062_2_2	492	1.6	50
P1001B_M1053_m1011_IP10142_24C26CN_L'2FC2_S1062_1_2	14	0.2	1
P1001B_M1053_m1011_IP10142_24C26CN_L'2FC2_S1061_7_2	567	4.9	63
P1001B_M1053_m1011_IP10142_24C26CN_L'2FC2_S1061_6_2	214	3.3	23
P1001B_M1053_m1011_IP10142_24C26CN_L'2FC2_S1061_5_2	748	1.9	76
P1001B_M1053_m1011_IP10142_24C26CN_L'2FC2_S1061_4_2	889	2.5	92
P1001B_M1053_m1011_IP10142_24C26CN_L'2FC2_S1061_3_2	593	1.7	60
P1001B_M1053_m1011_IP10142_24C26CN_L'2FC2_S1061_2_2	558	1.8	57
P1001B_M1053_m1011_IP10142_24C26CN_L'2FC2_S1061_1_2	894	2.8	93
P1001B_M1053_m1011_IP10142_24C26CN_L'2FC2_S1060_3_2	197	0.4	20
P1001B_M1053_m1011_IP10142_24C26CN_L'2FC2_S1060_2_2	757	1.2	76
P1001B_M1053_m1011_IP10142_24C26CN_L'2EM_S1060_1_3	4	0.0	0
P1001B_M1053_m1011_IP10142_24C26CN_L'2FC2_S1059_2_2	1112	4.6	123
P1001B_M1053_m1011_IP10142_24C26CN_L'2FC2_S1059_1_2	16	0.2	2
P1001B_M1053_m1011_IP10142_24C26CN_L'2FC2_S1058_3_2	396	1.7	40
P1001B_M1053_m1011_IP10142_24C26CN_L'2FC2_S1058_2_2	669	1.8	68
P1001B_M1053_m1011_IP10142_24C26CN_L'2FC2_S1058_1_2	587	1.5	59
P1001B_M1053_m1011_IP10142_24C26CN_L'2FC2_S1057_6_2	475	2.3	49
P1001B_M1053_m1011_IP10142_24C26CN_L'2FC2_S1057_5_2	456	1.7	46
P1001B_M1053_m1011_IP10142_24C26CN_L'2EM_S1057_4_3	2	0.0	0
P1001B_M1053_m1011_IP10142_24C26CN_L'2FC2_S1057_3_2	460	2.7	48
P1001B_M1053_m1011_IP10142_24C26CN_L'2FC2_S1057_2_2	299	2.0	30
P1001B_M1053_m1011_IP10142_24C26CN_L'2FC2_S1057_1_2	454	1.9	46
P1001B_M1053_m1011_IP10142_24C26CN_L'2FC2_S1056_3_2	103	0.6	10
P1001B_M1053_m1011_IP10142_24C26CN_L'2FC2_S1056_2_2	505	0.9	51
P1001B_M1053_m1011_IP10142_24C26CN_L'2FC2_S1056_1_2	979	3.6	104
P1001B_M1054B_m1007_IP10143_24C26CN_L'2FC2_S1014_2_2	1072	2.3	110
P1001B_M1054B_m1007_IP10143_24C26CN_L'2FC2_S1014_1_2	996	3.3	105
P1001B_M1054B_m1007_IP10143_24C26CN_L'2FC2_S1013_2_2	577	1.8	59
P1001B_M1054B_m1007_IP10143_24C26CN_L'2FC2_S1013_1_2	616	2.3	63
P1001B_M1054B_m1007_IP10143_24C26CN_L'2FC2_S1010_2_2	390	1.3	39
P1001B_M1054B_m1007_IP10143_24C26CN_L'2FC2_S1010_1_2	549	0.6	55
P1001B_M1054B_m1007_IP10143_24C26CN_L'2FC2_S1010_1_3	550	0.6	55
P1001B_M1054B_m1007_IP10143_24C26CN_L'2EM_S1010_4_3	14	0.1	1
P1001B_M1054B_m1007_IP10143_24C26CN_L'2EM_S1010_3_3	0	0.0	0
P1001B_M1054B_m1007_IP10143_24C26CN_L'2FC2_S1012_1_3	1004	0.5	100
P1001B_M1054B_m1007_IP10143_24C26CN_L'2FC2_S1011_2_3	630	1.7	64
P1001B_M1054B_m1007_IP10143_24C26CN_L'2FC2_S1011_1_3	152	0.8	15
P1001B_M1054B_m1007_IP10143_24C26CN_L'2FC2_S1015_2_3	339	0.3	34
P1001B_M1054B_m1007_IP10143_24C26CN_L'2FC2_S1015_1_2	509	0.3	51
P1001B_M1054B_m1010_IP10143_24C26CN_L'2FC2_S1028_2_2	472	0.8	47

P1001B_M1054B_m1010_IP10143_24C26CN_L'2FC2_S1028_1_2	969	1.8	98
P1001B_M1054B_m1010_IP10143_24C26CN_L'2FC2_S1027_2_2	474	2.0	48
P1001B_M1054B_m1010_IP10143_24C26CN_L'2FC2_S1027_1_2	475	1.3	48
P1001B_M1054B_m1010_IP10143_24C26CN_L'2FC2_S1026_2_2	1114	2.6	115
P1001B_M1054B_m1010_IP10143_24C26CN_L'2FC2_S1026_1_2	1068	3.2	112
P1001B_M1054B_m1010_IP10143_24C26CN_L'2FC2_S1025_2_2	848	4.6	93
P1001B_M1054B_m1010_IP10143_24C26CN_L'2FC2_S1025_1_2	412	1.6	42
P1001B_M1054B_m1010_IP10143_24C26CN_L'2FC2_S1022_1_2	6	0.2	1
P1001B_M1054B_m1010_IP10143_24C26CN_L'2EM_S1022_1_3	6	0.2	1
P1001B_M1054B_m1010_IP10143_24C26CN_L'2EM_S1022_2_3	5	0.0	0
P1001B_M1054B_m1010_IP10143_24C26CN_L'2FC2_S1021_6_2	1044	3.6	111
P1001B_M1054B_m1010_IP10143_24C26CN_L'2FC2_S1021_5_2	1009	3.3	106
P1001B_M1054B_m1010_IP10143_24C26CN_L'2FC2_S1021_4_2	1036	2.9	108
P1001B_M1054B_m1010_IP10143_24C26CN_L'2FC2_S1021_3_2	37	0.4	4
P1001B_M1054B_m1010_IP10143_24C26CN_L'2FC2_S1021_2_2	620	1.9	63
P1001B_M1054B_m1010_IP10143_24C26CN_L'2FC2_S1021_1_2	388	1.4	39
P1001B_M1054B_m1010_IP10143_24C26CN_L'2FC2_S1020_2_2	421	1.5	43
P1001B_M1054B_m1010_IP10143_24C26CN_L'2FC2_S1020_1_2	391	0.9	39
P1001B_M1054B_m1012_IP10143_24C26CN_L'2FC2_S1080_3_1	984	3.3	104
P1001B_M1054B_m1012_IP10143_24C26CN_L'2FC2_S1080_2_2	29	0.2	3
P1001B_M1054B_m1012_IP10143_24C26CN_L'2FC2_S1080_1_2	1005	3.6	107
P1001B_M1054B_m1012_IP10143_24C26CN_L'2FC2_S1079_2_2	397	0.7	40
P1001B_M1054B_m1012_IP10143_24C26CN_L'2FC2_S1079_1_2	949	4.1	102
P1001B_M1054B_m1012_IP10143_24C26CN_L'2FC2_S1078_2_2	562	2.6	58
P1001B_M1054B_m1012_IP10143_24C26CN_L'2FC2_S1078_1_2	612	1.8	62
P1001B_M1054B_m1012_IP10143_24C26CN_L'2FC2_S1077_2_2	1245	5.0	139
P1001B_M1054B_m1012_IP10143_24C26CN_L'2FC2_S1077_1_2	824	4.2	89
P1001B_M1054B_m1012_IP10143_24C26CN_L'2EM_S1076_3_2	5	0.0	0
P1001B_M1054B_m1012_IP10143_24C26CN_L'2FC2_S1076_2_2	656	1.4	66
P1001B_M1054B_m1012_IP10143_24C26CN_L'2FC2_S1076_1_2	581	1.9	59
P1001B_M1054B_m1012_IP10143_24C26CN_L'2FC2_S1075_3_1	447	1.7	45
P1001B_M1054B_m1012_IP10143_24C26CN_L'2FC2_S1075_2_2	853	3.0	89
P1001B_M1054B_m1012_IP10143_24C26CN_L'2FC2_S1075_1_2	895	3.3	94
P1001B_M1054B_m1012_IP10143_24C26CN_L'2FC2_S1074_2_2	518	0.8	52
P1001B_M1054B_m1012_IP10143_24C26CN_L'2FC2_S1074_1_2	543	0.4	54
P1001B_M1054B_m1012_IP10143_24C26CN_L'2FC2_S1073_4_2	577	2.1	59
P1001B_M1054B_m1012_IP10143_24C26CN_L'2FC2_S1073_3_2	1261	7.7	159
P1001B_M1054B_m1012_IP10143_24C26CN_L'2FC2_S1073_2_2	469	1.6	48
P1001B_M1054B_m1012_IP10143_24C26CN_L'2FC2_S1073_1_2	481	1.2	49
P1001B_M1054B_m1012_IP10143_24C26CN_L'2FC2_S1072_2_2	154	0.2	15
P1001B_M1054B_m1012_IP10143_24C26CN_L'2FC2_S1072_1_2	351	4.6	39
P1001B_M1054B_m1012_IP10143_24C26CN_L'2FC2_S1071_2_2	1091	4.4	119
P1001B_M1054B_m1012_IP10143_24C26CN_L'2FC2_S1071_1_2	24	0.2	2
P1001B_M1054B_m1012_IP10143_24C26CN_L'2FC2_S1070_2_2	736	2.6	76
P1001B_M1054B_m1012_IP10143_24C26CN_L'2FC2_S1070_1_2	921	3.9	99
P1001B_M1054B_m1012_IP10143_24C26CN_L'2FC2_S1069_1_2	877	3.5	93
P1001B_M1054B_m1012_IP10143_24C26CN_L'2FC2_S1068_2_2	806	1.2	81
P1001B_M1054B_m1012_IP10143_24C26CN_L'2FC2_S1068_1_2	665	2.4	68
P1001B_M1055_IP10143_24C26CN_L'2FC_S1317_1	686	0.7	69
P1001B_M1055_IP10143_24C26CN_L'2FC_S1317_2	648	1.8	66
P1001B_M1055_IP10143_24C26CN_L'2FC_S1317_3	587	6.7	71
P1001B_M1055_IP10143_24C26CN_L'2FC_S1317_4	888	13.8	151
P1001B_M1055_IP10143_24C26CN_L'2FC_S1317_5	530	1.8	54
P1001B_M1055_IP10143_24C26CN_L'2FC_S1317_6	795	1.4	80
P1001B_M1055_IP10143_24C26CN_L'2FC_S1317_7	397	4.3	43
P1001B_M1055_IP10143_24C26CN_L'2FC_S1317_8	539	2.6	56
P1001B_M1055_IP10143_24C26CN_L'2FC_S1317_9	616	0.7	62
P1001B_M1055_IP10143_24C26CN_L'2FC_S1317_10	138	0.5	14

Calibration based up 26/24 = 0.00229 equivalent to 420 ppm N (S0011G diamond)
1-within-spot uncertainty, for comparing data within this data set only
2-estimated overall uncertainty, for comparison with other data sets